Kurdistan Regional Government
Ministry of Higher Education and Scientific Research
University of Sulaimani
College of Science

COMPUTER AIDED DIAGNOSIS FOR EARLY DETECTION OF BRAIN TUMOR

A Dissertation
Submitted to the Council of the College of Science at the University of Sulaimani in Partial Fulfillment of the Requirements for the Degree of Doctor of Philosophy
In Computer Science

Image Processing

By

Dalia Mohammad Toufiq

M.Sc. Information Technonlogy (2011), University of JNTUH, India

Supervisor (s)

Prof. Dr. Ali Makki Sagheer

Assoc. Prof. Dr. Hadi Veisi

Rezber 2722 October 2022

بِسْمِ اللَّهِ الرَّحْمَنِ الرَّحِيمِ

﴿ وَيَرَى الَّذِينَ أُوتُوا الْعِلْمَ الَّذِي أُنْزِلَ إِلَيْكَ مِنْ رَبِّكَ هُوَ الْحَقَّ وَيَهْدِي إِلَى صِرَاطِ الْعَزِيزِ الْحَمِيدِ ﴾ (6)

صدق الله العظيم

سورة سبأ

Supervisor Certification

We certify that the preparation of this dissertation entitled "**Computer Aided Diagnosis for Early Detection of Brain Tumor**" accomplished by **Dalia Mohammad Toufiq**, was prepared under our supervision in the College of Computer Science and IT at the University of Anbar and the Faculty of New Sciences and Technologies at the University of Tehran in partial fulfillment of the requirements for the degree of Doctoral of Philosophy in **Computer Science (Image processing).**

Signature:

Supervisor: **Dr. Ali Makki Sagheer**

Title: **Professor**

Department of Computer Science,

College of computer Science and IT,

University of Anbar

Date: 14 /12 /2022

Signature: 

Co- Supervisor: **Dr. Hadi Veisi**

Title: **Associate Professor**

Department of Computer Engineering,

Faculty of New Sciences and Technologies,

University of Tehran

Date: 14 /12 /2022

Certification of the Department

In view of the available recommendation, I forward this dissertation for debate by examining committee.

Signature:

Name: **Dr. Mustafa Ibrahim Khaleel**

Title: **Assistant Professor**

Department of Computer Science, College of Science, University of Sulaimani

Date: 14 / 12 / 2022

Examining Committee Certification

We certify that we have read this dissertation entitled **"Computer Aided Diagnosis for Early Detection of Brain Tumor"** prepared by **Dalia Mohammad Toufiq**, and as the Examining Committee, we examined the student in its content and in what is connected with it, and in our opinion, it meets the basic requirements toward the degree of Doctoral of Philosophy in **Computer Science (Image Processing).**

Signature:
Name: **Abdulbasit Kamil Faeq**
Title: **Assistant Professor**
Affiliation: **Koya University**
Date: 14 /12 / 2022
Member

Signature:
Name: **Haval Mohammed Sidqi**
Title: **Assistant Professor**
Affiliation: **Sulaimani Polytechnic University**
Date: 14 /12 / 2022
Member

Signature:
Name: **Harith Raad Hasan**
Title: **Assistant Professor**
Affiliation: **Sulaimani Polytechnic University**
Date: 14 /12 / 2022
Member

Signature:
Name: **Alan Anwer Abdulla**
Title: **Assistant Professor**
Affiliation: **University of Sulaimani**
Date: 14 /12 / 2022
Member

Signature:
Name: **Dr. Ali Makki Sagheer**
Title: **Professor**
Affiliation: **University of Anbar**
Date: 14 /12 / 2022
Supervisor-Member

Signature:
Name: **Dr. Hadi Veisi**
Title: **Associate Professor**
Affiliation: **University of Tehran**
Date: 14 /12 / 2022
Supervisor-Member

Signature:
Name: **Muzhir Shaban Al-Ani**
Title: **Professor**
Affiliation: **University of Human Development**
Date: 14 /12 / 2022
Chairman

Approved by the Dean of the College of Science

Signature:
Name: **Dr. Soran Mohammed Mamand**
Title: **Assistant Professor**
Date: 14 /12 / 2022

DEDICATION

I **DEDICATE** this dissertation to…

My father's soul

My precious mother

My beloved brother and sisters

My friends who encourage and support me

All the people in my life who touch my heart

ACKNOWLEDGMENTS

First and foremost, I must express my unending gratitude for Allah's assistance and blessings, the Ever-Magnificent, the Ever-Grateful. Without His guidance, I am totally sure that this work would never have come to pass.

I would like to express my deep and sincere gratitude to my research supervisor, **Prof. Dr**. **Ali Makki sagheer**, for giving me the opportunity to do research and providing invaluable guidance throughout this research. His dynamism, vision, sincerity, and motivation have deeply inspired me. He taught me the methodology for conducting the research and presenting the findings as clearly as possible. I am extremely grateful for what he has offered me. I would also like to thank him for his friendship, empathy, positive encouragement, and warm spirit in helping me finish this dissertation. Also, this dissertation would not have been possible without the guidance and help of **Assoc. Prof. Dr. Hadi Vesie**, my co-supervisor, for the continuous support of my Ph.D. study and research and for his motivation, valuable comments, and immense knowledge. I was impressed by his never-ending energy and blessed by his keenness towards his students.

I would like to express my wholehearted thanks to my family, especially my mother, for the generous support they provided me throughout my entire life and particularly through the process of pursuing the Ph.D. degree. Because of their unconditional love and prayers, I have the chance to write and complete this dissertation. I also would like to thank my dearest sister **Taban** for her support, endless patience, and sincere help during my studies.

I would like to express my very great appreciation to the Dean of the College of Medicine, **Asst. Prof. Dr. Kosar Mohammad Ali,** the Head of the Department of Family and Community Medicine, **Prof. Dr. Bushra Mohammed Ali**, and my colleagues. Their enlightening suggestions, helping and encouragements made me feel I was not isolated in my research. I am extending my thanks to **Ammar Hamid Ali**, who has been with me and so supportive from the beginning until the completion of my dissertation.

I would like to take this opportunity to say warm thanks to all my beloved friends, especially to **Srwa Hasan Abdulla,** who has been so supportive along the way of doing my dissertation.

Last but not least, my deepest thanks go to all the people who took part in making this dissertation real.

Dalia Mohammad Toufiq

ABSTRACT

Brain tumors are the tenth leading cause of death worldwide. Tumors can be benign or malignant, and early diagnosis of malignant tumors can save lives. To diagnose and treat brain tumors early, magnetic resonance imaging (MRI) is the most common type of diagnostic scan. Processing MRI images manually is a time-consuming and difficult task, in which its speed and accuracy can be improved using machine learning techniques. Although there are various techniques for the automatic classification of brain tumor images, their performance needs to be improved. Furthermore, the computer-aided diagnostic system (CAD) is a pattern recognition tool that is used to help radiologists make accurate diagnoses. Due to the difficulties of analyzing medical data (signals or images) and the reliance on the expertise of the physician, the CAD system is crucial. In this dissertation, two methods are presented to address this challenge.

- The first method proposes a hybrid feature extraction technique based on discrete wavelet transform (DWT) and principal component analysis (PCA) to improve the normal and abnormal classification performances. Due to the complexity of brain structure, accurate mechanistic segmentation of brain tumors on MRI images is difficult due to density distributions in which skull intensity overlaps with tumor intensity and a lack of models that maximize accuracy and minimize time complexity. In this method, after image segmentation and wavelet transformation, the features are extracted using the gray-level co-occurrence matrix (GLCM) from the PCA components, and a random forest classifier (RF) is used for the classification. The experimental results obtained an accuracy of 98.3%, a sensitivity of 99%, and a specificity of 97.6% on the Harvard and OASIS datasets, which is higher than the reference methods.

- The second method presents a technique to segment brain tumors. When dealing with tumor segmentation, tumors are areas of higher density than the rest of the image. In this method, the dataset contains brain images in which tumors are less dense than the rest of the image, so this research proposes an optimized thresholded difference (OTD) and a rough set theory (RST) method to overcome the segmentation problem. Then GLCM is utilized to extract features, and Iterative Dichotomizer 3 (ID3) is utilized to perform the classification. This method achieves 98.9% accuracy on the Figshare dataset, which surpasses the reference methods.

TABLE OF CONTENTS

LIST OF TABELS

LIST OF FIGURES

LIST OF ABBRIVIATIONS

Abbreviation	Description
AI	Artificial Intelligence
ANN	Artificial Neural Network
AUC	Area Under the Curve
BWT	Berkeley Wavelet Transformation
CAD	Computer Assisted Diagnosis
CE	Contrast-Enhanced
CNN	Convolutional Neural Network
CPU	Central Processing Unit
CSF	Cerebrospinal Fluid
CT	Computed Tomography
DCNN	Deep Convolutional Neural Network
DFT	Discrete Fourier Transform
DMWT	Discrete Multiwavelet Transform
DNA	Deoxyribonucleic Acid
DT	Decision Tree
DWT	Discrete Wavelet Transform
EFD	Elliptic Fourier Descriptors
ELM	Extreme Learning Machine
ERR	Error Rate
FLAIR	Fluid Attenuated Inversion Recovery
FN	False Negative
FP	False Positive
GA	Genetic Algorithm
GBM	Glioblastoma Multiform
GLCM	Gray-level Co-occurrence Matrix
GLRL	Gray Level Run Length Matrix
GMM	Gaussian Mixture Model
HGG	High-Grade Glioma
HH	High-High
HL	High-Low
HOG	Histogram of Oriented Gradients
HPF	High Pass Filter
ID3	Iterative Dichotomiser3
IDM	Inverse Difference Moment
IND	Indiscernibility Relation
IST	Information System Table

KELM	Kernel Extreme Learning Machine
KNN	K-Nearest Neighbors
KURT	Kurtosis
LBP	Local Binary Pattern
LGG	Low- Grade Glioma
LH	Low-High
LL	Low-Low
LOOCV	Leave-One-Out-Cross Validation
LPF	Low Pass Filter
MGLCM	Modified Grey Level Co-Occurrence Matrix
ML	Machine Learning
MLP	Multilayer Perceptron
MRI	Magnetic Resonance Imaging
MSE	Mean Squared Error
NN	Neural Network
OASIS	Open Access Series of Imaging Studies
OTD	Optimized Thresholded Difference
PCA	Principle Component Analysis
PET	Positron Emission Tomography
PNN	Probabilistic Neural Network
RAM	Random Access Memory
RELM	Regularized Extreme Learning Machine
RF	Random Forest
ROC	Receiver Operating Characteristics
ROI	Region of Interest
RST	Rough Set Theory
SD	Standard Deviation
SIFT	Scale-Invariant Feature Transform
SVM	Support Vector Machine
SWT	Stationary Wavelet Transform
T1	Longitudinal Relaxation Time
T2	Transverse Relaxation Time
TE	Time to Echo
TL	Transfer Learning
TN	True Negative
TP	True Positive
TR	Time Repetition

Chapter One

Introduction

1.1 Introduction

A tumor is the term for abnormal cell proliferation in the human body that forms inside the skull. Tumors can be benign or malignant (cancerous), depending on their nature. Malignant tumors are those that spread to other regions of the body, whereas benign tumors do not. Because they infiltrate other areas of the brain, malignant tumors are more dangerous than benign ones. Though benign tumors may not infect other regions of the body, they are still damaging because they press on other brain tissues, causing complications. As a result, early diagnosis of malignant cancers can save lives. According to statistics, brain tumors are the tenth highest cause of mortality in both men and women [1]. Thousands of people suffer and die every year as a result of brain tumors. However, this rate is reduced significantly due to the early and accurate diagnosis of brain tumors. Early diagnosis is the key to improving medical treatment and saving lives. As a result, scientists and researchers have been attempting to create advanced tools and procedures for determining the type and stage of brain tumors.

There are two modalities that are widely used in examining and determining the abnormalities in brain tissues regarding their size, shape, and location. These modalities are magnetic resonance imaging (MRI) and computed tomography (CT), which are explained in detail in the next chapter. Radiologists and doctors prefer MRI over CT as it monitors brain tissue in depth and it is a non-invasive imaging modality [2]. Processing MRI images manually on a daily basis by the medical staff is a tedious and difficult task. Furthermore, it is a difficult process when there is a huge amount of data that needs to be examined with a wide range of brain tumors. An automated tumor classification system is critical to assist radiologists and clinicians in identifying brain tumors. Therefore, there is a need for machines to do these routine tasks accurately and within a short time. These tasks are based on artificial intelligence (AI) or computer-aided

diagnosis (CAD). The medical community recommends automatic image analysis for medical images to help doctors diagnose diseases and plan treatment. The main stages for a CAD system to diagnose brain tumors are detection, segmentation, feature extraction, and classification processes. The quality of images that enter a diagnosis system determines the performance of such a system and obtains high results. Therefore, enhancing these images prior to feeding them to classification methods is essential to the success of a classification process. In addition, selecting the best approaches for feature extraction from the obtained images is important to gain better performance. Feature extraction aims to extract the most important information from the original image in order to reduce dimensionality, speed up processing and achieve accurate prediction. The classification process is based on features that are fed as input to the machine learning. Therefore, the performance of the system can suffer from overfitting if the features are not chosen properly [3].

The next section explains the studies that have been proposed by the research community to enhance the ability of the brain tumor system to detect the tumor types (i.e., normal or abnormal) more accurately and efficiently. The scholar utilized different techniques for this purpose, such as segmentation methods, feature extraction, and machine learning.

1.2 Literature Review

This section provides a review of the previous related works with respect to this dissertation.

The authors **P. Dvoˇrák et al. (2013)** presented an approach to determine if the brain tissue has a tumor or not and then localize this tumor. The propose approach was tested based on dataset that included 203 T2-weighted images, 131 of them do not contain any tumor while the remaining images are infected. Multi-resolution symmetry analysis is used to determine whether the image depicts an afflicted brain and where a pathological area exists. Five-fold cross-validation technique was applied for the selected database, the results for the first part showed that the true negative rate of 93.14% and the true positive rate is 87.52% for afflicted brain detection. The second component of the method was evaluated by comparing the estimated tumor location to the actual tumor location. The percentage of correct anomaly identification is 95.83%, while the rate of correct tumor location is 87.5% [4].

The authors **Nooshin N. and Miroslav K. (2015)** utilized a single-spectral anatomical MRI images to detect brain tumors and to reduce the time and cost that occurs due to a multi-spectral MRI scans. They demonstrated a completely autonomous system that can identify slices containing tumors and identify the tumor region. The experimental findings using a single contrast mechanism showed that the suggested approach is effective at accurately and efficiently segmenting brain tumor tissues while requiring little processing effort. The results obtained are as follow 77.2%, 81.3% and 79.3% for sensitivity specificity and accuracy receptively [5].

Cheng J. and Huang W. (2015) classified three types of brain tumors which are meningioma, glioma, and pituitary based on large dataset of T1-weighted MRI images. The proposed approach firstly localized the region of tumor and then drew various circles with different radius around the region. The authors

claimed that the tumor-surrounding tissue is distinct among the various tumors types. Firstly, the approach improves classification performance by setting the ROI to the augmented tumor region rather than the original tumor location. Secondly, the enhanced tumor is subdivided into progressively fine ring-shaped sub regions. The proposed method evaluated by comparing with other feature extraction methods which are intensity histogram, bag-of-words (BoW) model, and grey level co-occurrence matrix (GLCM), and. The accuracies were improved to 82.31% from 71.39%, 88.19% from 83.54%, and 84.75%from 78.18%, respectively. Although the experimental results showed that this method performed better accuracy than the others, but the accuracy is still low [6].

The authors **Ali M. Hasan and Farid M. (2016)** developed an algorithm to detect and classify MRI images into two classes which are normal and abnormal. A modified grey level co-occurrence matrix (MGLCM) method was applied for analyzing and measuring the two parts of brain hemispheres, 21 features are used to present the selected images. The experimental findings showed how effective the suggested method for accurately and quickly identifying brain abnormalities. The dataset included in the study consists of 165 individuals, 88 of whom have various types of brain abnormalities while the remaining patients don't show any obvious abnormality. The algorithm was evaluated using a ten-fold cross-validation approach with 100 repeats. With a multi-layer perceptron neural network, the highest detection accuracy for brain cancers was 97.8% [7].

Also, MF Siddiqui et al. (2017) proposed an automatic computer-aided multi-class decision support system for classifying magnetic resonance imaging (MRI) scans of the human brain using benchmark MRI datasets (OASIS and Harvard) with 310 patients verified the performance of the suggested system. A fast discrete wavelet transform (DWT) is used to extract the images' master

features, and principal component analysis (PCA) is then used to further examine these distinguishing features. The J48 decision tree, k-nearest neighbor (kNN), random forest (RF), and least-squares support vector machine (LS-SVM) with polynomial and radial basis kernels are some of the classification models. The RF-based classifier surpassed all other decision models with an accuracy of 95.70%. The provided medical decision support system shows prospective proof for reliable multi-class classification of brain abnormalities; hence, it has the potential to be used as a diagnostic tool by medical professionals [8].

H. Mohsen et al. (2018) proposed a system to classify a dataset of 66 brain MRIs into 4 classes e.g. normal, glioblastoma, sarcoma and metastatic bronchogenic carcinoma tumors. The deep neural network (DNN) classifier was integrated with discrete wavelet transform (DWT) the effective feature extraction tool and principal components analysis (PCA). Finally, DNN was used for classification issues with an accuracy, sensitivity and precision of 96.97%, 97% and 97% respectively [9].

Other studied tried to identify a type of brain tumor as a next stage after determining the brain cancer. For example, the authors **M. R. Ismael et al. (2018)** introduced a framework that is capable to classify brain tumors relaying on MRI modality. The framework used statistical features and neural network algorithms to determine well known brain tumors glioma, meningioma, and pituitary tumor. In addition, the approach utilized region of interest (ROI) techniques to segment a brain tumor as pre-processing. The study used 2D discrete wavelet transform and 2D gabor filter methods for selecting appropriate features. A dataset that included 3,064 slices of T1-weighted MRI images was used to evaluate the framework with accuracy reached to 92% and specificity 96.29%, 96%, and 95.66% for glioma, meningioma, and pituitary tumor respectively. The authors stated that the selected features could be utilized in

different frameworks with different classification techniques to improve the accuracy. This study uses large dataset samples compared with previous study and achieved high accuracy about 92%. However, the study utilized additional methods and filters to select the appropriate features that caused in extra computational time [10].

For instance, **M. Sharif el al. (2018)**, in a study proposed a method for detection a malignant tumor in a human brain for MRI images based on the first category. The method carried out four steps to segment and classify brain tumor whether it is normal or abnormal. In the first step, a manual skull stripping was used to determine the region of interest and Gaussian filter to remove any noise effects. In the next step, a binomial mean, standard deviation, and variance were utilized to enhance a thresholding method that segmented the tumor. Afterwards, a serial based method and genetic algorithm (GA) were suggested for feature extraction and selecting a best features respectively. Finally, a classification method was applied based on support vector machine (SVM) to classify a brain's tissue as normal or abnormal. The proposed approach was evaluated by using two datasets (i.e., Harvard and Private) with accuracy above 90% which is also still low [11].

The authors **N. Varuna Shree and T. N. R. Kumar in study (2018)** collected MRI dataset from web site www.diacom.com to classify brain tumors into normal and abnormal. The first stage was pre-processed these images to reduce a noise ratio and do smoothing. Next, the images were decomposed into several sub-bands using DWT to reduce image size with maintaining the important information. Afterwards, the features were extracted from these images in which represent samples by utilizing gray-level co-occurrence matrix (GLCM). These samples were the input to probabilistic neural network (PNN) classifier that distinguish whether the tissue is normal or not with maximum

accuracy of 95%. This study identify only weather the tissue is infected or not without determine the type of tumor [12].

H. Byale et al. (2018) built four stages to perform automatic classification for brain tumors. The first stage involved adaptive median filter to remove any noise in the image, then, the next stage included gaussian mixture model (GMM) to segment the tumor region. The third stage utilized grey level co-occurrence matrix (GLCM) to extract feature from the segmented image, and finally, neural network (NN) was used to determine the tumor types. The model was evaluated and showed high performance, the study utilized the accuracy, specificity, sensitivity and precision as evaluation metrics and they scored with 93.33%, 96.6%, 93.33%, and 94.44% respectively. The authors achieved good accuracy, but they used neural network which is need more computational resources [13].

The authors **Pashaei A. et al. (2018)** extracted features by the convolution and maxpooling layers are taught to CNNs. Extreme learning machines (ELM) are a type of learning algorithm that uses one or more layers of hidden nodes to learn. These networks are utilized in a number of applications, including classification and regression. This work attempts to extract hidden features from images using a CNN. The images are then classified using these extracted characteristics by a kernel ELM (KELM). In this study, a dataset was used to assess the efficacy of our proposed technique, which includes T1-weighted contrast-enhanced MRI (CE-MRI) scans of three types of brain tumors: meningioma, glioma, and pituitary tumor. The proposed technique achieved an accuracy of 93.68% [14].

Hussain L. (2019) proposed in a strategy to identify brain tumor based on multimodal feature extraction; these features were texture, morphological, Scale invariant feature transform (SIFT), entropy based and elliptic Fourier descriptors (EFDs) that extracted from the MRI imaging dataset. Afterwards, three machine

learning algorithms were applied for detection brain tumors (i.e., SVM, decision tree (DT), and naïve Bayes). The naïve Bayes followed by decision tree contributes higher accuracy for tumor detection that achieved very high accuracy 100% and 97.8 respectively. The high accuracies obtained with considering using three methods for feature extraction which is also time consuming and increases the complexity of the system proposed [15].

The authors **Deepak S. and Ameer P. (2019)** focused on a three-class classification issue to distinguish between three forms of brain malignancies: glioma, meningioma, and pituitary tumors. To extract characteristics from brain MRI scans, the proposed classification method employs deep transfer learning and a pre-trained GoogLeNet. The collected features are classified using proven classifier models. On an MRI dataset from figshare, the experiment uses a patient-level five-fold cross-validation approach. The suggested system outperforms all current approaches with a mean classification accuracy of 98 percent [16].

The authors **Khan M. et al. (2019)** developed an automated system for extracting and classifying MRI brain tumors. The proposed approach used marker-based watershed segmentation and features selection. Five stages are carried out in the proposed system, which are tumor contrast, tumor extraction, multi-model features extraction, features selection, and classification. To improve the contrast of a tumor, a gamma contrast stretching method is used. After that, a marker-based watershed technique is used to segment the data. In the next stage, shape, texture, and point features are extracted, and only the top 70% of features are selected using the chi-square max conditional priority features approach. Before classifying with a support vector machine, selected features are fused using a serial-based concatenation method. All of the experiments are run on three data sets: Harvard, (BRATS 2013), and a set of privately obtained MR pictures. The suggested approach clearly exceeds

existing systems in terms of precision and accuracy, according to simulation findings[17].

In addition, **A. Gumaei et al. (2019)** proposed an approach for accurate brain tumor identification based on a hybrid feature extraction method and a regularized extreme learning machine (RELM). Firstly, the brain images were preprocessed to detect edge regions of the tumor through utilizing a min-max normalization rule. Afterwards, features were extracted based on a hybrid method referred to as PCA-NGIST. The proposed approach was evaluated by using a new dataset of medical images for brain tumors which is publically available. RELM classifier was used to classify brain tumors with accuracy reached to 94.2%. The work utilized hybrid method for feature extraction that cost time[18].

On the other hand, other papers used the both categories to identify brain tumors as **Mohammed M. et al. (2019)** the authors used the brain T1-weighed CE-MRI dataset that are provided by [6, 19]to identify brain tumors by applying Fuzzy C-Means clustering method. The dataset included different images for brain tumors that have various sizes, shapes, and locations. The following step was utilizing six methods of machine learning (i.e., support vector machine (SVM), k-nearest neighbor (KNN), multilayer perceptron (MLP), logistic regression, naïve Bayes and random forest. In addition, convolutional neural network (CNN) was applied and achieved higher accuracy than the traditional ones. The proposed method is able to distinguish whether a tissue is normal or abnormal with accuracy 97.87% [20].

The authors **Zar N. et al. (2019)** tried to solve the limitation of the small dataset, they pre-trained CNN model and suggested a fine tuning approach that based on transfer learning. MRI benchmark dataset was used to evaluate the proposed approach. This approach is more universal since it does not rely on custom features, it needs less preprocessing, and it obtained an average accuracy

of 94.82%. The findings not only compared with deep learning techniques utilizing CNNs but also with more conventional machine learning techniques. On the CE-MRI dataset, experimental findings demonstrate that the suggested technique outperforms state-of-the-art classification [21].

The authors **S. Deepak and P. M. Ameer (2020)** proposed a scheme that merges two machine learning algorithms (i.e., convolutional neural network (CNN) and support vector machine (SVM)) to classify the medical images. This combination is to mitigate the challenge of availability of large medical images to train neural network. Figshare open dataset that included MRI images was used to evaluate the fully automated system. The study utilized CNN for extracting features from the brain MRI images and a multiclass SVM to improve the performance of the system. the system achieved high accuracy compared with the other studies that reached to 95.82% [22].

S. Dutta et al. (2020) proposed a work to classify five main types of brain tumors using the Adaptive Neuro Fuzzy Inference System (ANFIS), a classifier built on the Fuzzy Inference System (FIS), where initially a normalized MRI image is used as input. In the second stage, feature vectors are extracted from the image using GLCM, which reduces the amount of redundant data used as the classifier's input. The overall accuracy of the suggested technique, which is evaluated on Harvard dataset is about 96.34% [23].

WAK Naser et al. (2021) suggested multi-kernel SVM technique for MRI brain tumor detection. The stages of image acquisition, image preprocessing, feature extraction, and tumor classification are involved in the work. During the preprocessing stage, thresholding was performed automatically using the Otsu region-based segmentation algorithm. To distinguish between normal and abnormal images, the classification system uses four distinct kernels. SVM with a quadratic kernel achieves the best classification accuracy of 86.5% [24].

Similarly, **Naralasetty N. et al. (2021)** proposed a method for developing a mechanized system that distinguishes benign and malignant tumor images and improves classification accuracy. K-means and the Gaussian mixture model (GMM) were used to segment brain tumors. Discrete wavelet transform (DWT) and principal component analysis (PCA) were used for feature extraction and feature reduction, respectively. In addition, they utilized an SVM classifier to identify benign and malignant tumors [25].

Sathi K. and Akhter S. (2021) proposed a framework for the classification of brain tumors into three categories, which are glioma, meningioma, and pituitary using an artificial neural network (ANN). The Min-max normalization rule was applied as a preprocessing stage and then statistical features were extracted from the medical image based on two techniques, which are stationary wavelet transform (SWT) and gray level co-occurrence matrix (GLCM). These techniques aimed to enhance the performance of the classifier which achieved better accuracy than other multi-classification methods that reached into 96.2% [26].

The authors **MH Siddiqi et al. (2022)** suggested a novel feature extraction method. The proposed technique selects the most valuable features from MRI images of various disorders. Additionally, this method uses recursive values like the partial Z-value to distinguish between multiple classes. The model is trained by applying a support vector machine (SVM) to assign the predicted labels to the relevant MRI images after extracting and selecting the most effective features. The work used a publicly available standard dataset, such as Harvard Medical School and the Open Access Series of Imaging Studies (OASIS), to show the importance of the suggested model, and the proposed approach achieved an accuracy of 96.4% [27].

The authors **MH Siddiqi et al. (2022)** provided a reliable method that can assess and identify many kinds of brain abnormalities using MRI images.

Unwanted details are eliminated using global histogram equalization. After the image has been enhanced, the best features from the MRI images can be extracted for feature extraction using a symmetric wavelet transform-based method. After the best feature has been extracted, the linear discriminant analysis (LDA) was used to reduce the size of the feature space. A logistic regression for training and evaluation is utilized, and the model successfully identified several types of brain diseases from MRI images. The Open Access Series of Imaging Studies (OASIS), which includes 24 distinct brain diseases (including normal), and a standard dataset from Harvard Medical School are both utilized. The best classification accuracy was achieved by the suggested method, which was 96.6% [28].

1.3 Problem Statement

Doctors and radiologists commonly use MRI images to detect brain tumors manually in the medical world. The experts in this field have the ability to read and diagnose brain tumors; however, this task becomes difficult and could lead to human errors when repeated many times and for many images. Furthermore, the structure's complexity in the brain tissue could prevent a doctor from taking the right decision [29], [30]. Therefore, computer-aided diagnostic systems (CAD), which utilize machine learning (ML) techniques, are used to help radiologists make accurate diagnoses.

The literature review for ML-based brain tumor identification shows that these methods make a compromise between accuracy, design complexity, and execution time. As the studies in the literature review noticed, some methods result in high accuracy, but they are mainly complicated in which more resources are needed and more execution time is required. On the other hand, there are other studies that speed up the processing time for identifying the brain tumors, but they suffer from low accuracy. This dissertation takes this trade-off

into consideration and proposes a technique with low complexity but acceptable performance.

Another issue addressed in this dissertation is the segmentation of brain tumor MRI images, which is an important step in CAD systems. The low contrast and high correlation in these images make the segmentation of brain tumors a challenging task.

When dealing with tumor segmentation, tumors are an area of higher density than the rest of the image, so the segmentation process is to split the higher-density pixels from the rest of the image when using thresholding algorithms. This fact differs in some cases, such as the Figshare dataset samples, which also contain brain images in which tumors are less dense than the rest of the image. Therefore, the threshold-based segmentation process is used to split the pixels that are less dense than the rest of the pixels in the image. Furthermore, traditional threshold techniques will not be able to identify both low and high intensities at the same time, so they will only be able to find either low or high intensities.

1.4 Aim of Dissertation

This dissertation aims to propose an approach that has a simple design in order to achieve higher accuracy with less execution time for brain tumor classification. The dissertation aims to propose and investigate novel mechanisms for accurate, efficient detection and classification to reduce the computational complexity of the model. In the first model, a hybrid approach that consists of the following techniques (DWT, PCA, and GLCM) is proposed to enhance the classification results. It can also locate the area of the tumor in the brain and distinguish between the normal and abnormal MRI images based on random forest. In the second model, we suggests an optimized thresholded difference (OTD) and rough set theory (RST) for automatic segmentation of brain tumors that can isolate the infected tissue in the brain from the healthy

ones in MR images by determining the position of the tumor and drawing statistical analysis for the selected area. The features are extracted from the segmented images using the gray-level co-occurrence matrix (GLCM). An RST is employed to improve the performance of the system that is validated based on the Figshare open dataset using the ID3 classifier.

1.5 Contributions

The following are the dissertation's key contributions, which are the suggested solutions to the issues listed in the problem definition section:

1. To speed up the processing time to identify brain tumors while achieving a high accuracy level, a hybrid approach consisting of three techniques (i.e., DWT, PCA, and GLCM) is proposed to classify normal and abnormal MRI images using a random forest (RF) classifier. The proposed technique obtained high accuracy of 98.3%, compared to other popular methods in recent literature.

2. To overcome the limitations of the traditional thresholding algorithms, an optimized thresholded difference (OTD) and rough set theory (RST) are proposed to segment brain tumors. In this method, features are extracted from the segmented images using the gray-level co-occurrence matrix (GLCM), and the RST is employed to improve the performance of the system. The proposed system achieved an accuracy of 98.9%, leading to the conclusion that it allows clinical experts to decide and diagnose.

1.6 Dissertation Structure

This dissertation is structured as follows:

- **Chapter One:** This chapter gives an introduction to the brain tumor subject, followed by a review of the most recent studies in this field. Later on, the chapter outlines the problem that faces the medical staff in identifying the brain tumors. This chapter includes the main aim of the study and the main contributions of the researchers. Finally, it presents the dissertation structure.
- **Chapter Two:** This chapter presents the brain anatomy of the human body, its structure, and types of brain tumors that infects the brain; also, it introduces the imaging modalities such as MRI. The next part of this chapter includes sections about digital imaging processing and displays the main components of designing digital imaging processing. In addition, the chapter shows the most evaluation metrics that are used in calculating the efficiency of the system. Finally, the chapter gives an explanation to the most popular datasets that are utilized in this study.
- **Chapter Three:** This chapter explains the proposed methodology that contains various steps to implement tumor type's detection. There are different stages to carry out this task which are image acquisition, pre-processing, segmenting tumor regions. Finally, applying machine learning algorithms to train and evaluating models.
- **Chapter Four:** This chapter presents the results by utilizing the evaluation metrics for evaluation such as accuracy, sensitivity, and the confusion matrix. Also, the chapter discusses these results.
- **Chapter Five:** This chapter introduces the main conclusions from the research, highlighting the key achievements and limitations. The chapter also discusses future research and development.

Chapter Two

Theoretical Background

2.1 Introduction

Medical imaging is a technique used to view an inner structure of the body for medical and scientific purposes. It is a vital tool to recognize and diagnoses anomalies early and in easy way. Classifying these images have been taken attention by medicine industry and research community as it discovers the infected area in early stages and knows the progress of the disease such as brain tumors [31]. An accurate diagnosis is the key to minimizing the percentage of deaths that have recently reached significant numbers. Techniques such as computed tomography (CT) scans and magnetic resonance imaging (MRI) imaging are widely used nowadays, and the latter is more common as it offers high resolution images of the brain tissues from various angles. Determining the correct type of brain tumor manually requires an expert who has good knowledge of brain diseases [32]. Additionally, it is time-consuming and tedious for a lot of images. Moreover, human errors are possible, and consequently, false detection may cause a wrong procedure and treatment. Therefore, scientists and researchers have introduced different approaches for classifying tumor types automatically and efficiently without need for human expertise [33]. Brain tumor classification by utilizing machine learning algorithms has become essential due to its importance in people's lives. This chapter presents these approaches, which are mainly utilizing machine learning (ML) algorithms. These algorithms can be divided into two main categories: supervised and unsupervised. The most popular algorithms that are used for this topic and have achieved high accuracy in classifying brain tumors are random forest (RF) and decision tree (DT). In addition, this chapter shows the main steps that are important for successful diagnosis tumors which include: pre-processing, segmentation, feature extraction/selection, and classification. Image processing is an approach that converts an image into digital form and applies specific functions on it in order to extract important information. Moreover, evaluation metrics such as accuracy, specificity, and sensitivity are reviewed in this

chapter. Also, this chapter introduces brain anatomy, its architecture, and the main types of brain tumors, which are benign and malignant. Furthermore, this chapter reviews the main modalities of brain tumor imaging such as MRI, CT, and (PET) scans. Finally, the chapter contained main datasets that are available publicly on the web.

2.2 Brain Anatomy

The brain forms the most complicated organs in the human body. It is made up of around 100 billion nerves that interact in billions of synapses to communicate. This spongy mass of fat and protein, which averages three pounds, is made up of two major types of cells glia and neurons that comprise many billions of each. Neurons are known for their axons and dendrites, which are branch-like projections that collect and transmit electrochemical impulses. Glial cells come in a variety of shapes and sizes, and they protect neurons and keep the brain healthy [34]. The brain is responsible for the main functions such as thinking, breathing, sleeping, and remembering. The brain's functions are similar to a council of experts. Although all of the brain's sections operate together, each one has its own unique characteristics. The cerebrum, which makes about 85 percent of the brain's weight, is the largest component of the organ. The cerebral cortex is distinguished by its severely wrinkled outer surface. The cerebrum is what makes the human brain and thus humans so powerful [35]. Elephants, dolphins, and whales have larger brains than humans, yet humans have the most developed cerebrum. The brain is made up of a variety of specialized sections that collaborate, these sections are illustrated on the left side of Figure 2.1 and as follows [34]:

- The cortex is the brain's outermost layer, where thinking and voluntary activities start.

- The brain stem is located between the spinal cord and the remaining portion of the brain. This part regulates two fundamental processes: breathing and sleeping.
- The basal ganglia are a group of structures in the brain's core. Messages between several brain areas are coordinated by the basal ganglia.
- The cerebellum is located at the brain's base and back. The cerebellum is responsible of balance and coordination.

The brain also includes four lobes as shown on right side of the figure and are explained as follows [36]:

- Problem solving, judgment, and motor performance are all controlled by the frontal lobes.
- Sensation, penmanship, and bodily posture are all controlled by the parietal lobes.
- Memory and hearing are both aided by the temporal lobes.
- The visual processing system of the brain is housed in the occipital lobes.

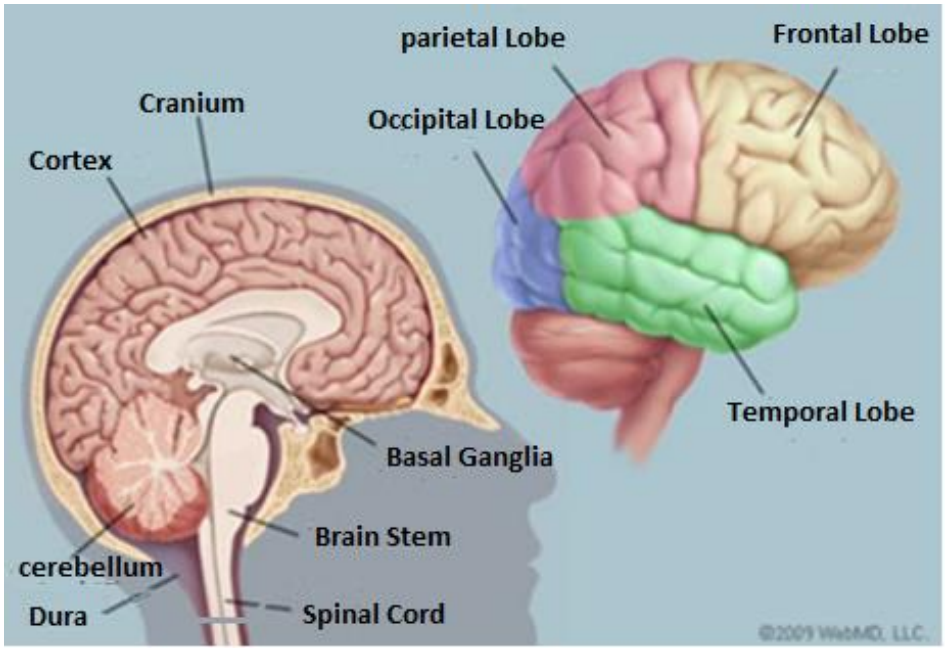

Figure 2. 1 Anatomy of the brain [34]

2.3 Brain Tumor

A brain tumor is an uncontrolled growth of brain cells. There are many distinct types of brain tumors. Some benign (noncancerous) brain tumors are different from cancerous ones (malignant). Brain tumors may originate from the brain (primary brain tumors) or from another part of the body and spread to the brain (metastatic brain tumors). A brain tumor can develop at many different rates [37]. According to a brain tumor's development rate and location, it can have an impact on how the neurological system works [38]. Figure 2.2 shows different types of brain tumors.

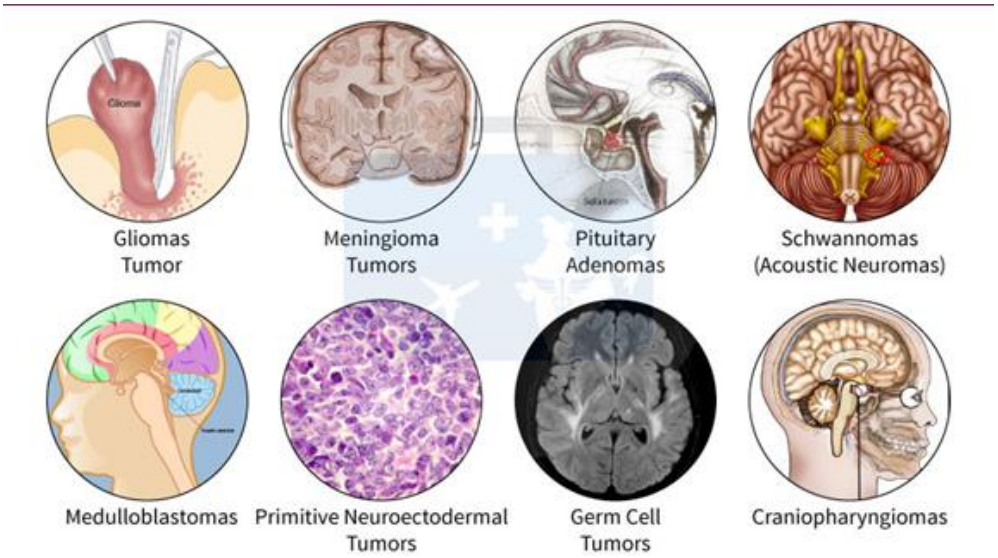

Figure 2. 2 Types of brain tumors [39]

Different types of tumors that grow in the brain region could be classified into primary and secondary tumors. Primary tumors refer to tumors in the early stages, while a secondary refer to advance stages that are spreading to additional brain cells [40]. Due to the human skull is a hard and volume-limited body, any unexpected growth may have an impact on human functions. The primary type represents around 70% of all brain tumors, while the secondary tumor represents the remaining 30%. This categorization is based on the origin of the tumor, with

primary tumors being those that begin in the brain. Secondary tumors, on the other hand, start in another region of the body and subsequently spread to the brain, and the majority of them are malignant [41].

2.3.1 Types of Benign Brain Tumors

There are different types of benign brain tumors that are introduced some of them underneath:

Chordomas: They are slow-growing benign tumors that are most frequently affect adults between the ages of 50 and 60 [42]. The base of the skull and the lower section of the spine are the most typical sites for them. Even though Chordomas are benign tumors, they have the ability to invade nearby neural tissue and impose pressure on the local brain tissue. As only 0.2% of primary brain tumors, these tumors are incredibly uncommon.

Craniopharyngiomas: They are often benign tumors that are difficult to remove due to their proximity to important brain regions. Therefore, they require hormone replacement therapy since they develop from a part of the pituitary gland. These kinds of tumors are slow-growing that don't spread to other areas of the brain or body [43]. However, they could expand and push on adjacent brain structures such as the pituitary gland, hypothalamus, optic chiasm, optic nerves, and fluid-filled areas. This might affect the growth of the human, eyesight, and the production of certain hormones. Craniopharyngiomas are more common in children and teenagers [44].

Meningiomas: The most common type of primary brain tumor, this tumor begins in the brain or spinal cord. On the other hand, low-grade meningiomas are extremely rare. [45]. Based on tumor features, meningiomas are classified into three categories. There are numerous subtypes of meningiomas in each grade. Molecular testing is used to discover subtypes that are linked to illness features and location.

Pituitary adenomas: Pituitary adenomas are usually slow-growing and benign, meaning they aren't cancerous and don't spread to other regions of the body [46]. They can, however, impose pressure on adjacent tissues, such as the nerves that connect the eyes to the brain, and produce discomfort as they become larger. The pituitary gland is a small gland attached to the base of the brain, about the size of a pea. It can be found in the sphenoid sinus and behind the nose. Pituitary adenomas are unknown in their specific cause. However, some have been related to change in deoxyribonucleic acid (DNA), the material that makes up genes and is found within cells [47]. These modifications cause aberrant pituitary cells to develop out of control, resulting in a tumor. The alterations can be passed down the generations, but they usually occur on their own at some point throughout a person's life. Adenomas are the most prevalent illness of the pituitary gland. Although they can be identified in youth, they primarily affect people in their 30s and 40s. The majority of these tumors are treatable with success. The general symptoms for these tumors could be headaches, problems in vision, vomiting, change in the sense of smell, change in the monthly periods for the women, and others.

2.3.2 Types of Malignant Brain Tumors

Three main types of malignant brain tumors are explained as follow:

Gliomas: It is the most common kind of malignant brain tumor in adults that account for about 78% of all malignant brain tumors. Astrocytes, ependymal cells, and oligodendroglial are such types of these tumors, [37]:

Astrocytomas: A tumor known as an astrocytoma can grow in either the brain or the spinal cord. The astrocytes, which support nerve cells, are where astrocytoma begins. Astrocytomas can affect people of any age, but they are more common in adults, especially middle-aged males. Depending on where the tumor is located, different astrocytoma signs and symptoms may be present. The symptoms of brain astrocytomas can include nausea, headaches, and seizures

[48]. In the area where the tumor is growing, astrocytomas in the spinal cord may cause paralysis and impairment. An astrocytoma can either be a slow-growing tumor or a malignancy that spreads swiftly[49].

Ependymomas: They are malignant tumors that can develop in the brain or any portion of the spine, including the neck, upper and lower back. They start out as ependymal cells in the center of a spinal cord and ventricles, which are fluid-filled regions in your brain. Ependymomas, unlike other types of cancer, seldom spread to other sections of the body. They can, however, spread to multiple areas of your brain or spine. These tumors are more likely to occur in children after treatment. Because most ependymomas begin tiny and expand slowly over time, it is difficult to notice any symptoms. These symptoms vary based on the location of the tumors. If the tumor is in the brain, the symptoms are headaches, nauseousness, and the patient could not be in balance or lose some vision. While the symptoms are painless in the neck or back, the patient has weakness in the legs or arms when the tumors are in the spine [50]. There are four types of cancer, depending on where it starts and how quickly it spreads.

Grade I: these normally appear around a brain ventricle and expand slowly. Adults and elderly men are the most commonly affected [51].

Grade II: this is the most frequent kind of ependymoma, and it mainly develops in the brain.

Grade III: these ependymomas nearly usually occur in the brain or skull, and they grow more quickly than other types of ependymomas [52].

The majority of ependymomas in children develop towards the base of the brain. The majority of people over the age of 12 are affected by spinal tumors.

Glioblastoma multiform (GBM): It is the most invasive type of glial tumor; it develops quickly, spreads to other parts of the body, and has a terrible

prognosis. It can be made up of a variety of cells, including astrocytes and oligodendrocytes. GBM is more common in men than in women, and it affects persons between the ages of 50 and 70 [53].

2.4 Brain Tumor Imaging Modalities

Detection brain tumours mainly depends on medical imaging as this technique display in depth different texture features of different tissues without a need to do a surgery. Therefore, doctors cannot detect these tumours precisely without medical imaging. Different techniques are used to diagnose brain tissues such as magnetic resonance image (MRI), computed tomography (CT) scan, positron emission tomography (PET) scan, and X-ray [54].

2.4.1 Magnetic Resonance Imaging (MRI)

The interior organs of the human body can be visualized with this more effective and potent method, which uses a magnetic field and radio waves. The high resolution afforded by this approach results in images that provide useful information regarding the anatomy of the brain tissues. As a result, the research community employs MRI technology to suggest several methods for precisely determining the location and severity of brain tumors automatically and without the need for human intervention [55]. Additionally, the MRI medical imaging technique accurately and clearly depicts the shape of the brain in 2D and 3D [56]. Among the different imaging techniques, MRI technique is the more powerful one. An internal organ of a human body is imaged using magnetic resonance imaging (MRI). It is a non-invasive technology that helps medical professionals identify abnormalities in internal body structures like bone and soft tissues. The MRI imaging technology, in contrast to X-ray, does not use hazardous radiation. The hydrogen atoms in the human body are arranged when radio frequency (RF) waves are applied to it. The pictures may be obtained with varying intensities using the MRI technology by adjusting the imaging parameters related to longitudinal relaxation time (T1) and transverse relaxation

time (T2). The structure of the brain, chest, belly, and pelvis may be determined via MRI imaging. It also aids doctors in the diagnosis of numerous disorders. It is the most common tool for detecting white matter disorders that cannot be detected by CT imaging is MRI. The T1 and T2 relaxation durations are used to determine the intensity and contrast of MRI images. Figure 2.3 shows the MRI machine.

The following are some of benefits of MRI technique:

1. The MRI method provides excellent soft tissue imaging.
2. MRI imaging offers a high resolution.
3. The signal-to-noise ratio is high.

The only drawback is that imaging with an MRI takes longer than with a CT. [57].

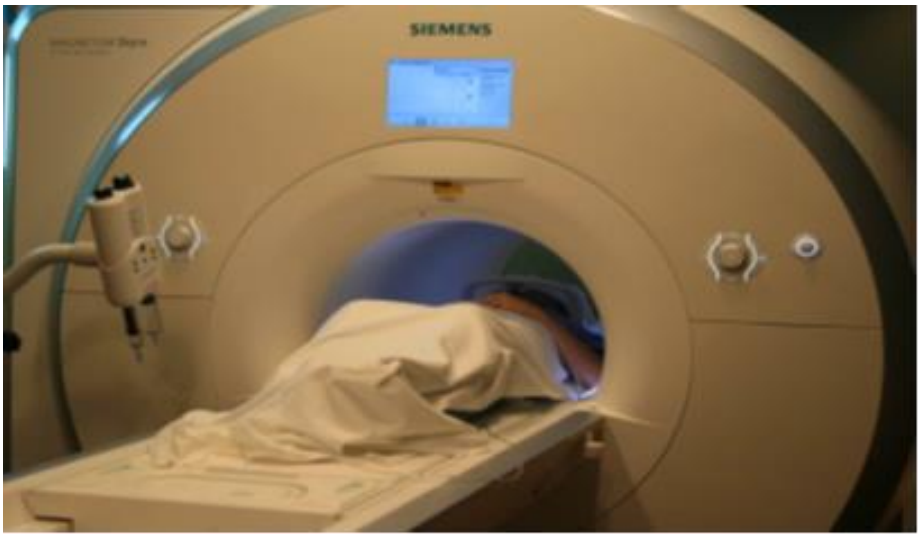

Figure 2. 3 MRI machine [57]

Even for experts, identifying different shapes for brain tumors and comparing their tissues to nearby healthy cells may not be an easy process. As a result, diagnosis based on human vision is difficult and time-consuming. Additionally, human mistake may occur and result in a missed diagnosis, which results in the erroneous course of action and response. On the other hand, a prompt and

appropriate intervention might save lives and raise the survival rate. Therefore, it is critical to use an automatic system that loads MRI medical images utilizing computerized technology in order to get quick results with little effort. With the aid of creative computer-aided diagnostics, this approach intends to assist radiologists and clinicians in identifying and categorizing brain tumors (CAD). For those working in radiology diagnostic and medical imaging, specifically for the classification of cancer, the CAD has become a popular topic [53].

2.4.2 Types of MRI Image

T1- weighted, T2- weighted, and fluid attenuated inversion recovery FLAIR are three forms of brain MR images that vary in the contrast of the brain tissues. These three types also have three orientations: axial, coronal, and sagittal. The axial direction of an MR image is from the neck to the head, while the coronal orientation is from the nose tip to the rear of the head and the sagittal orientation is from ear to ear [58]. Studying the meaning of time to echo (TE) and repetition time (TR) is important to understand different types of MRI images. TE is the difference in time between the delivery of an RF pulse and the reception of an echo signal. TR is the time it takes for two continuous pulses to be received in the same order [59]. A brain MRI provides a very detailed image. Figure 2.4 shows an example of a brain scan image.

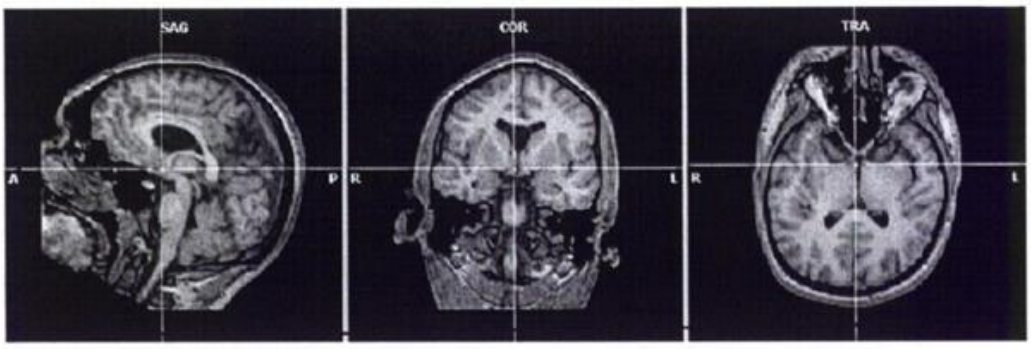

Figure 2. 4 the three types of MRI images sagittal, coronal and axial planes (from left to right) [60]

- **T1-weighted image:**

T1 is based on short TE and TR timings that are used to create this type of MRI image. The brightness of the image is determined by the T1 characteristics of tissue, therefore; the cerebrospinal fluid (CSF) appears dark in these MRI images. The contrast in a T1-weighted image is mostly determined by changing in T1 timings across tissues such as water and fat [61]. Figure 2.5 presents the T1-weighted image.

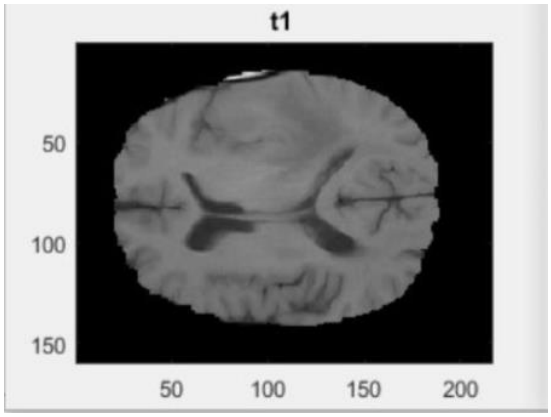

Figure 2. 5 T1-weighted image [62]

- **T2-weighted image:**

In contrast, T2-weighted images are generated with longer TE and TR than T1-weighted images, and the CSF area appears brighter. The contrast in a T2-weighted image is mostly determined by changing in T2 timings across tissues such as water and fat. The TE time adjusts the amount of T2 decay that may occur before the signal is received [61]. Figure 2.6 presents the T2-weighted image.

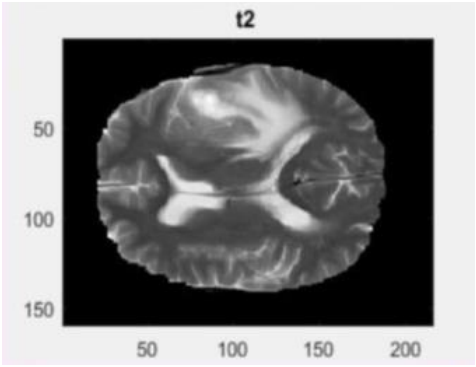

Figure 2. 6 T2-Weighted Image [62]

- **Fluid Attenuated Inversion Recovery (FLAIR):**

The third type of MRI imaging is FLAIR, which has much longer TE and TR periods compared with other types. In this type, the abnormalities stay bright while normal CSF fluid is attenuated and darkened. Abnormalities and CSF are discriminated against in this sort of imaging as these features are particularly sensitive to disease. The tiny hyperintense lesion is better detected by FLAIR [62]. Figure 2.7 presents the FLAIR image.

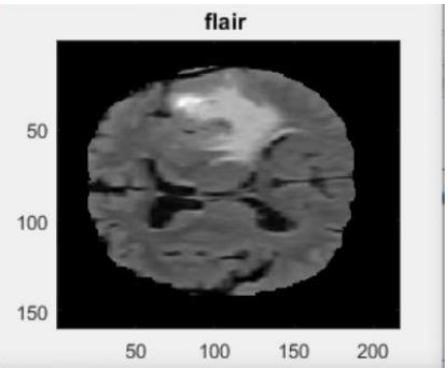

Figure 2. 7 FLAIR image [62]

2.4.3 Other Modalities

- **Computed Tomography (CT):**

Another type of brain tumors imaging is computed tomography (CT) that employs an X-ray and a large number of detectors to collect numerous exposures. When the instrument revolves around the patient and for different angles, the data from the detectors, which is essentially a body density map, is reconstructed into an image that may be altered in any plane. The development of CT in the 1970s marked the beginning of sophisticated cross-sectional imaging. Diagnostic investigation for many clinical diseases has changed as a result of these cross-sectional pictures, and demand for imaging continues to increase inexorably [63].

Comparing with MRI imaging technique, the CT delivers less information than an MRI. The functional and structural state of clinically significant symptoms of disease was evaluated using the CT scan. CT is inferior to MRI in

terms of the use of ionizing radiation and the ability to characterize soft tissues like the brain. A CT scan may provide more thorough imaging of the skeletal elements surrounding a brain tumor, such as the skull and spine [64].

- **Positron Emission Tomography (PET):**

The other type of imaging modality is a PET scan or named PET imaging, which is a nuclear medicine imaging technique. Radiotracers, which are tiny quantities of radioactive material, are used in nuclear medicine. This nuclear medicine is used by doctors to diagnose, assess, and treat a variety of diseases such as cancer, heart disease, neurological disorders, and others [65]. Nuclear medicine tests molecular activity, which allows detecting disease in its early stages. Also, It is able to detect whether a patient is responding to treatment or not. The radiologists carry out PET scan for the following purposes:

- Examine anomalies in the brain, such as tumors and memory problems.
- Determine the presence of cancer and/or do a diagnosis.
- Detect if cancer is spread in the patient.
- Draw how the brain and heart work properly.
- Evaluate the efficiency of the treatment.

Any type of radiation exposure has a tiny risk of tissue damage that might lead to cancer later on, but this amount of radiation is still in the standard PET scans. Over time, the radiotracer loses its radioactivity and is typical passes out of the patient's body naturally within a few hours. After the scan, drinking plenty of water can help to flush it out of the body [66].

- **X-ray:**

Another type of imaging modality is X-ray that can create images of the skull using invisible electromagnetic energy beams. X-rays are used to diagnose diseases such as cancers, tumors, and infections. X-rays employ external radiation to create images of the body and its organs. The X-ray move over plates that are similar to camera film, the solid structure such as bone appears as

white in the film. With developing computer technology, digital images can be used instead of camera films. The X-ray of the skull can reveal abnormalities in the bones caused by a tumor. Calcium deposits, which are prevalent in some kinds of brain tumors, can also be visible. However, ionizing radiation found in X-rays is the most well-known environmental risk factor for meningioma brain tumors, which are mostly benign. In the United States, it is found that frequent dental X-rays are the most popular sources of radiation [67]. They have the advantage of being cheaper than other modalities. They do not offer exact images, and extended exposure to X-rays may be harmful to tissues. In addition, they cannot be used to evaluate delicate tissues [66], [68].

2.5 Digital Image Processing

The definition of an image is a two-dimensional function (x, y), where x and y are the spatial coordinates. At any pair of coordinates (x, y), the amplitude is represented by the letter f, and is known as the intensity of the image at that point. If the values of x, y, and f of the image are finite, then the image is called a digital image. Therefore, this type of image can be expressed in an array, which contains rows and columns [69]. In other words, each coordinate of the image has a value and it is named element or pixel, which is the smallest part of the image and a common phrase for the element. There are three types of images, which are binary, grayscale, and colour [70].

- **Binary Image:** This type of image is one that consists of pixels that can have one of exactly two colors, usually black and white. This means that each pixel is stored as a single bit 0 or 1.
- **Grayscale Image:** This type of image is called grayscale and has a range of values starting from 0 until 255. It means that each pixel has a gray value and is located between 0 and 255.
- **Colour Image:** In the previous types of images, they have only 2-dimensional arrays and each pixel has only one value. In contrast, the colour image needs

three values for each pixel to represent a colour. The colour is formed by mixing at least three base colours, Red, Blue, and Green.

Digital image processing is a field that an image is processed by a computer starting from acquiring a digital image, pre-processing that image, extracting and describing features in a form suitable for a computer. In other words, digital image processing is concerned with the development of a computer system that is capable of doing image processing [71]. In medical imaging and diagnostic radiography, computer-aided diagnosis (CAD) has become a major study topic.

2.5.1 Computer-Aided Diagnosis (CAD)

The computer-aided diagnosis (CAD) is an application of pattern recognition that tries to assist doctors and radiologists in making an accurate diagnosis [61]. Computer-assisted diagnosis is based on utilizing a computer program to analyze and alter multidimensional medical images of a patient's anatomical structures to see diagnostic information. In MRI and CT imaging, CAD is employed for identification and segmentation of brain anatomical structures, breast and brain cancer tissues, and other bodily organs. This technology is significant in medicine to enhance a diagnostic precision for the radiologist to make final choices. It also saves processing time, allowing clinicians to promptly determine the appropriate therapy for a detected illness. However, automated identification and segmentation of diagnostic brain regions remains a difficult topic owing to the diversity of scanning techniques and patient orientation. However, medical image analysis and machine learning methods to develop a CAD system capable of assessing brain tumors is advantageous [72].

2.5.2 Classification of Brain Tumor Images

Medical image classification is essential for clinical treatment tasks. Classifying images into relevant groups based on their imaging modalities is becoming more vital in the development of a successful medical information management system. The ability to track and classify these images in order to

support a doctor's diagnosis for future inquiries could be a useful secondary diagnosis tool. As mentioned earlier, brain tumor disease has a significant mortality rate worldwide. As a result, researchers have focused a lot of their attention on automatically segmenting and diagnosing brain tumors. It is difficult to create a technology that can accurately identify the tumor without human assistance [73]. The block diagram of brain tumors classification is presented in Figure 2.8. The figure illustrates the key phases in image classification, which includes pre-processing and segmenting medical MRI images, extracting features, choosing the most important ones, and then using machine learning algorithms [74]. The following subsections depict each step's full description in detail.

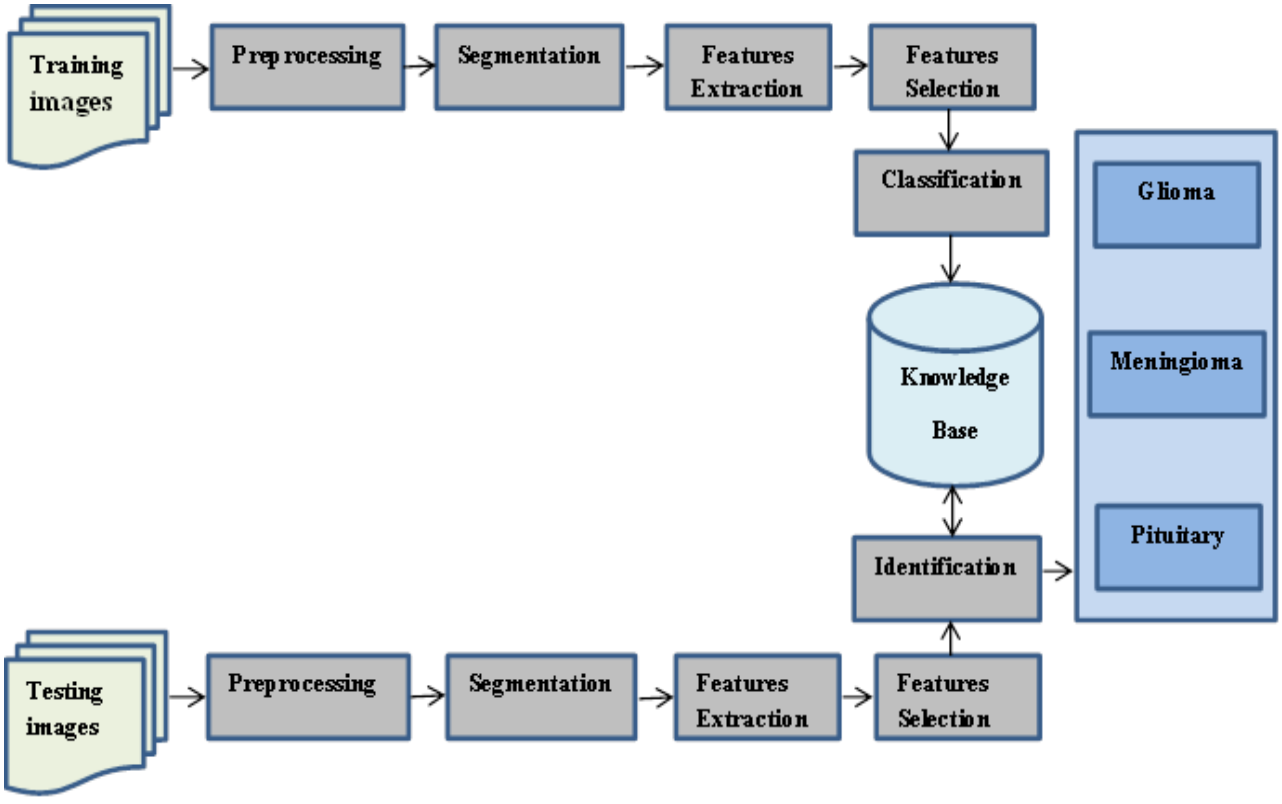

Figure 2. 8 The block diagram of brain tumors classification [74]

2.5.2.1 Data Acquisition

Imaging modalities include X-rays, computed tomography (CT), and magnetic resonance imaging (MRI). And positron emission tomography (PET), are further types of imaging. A sample of an image modality for a brain tumor is shown in Figure 2.9. The X-ray emits a high degree of dangerous radiation that might cause cancer or skin disorders. PET displays the functionality of certain sections of the human body rather than a clear image of these organs; yet, it works by detecting radiation emitted by a radiotracer and should be administered into the organ accordingly [75]. In contrast, MRI technology utilizes powerful magnets to produce a strong magnetic field in order to display an organ in more detail and from several perspectives. This tool has two modes of operation: the first mode uses a high field to create high-quality images, while the second mode uses a low field for straightforward diagnosis. The following data repositories have publicly accessible datasets [76], [77].

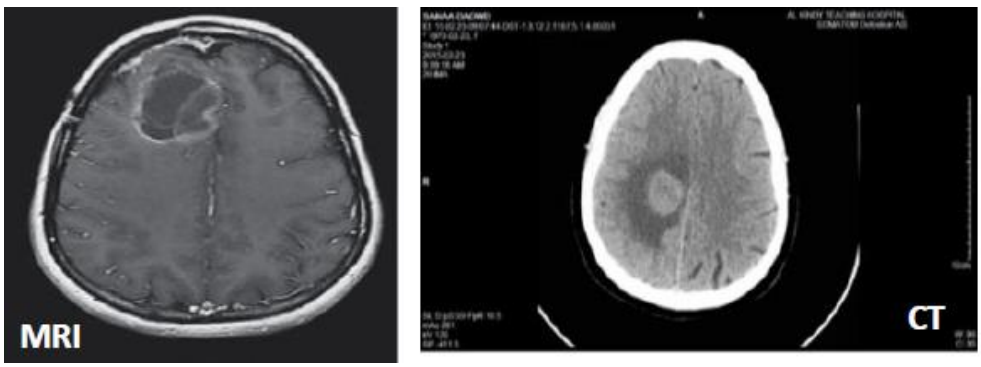

Figure 2. 9 Examples of MRI and CT images for brain tumor [78]

2.5.2.2 Pre-processing

After data acquisition, a preprocessing is essential to prepare data for the next steps of segmentation and applying machine learning algorithms. This stage includes removing artifacts, modifying image resolution, and addressing contrast variations caused by differing capture devices and settings [79]. Artifacts are additional characteristics that are unrelated to the underlying image. Therefore, a

method is required for removing visual artifacts and variations in intensity that is effective. The tasks of pre-processing are to prepare the image for future processing, improve the image's quality and eliminate any noise present in the image. Different pre-processing approaches try to improve an image without changing its informational content [80]. In order to improve the quality of the image in preparation for the subsequent segmentation stage, any noise or labels, such as the time and date, are removed in this step [81]. This process is carried out using a variety of approaches, including as cropping, image resizing, histogram equalization, filtering, and image normalizing.

The aim of data preprocessing is to facilitate the training/testing process through scaling and converting the entire dataset. It is important step before applying training of the machine learning models [82].

2.5.2.3 Segmentation

The most critical step in image processing is segmentation. This method includes a step to extract the information necessary to determine if a region is infected or not. Multiple challenges, including imaging noise, poor contrast, loss borders, shifting intensities within tissues, and different tissue types, make it challenging to segment brain tumors [54]. The scholars such a [31], [83] divided segmentation into various methodologies (i.e., threshold-based, region-based, boundary-based, and pixel classification techniques). The former, a threshold-based method, makes the assumption that pixels are assigned to a class when they fall inside a certain range [84]. The region-based approach makes the assumption that adjacent pixels within a region share the same characteristics [85]. The third method assumes that the pixels' properties abruptly change from region to region in the boundary line [84]. The latter one is predicated on the idea that pixels are categorized based on feature space, where features may depend on local texture, color components, and gray levels [86]. A hybrid

strategy is one that is created by combining two or more of the preceding techniques [54].

- **Morphological Operation:**

Morphology is the study of forms and the derivation of boundary areas from brain tumor images. The morphological operation is the reordering of pixel values that acts on input element and image structures. Structuring components are characteristics that investigate a characteristic of interest. The fundamental actions are based on dilation and erosion; dilation process adds pixels to the border region, whereas erosion removes pixels from the object's boundary region. These operations are conducted in accordance with the structural components. Dilation selects the greatest value by comparing all pixel values in the vicinity of the input picture represented by the structuring element, whereas erosion selects the lowest value by doing the same comparison [87]. The erosion of *A* by *B* is as follows:

$$A\Theta B = \{a \in A | \, a + b \in A, b \in B\} \quad (2.1)$$

Where *A* represents the image with pixels *a*, and *B* represents the structuring element with elements *b*. And the Dilation of *A* by *B* is as follows

$$A \oplus B = \{c \in A | \, c = a + b, a \in A, b \in B\} \quad (2.2)$$

Where *A* represents the image with pixels *a*, *B* represents the structuring element with elements *b*, and *c* represents the new pixels in *A* after dilation.

- **Region of Interest (ROI):**

Region of interest is a segmentation approach in which pixels are assigned to specific regions based on their similarity. Adjacency spatial interactions between pixels are necessary for an appropriate basis for segmentation when using similarity criteria. The technique is started with distributing randomly a number of seed pixels in a region growing over the image. Afterward, pixels in the neighboring to the same region are appended if they meet the similarity criteria

based on intensity, statistical features, or colour. Figure 2.10 displays MRI and CT images after carrying out the segmentation process. The description of the method is illustrated in the following points:

- A candidate pixel's and a seed pixel's intensity differences must fall within a defined range.
- The difference between a candidate pixel and the interest region's running average intensity must fall within a predetermined range.
- The difference between candidate pixels of a specified local neighborhood and local neighborhood of the candidate pixels for the standard deviation in intensity has to or not override a certain threshold [88].

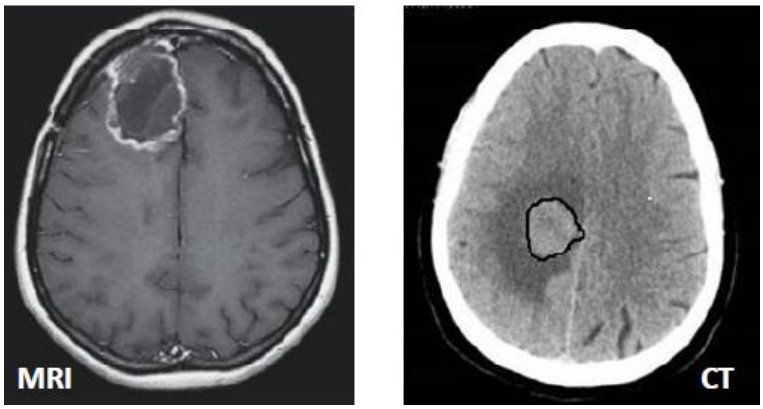

Figure 2. 10 MRI and CT images after carrying out the segmentation process [32]

- **Thresholding:**

This segmentation technique is sometimes referred to as a threshold-based approach, which is the simplest method and is frequently applied to two-dimensional pictures. They only assess the intensity of the current pixel and disregard its neighbors. Despite the fact that each pixel is segregated from its neighbors, these approaches are not considered segmentation techniques. Consequently, it cannot be ensured that the linked segments are actually acquired. The majority of pixel-based approaches rely primarily on measuring thresholds from an image's histogram. In these techniques, image objects are

identified by comparing the intensities of their pixels to one or more intensity thresholds. If the item can be distinguished from the image's backdrop using a single threshold, this is referred to as global thresholding. However, if there are more than two items, local thresholding should be used to segment the image. Automated threshold selection is mostly dependent on the image's histogram, which normally consists of two peaks that correspond to the pixels of the objects and the pixels of the background. The threshold must be selected so that these two peaks are clearly distinguished from one another. The most significant issue with thresholding is that the intensity information is analyzed, while the connections between the pixels are disregarded. There is no assurance that the thresholding will produce continuous pixels. In addition, it likely contains pixels that do not correspond to the intended region or the backdrop region. In most situations, threshold-based segmentation approaches are employed to segregate and eradicate the background of an MRI slice [89].

2.5.2.4 Feature Extraction

To improve the performance in classification of tumors based on medical imaging, the processes of dimension reduction and feature extraction are required. The objective of feature extraction is to find the smallest and most useful set of features (distinct patterns) to increase the performance of the classifier. Furthermore, in order to accomplish appropriate classification, features are extracted from the original image. It is a crucial element of classification because poorly picked features might impair classification performance [90]. Underneath some of these features, with their descriptions:

Cross correlation coefficient: cross correlation is a method for comparing two time series and determining objectively how they correspond to one another, in particular where the best match occurs. It may also identify any recurring patterns in the data. To determine how effectively one series may predict the values of another, a correlation coefficient is calculated. The sequences are then

shifted, and the procedure is repeated. The range of cross correlation is from (-1to +1) [91]. The formula is as follow:

$$\text{Cross Correlation Coefficient } \frac{\sum_{i=1}^{n}(x_i-\bar{x})(y_i-\bar{y})}{\sqrt{\sum_{i=1}^{n}(x_i-\bar{x})^2}} \quad (2.3)$$

Pearson correlation coefficient: it is commonly known as the Pearson coefficient. The two variables, labeled as *x* and *y*, are arranged on a scatter plot to determine the correlation. The Pearson coefficient is expressed numerically in the same manner as a linear regression correlation coefficient, ranging from (-1 to 1). The consequence of a complete positive association between two or more variables is a value of +1. Positive correlations suggest that the variables move in the same direction. In contrast, a number of -1 indicates an ideal negative connection. Negative correlations suggest that if one variable grows, the other variable falls; the variables are negatively connected. A zero shows no association [92]. The formula for Pearson Correlation Coefficient is as follow:

$$\text{Pearson Correlation Coefficient} = \frac{\sum_{i=1}^{n}(x_i-\bar{x})(y_i-\bar{y})}{\sqrt{\sum_{i=1}^{n}(x_i-\bar{x})^2}\sqrt{\sum_{i=1}^{n}(y-\bar{y})^2}} \quad (2.4)$$

Mean squared error (MSE): the MSE quantifies the error in statistical models. It measures the average squared deviation between observed and projected values. When there are no errors in a model, the MSE equals 0. As model inaccuracy grows, its value increases. The formula of the MSE is as follow:

$$\text{MSE} = \frac{\sum_{i=1}^{n}(y_i-x_i)^2}{n} \quad (2.5)$$

Where the variable y_i is the i^{th} of observed value, x_i is the corresponding predicted value, and n is the number of observations.

Mean: the Mean is a crucial mathematical and statistical concept. The mean is the average or most frequent value among a set of numbers. It is a measure of the central tendency of a probability distribution based on the median and the

mode. It is also known as the anticipated value. The mean can be computed by dividing the sum of all values in a set of numbers by the total number of numbers in the set [93]. The formula is as follow:

$$M = \frac{1}{m*n}\sum_{x=0}^{m-1}\sum_{y=0}^{n-1} f(x,y) \quad (2.6)$$

Standard deviation: It is a statistic that determines the square root of variance and measures how widely distributed a dataset is in relation to its mean. The standard deviation is calculated as the square root of variance by computing the deviation of each data point from the mean [94]. The Formula of standard deviation is as follow:

$$SD = \sqrt{\frac{\sum_{i=1}^{n}(x_i - y)^2}{n-1}} \quad (2.7)$$

Where x_i is the value of the i^{th} point in the data set, y is the mean value of the data set, and n is the number of data points in the data set.

Kurtosis (Kurt): the kurtosis is defined as a measure of a distribution's relative peakedness or flatness as compared to the normal distribution. Positive kurtosis shows that the distribution is relatively peaked. A flat distribution is indicated by a negative kurtosis [87], [95]. Kurtosis it denoted as Kurt(X) for the random variable X and it defined as:

$$K_{\text{urt}}(X) = \frac{\mu^4}{\sigma^4} \quad (2.8)$$

Where

μ: is the fourth central moment

σ: is the standard deviation

Energy: the energy is a physical system's ability to do work. The capital letter E is a typical sign for energy [96]. The joule, abbreviated J, is the standard unit. The formula for the energy is as follow:

$$E = m * c^2 \quad (2.9)$$

Where *E* denotes energy in joules, *m* denotes mass in kilograms, and *c* is the speed of light, which is around 2.99792 × 108 meters per second.

Coarseness (Cness): Coarseness is the textural analysis of an image as an indicator of roughness [87]. The formula for the coarseness is as follow:

$$\text{Coarseness} = \frac{1}{2^{m+n}} \sum_{x=0}^{m-1} \sum_{y=0}^{n-1} f(x,y) \quad (2.10)$$

Homogeneity: this phrase is used in statistics in its ordinary meaning, although it is most often associated with samples from diverse populations that are not necessarily similar. The populations are considered to be homogenous if they are identical, and the sample data are said to be homogeneous as well [97]. The formula for the Homogeneity is as follow:

$$\text{Homogeneity} = \sum_{x=0}^{m-1} \sum_{y=0}^{n-1} \frac{1}{1+(i-y)^2} . f(x,y) \quad (2.11)$$

Variance: Variance is a statistical evaluation of a data collection's value dispersion. Each number in the set is expressed in terms of its variance from the mean and, consequently, fromevery other number in the set. This symbol $\sigma 2$ is often used to represent variation [98]. The formula for the variance is as follow:

$$\sigma^2 = \frac{\sum(X-\mu)^2}{N} \quad (2.12)$$

Where σ is the population variance, X is the value of observation, μ is the population mean, and N is the number of values in the population.

Auto Correlation Predictor: It is defined as [99]:

$$\text{Auto Correlation Predictor} = \sum_{x=0}^{m-1} \sum_{y=0}^{n-1} (x * y) . f(x,y) \quad (2.13)$$

Dissimilarity: It is defined as [99]:

$$\text{Dissimilarity} = \sum_{x=0}^{m-1} \sum_{y=0}^{n-1} |x-y| . f(x,y) \quad (2.14)$$

Entropy: it is a measure of impurity or the randomness in the data being processed, the entropy is zero when the sample is homogeneous. A higher value for the entropy means more heterogeneous in the sample with more difficulty to

describe the data, until the value becomes 1, the sample becomes most heterogeneousness [100].

$$\text{Entropy} = \sum_i^M \sum_j^N S_{Img}(i,j) log(S_{Img}(i,j)) \quad (2.15)$$

Where $S_{Img}(i,j)$ is a segmented image

Contrast: the contrast describes the degree of color or grayscale distinction between various image characteristics in both analog and digital images. Images with a higher contrast level often exhibit more color or grayscale variance than images with a lower contrast level [101].

$$\text{Contrast} = \sum_i^M \sum_j^N |i-j|^2 S_{Img}(i,j)) \quad (2.16)$$

Correlation: the correlation is a statistical measure used to determine how closely two variables are related. The measure performs best when there is a linear relationship between the variables.

A scatterplot may be used to see how well the data fits together. We may analyze the connection between the variables and decide if they are correlated or not using a scatterplot [102]. The formula is as follow:

$$\text{Correlation} = \frac{\sum_i^M \sum_j^N (i-\mu_i)(j-\mu_j)}{\sigma_i \sigma_j} \quad (2.17)$$

The correlation coefficient measures the strength of the association between two variables. The coefficient may have values between -1 and 1, the value interpretations are as follows:

- The value -1 indicates a perfect negative correlation. In general, the variables move in opposing directions (i.e., when one variable increases, the other variable decreases).
- The value 0 indicates that the variables have no correlation with one another.

- The value 1 indicates a perfect connection exists. The variables often trend in the same direction (i.e., when one variable increases, the other variable also increases).

Inverse difference moment (IDM): high IDM values mean high local homogeneity of an image, while low IDM values indicate local inhomogeneity. The formula for IDM is as follow:

$$IDM = \sum_{i,j}^{M,N} \frac{S_{Img}(i,j)}{1+|i-j|} \quad (2.18)$$

Sum of square variance: The sum of squares equals the square of variation, where variation refers to the difference between each individual result and the mean. The distance between each data point and the line of best fit is squared and then totaled to produce the sum of squares. This value will be minimized by using the line of greatest fit [103]. The formula is as follow:

$$\text{Sum of square variance} = \sum_{i}^{M} \sum_{j}^{N} |i - \mu|^2 S_{Img}(i,j)) \quad (2.19)$$

There are different techniques to apply feature extraction such as principle component analysis (PCA), discrete wavelet transform (DWT), and gray-level co-occurrence matrix (GLCM). The method PCA is a statistical technique that reduces the number of features without losing its properties. After applying this approach, a huge amount of data is converted to a smaller set of uncorrelated features called principal components. This tool is used widely in various fields such as image processing, computer graphics, and face recognition [84].

- **Discrete Wavelet Transform (DWT)**

Through a wavelet transform, a signal can be decomposed into some basic functions, which are called wavelets. The wavelet is a well-known technique in image processing and computer vision, with applications including compression, detection, and identification, among others. Additionally, a wavelet is used as a multi-resolution technique to analyze an image's texture. Wavelet coefficients are used as feature vectors for classification. One technique used for extracting

features is the discrete wavelet transform (DWT). DWT is considered to be more efficient and less expensive in terms of computation. The DWT is capable of simultaneously locating a signal in time and frequency resolutions. DWT is regarded as the subsequent generation of discrete fourier transform (DFT). DWT decomposes the signal into many bands or frequencies; it employs DWT filters called the wavelet filter and scaling filter, both a high pass filter and a low pass filter comprise the wavelet filters. The DWT operates on many mother wavelet types, including Symlet, Daubechies, and Haar (Alfred Haar (1909) first introduced the Haar wavelet. It is the most basic wavelet. Haar wavelets are known as Haar transforms when they are used in a discrete manner. Haar wavelets are created in the same manner as the other wavelet transforms. The discrete input is divided into two half-length sub signals in Haar). Utilizing both the low pass filter (LPF), and high pass filter (HPF) concurrently, 2D-DWT is used in image processing to conduct operations across the rows of original pictures. The signal is then downsampled by a factor of 2 to produce a detailed portion (high frequency) and an approximating portion (low frequency). An additional procedure is done on each column of the image. At each decomposition level, four subbands are generated: an "approximation" subband (LL) and three "detail" subbands—vertical (LH), horizontal (HL), and diagonal detail (HH). See Figure 2.11 [104].

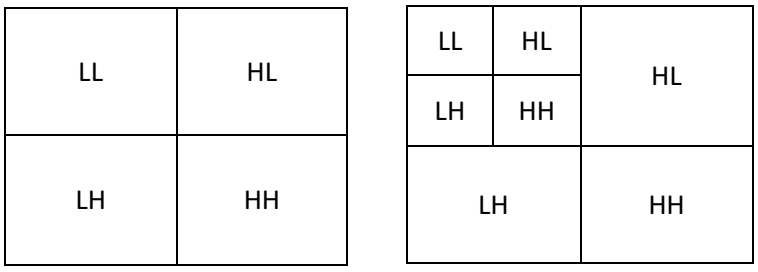

Figure 2. 11 Multilevel wavelet decomposition includes the following components: (a) specification for single-level components, and (b) specification for components with two levels [104]

- **Principle Component Analysis (PCA)**

Principal component analysis (PCA) is a regularly used feature extraction approach for dimensionality reduction. It is an unsupervised strategy for generating a new collection of characteristics known as principle components (PCs). Each PC is a linear combination of original variables with unique coefficients for each original variable. PCA modifies the original feature set such that all PCs are orthogonal to one another and eliminating duplicate information [105]. As discussed before, principal component analysis is a statistical technique that applies an orthogonal transformation to turn a collection of observations of potentially correlated variables into a set of values of linearly uncorrelated variables called principle components [106].

- **Gray-level Co-occurrence Matrix (GLCM)**

Texture is one of the most important identifying characteristics of an image. It is characterized by the geographical distribution of gray levels within a community. Co-occurrence matrix is the most prevalent mathematical representation of texture. In the gray level co-occurrence matrix (GLCM), the spatial association between pixels is examined using a statistical approach. GLCM is formed by computing the frequency with which a pixel with gray level value *i* appears horizontally next to a pixel with value *j*. The primary use of gray level co-occurrence matrix is to quantify the image's texture [107].

The GLCM contains information about the number of pairs of intensity values of pixels at various offset distances d in four different orientations ($\boldsymbol{\theta}$=0^o, 45^o, 90^o and 135^o) and has rows and columns that are equal to the number of gray levels in the image).

For an image *I* of size ($N \times N$), the GLCM is calculated using Eq. 2.20

$$\mathrm{GLCM}_{\theta}(i,j) = \sum_{x=1}^{N}\sum_{y=1}^{N}\begin{cases} 1, & if\ I(x,y) = i\ and\ I(x+\Delta_x, y+\Delta_y) = j \\ 0, & otherwise \end{cases} \quad (2.20)$$

Where Δ_x and Δ_y are the offset distances between the reference pixels of coordinates x, y, and its neighbors. i and j are the coordinates of GLCM [89].

2.5.2.5 Feature Selection

In machine learning, feature selection is a crucial data processing phase that must precede the application of the learning algorithm. Feature selection is a widely used method in machine learning to pick a subset of a dataset's characteristics in order to construct a robust model for learning. This approach assists researchers in gaining a better feature of the data by highlighting the significant characteristics and relationships of the data. There are three primary objectives of feature selection: enhancing the prediction performance of the predictors, more cost-effective and speed up predictors, and gaining a deeper knowledge of the underlying process of the data. Researchers exploring domains with hundreds to tens of thousands of variables or features often use the approach of feature selection. Therefore, several feature selection approaches are employed to choose important data and exclude unnecessary, duplicate, and noisy information from the data. There are several feature selection strategies, which are categorized into distinct technique types depending on how the selection algorithm and model construction are coupled. Filter technique, wrapper method, embedding method, and rough set theory (RST) are methods of feature selection [105]. In the next section, RST is explained as follow:

- **Rough Set Theory (RST)**

The rough set theory (RST) approach is a well-known algorithm for feature selection and reduction. Clearly, the RST approach applies a mathematical technique to uncover hidden patterns in data, as well as redundancies, dependencies, and dimensionality between data components. This approach was presented in 1982 by Z. Pawlak. Recent applications of RST to the investigation of limited and partial model information have proven very effective for machine intelligent systems. It plays a crucial role in advancing methods to artificial

intelligence, cognitive sciences, and machine learning. The rough set consists of mathematical techniques designed to address ambiguity and uncertainty. Lower and upper approximation sets are the exact sets related with the technique of rough sets. All items classed with unquestionably belong to the set denoted as the lower approximation set. The upper approximation set consists of all items that may belong to the set being characterized. RST is characterized by the following algebraic concepts: U referred to the universe, whereas the indiscernibility connection $R \subseteq U \times U$ represented partial understanding of U's characteristics. It is assumed, for the purpose of simplicity, that R is an equivalence relation. And X is contained inside U. Then, it is necessary to describe the set X in terms of R [108]. Rough set theory's fundamental concept may be separated into two pieces. Through the categorization of relational databases, the first step is to develop ideas and rules. The second step is to uncover knowledge by classifying the equivalence relation and the approximation aim. As a theory of data analysis and processing, the rough set theory provides a new mathematical instrument following probability theory for dealing with uncertain information [109].

2.5.2.6 Classification

There are three main categories for machine learning methods, supervised, unsupervised, and semi-supervised methods, see Figure 2.12. In supervised method, it can be classified into two phases, training and testing phase. In the first category, the data is labeled accurately based on the extracted features. In the second category, the model is first built and then used to specify the classes that are unlabeled in the testing phase [110]. In unsupervised methods, image pixels are classified automatically into different classes based on an algorithm without human intervention. In other words, in unsupervised methods, there is no need to train a model; the pixels are grouped together relying on common features. In semi-supervised learning method means using both supervised and

unsupervised methods to obtain high accuracy. Semi-supervised learning methods utilize both labeled and unlabeled data and these respective techniques have taken more attention in last decade [111]. Below are some of the supervised and unsupervised classifiers and their descriptions.

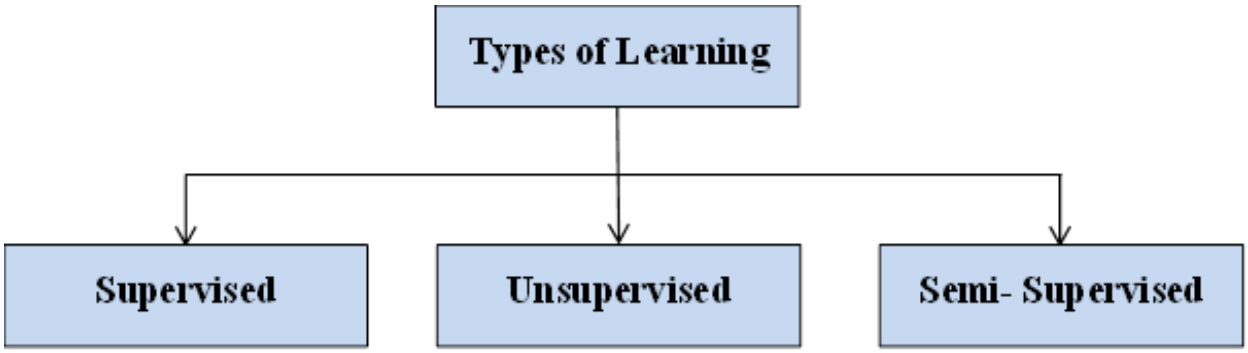

Figure 2. 12 Machine learning approaches

Training, testing, and cross validation: Commonly, in creating statistical and machine learning models, the dataset is divided into two sections: training and testing. The training phase is used to fit the model, or to estimate the model's unknown parameters. The accuracy of the model is then tested using the testing dataset. Utilizing the complete dataset for fitting, the model would be overfit to the data, which might result in inaccurate predictions for future situations. Therefore, reserving a part of the dataset and evaluating the effectiveness of the model before to deploying it in the field helps prevent against unanticipated problems that may result from overfitting. In addition, it is usual practice to reserve a part of the training set for validation. The validation set may be used to fine-tune the performance of the model, such as when selecting hyper-parameters. In reality, the training set may be subdivided into numerous sets, and the model may be trained via cross-validation [112]. The objective of constructing a machine learning model is not to achieve high performance just on the training data, but also on future cases the model has not encountered during training. In machine learning, it is standard practice to

divide training-test sets 70 percent - 30 percent or 80 percent - 20 percent. Typically, this holds true for relatively small datasets. When attempting to train a big deep neural network utilizing a dataset containing millions of instances, the training-test split may be 98 percent - 2 percent or 99 percent - 1 percent, according to [113].

Cross-validation: is often used to assess machine learning algorithms. It is used to indicate how well the model will predict future data. Cross-validation is accomplished by splitting a dataset and utilizing a portion to train the algorithm and the remaining data to test the method. The common cross validation strategies are:

- K-fold cross-validation. In this method, data are sorted at random and split into k folds (a common value of k is 10). One of the folds is utilized for testing, while the remaining folds are used for algorithm training. This circumstance occurs k times.
- Leave-one-out-cross validation (LOOCV). This methodology partitions the data using the k-fold method, where k equals the total number of observations in the dataset.
- Holdout. This method separates the data into two groups with a predefined ratio for training and testing [114].

- **Decision Tree (DT)**

Decision tree is a technique for data categorization and prediction analysis based on machine learning. It is a cross-disciplinary approach used in data mining, knowledge discovery, machine learning, and artificial intelligence challenges for prediction and classification. Decision learning algorithms generate decision trees from training data in order to solve classification and regression problems. Primarily, they are used as predictive models to estimate the value of a target variable using basic decision rules derived from the characteristics of the data. Typically, these rules take the form of if-then

expressions. The information gathered is then utilized to determine which characteristics to split on at each setup [115]. Figure 2.13 illustrates the general diagram of the decision tree.

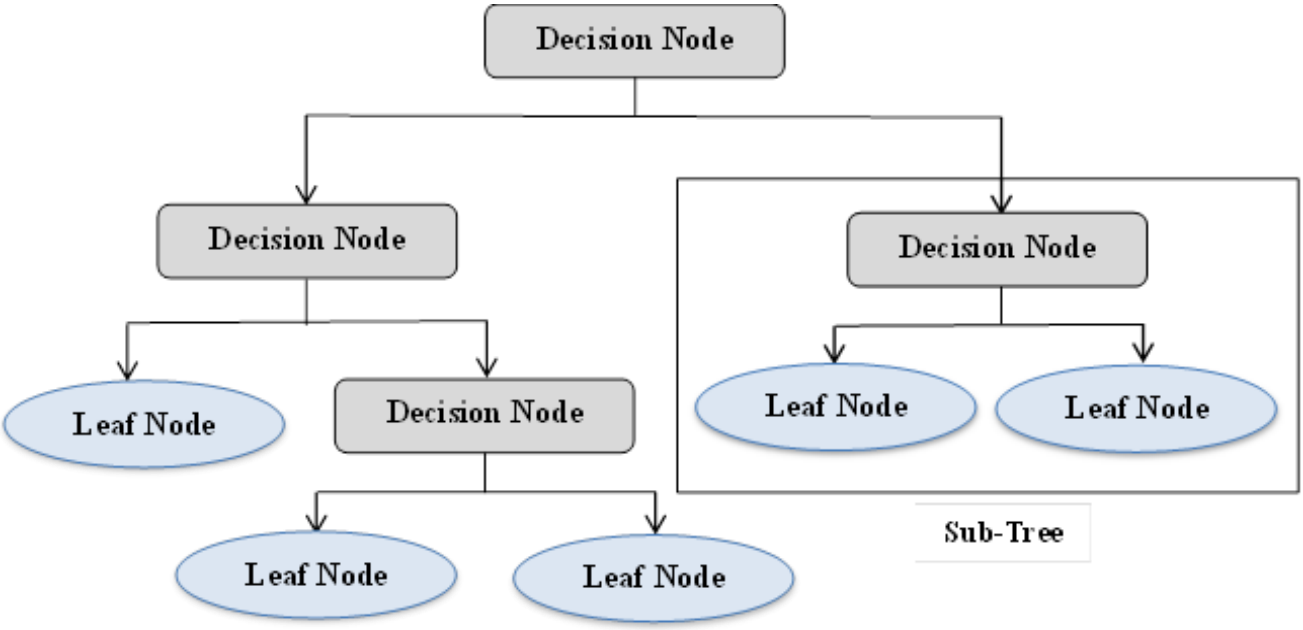

Figure 2. 13 Decision Tree [116]

- **Iterative Dichotomiser3 (ID3)**

Quinlan created decision tree algorithm in 1986. The ID3 algorithm was implemented serially and was based on Hunt's method. The ID3 tree was built in two phases: tree construction and tree pruning. During the tree-building step, each node's data is sorted to determine the optimum splitting attribute. The primary concepts behind the ID3 algorithm are as follows:

1. Each non-leaf node of a decision tree refers to an input attribute, whereas each arc corresponds to a potential value for that input property. A leaf node corresponds to the expected value of the output attribute when the input attributes are described by the path from the root to that leaf node.
2. In a "good" decision tree, each non-leaf node should correspond to the input attribute that is most informative about the attribute among all the input

attributes that have not yet been considered in the path from the root to that node. This is because we want to predict the output attribute with the fewest questions feasible on average.

3. Entropy is used to estimate how informative a specific input feature is regarding the output attribute for a portion of the training data. In communication systems, entropy quantifies unpredictability. As a result, ID3 employs the Entropy function and Information gain as metrics [115]. Figure 2.14 represents the ID3 diagram.

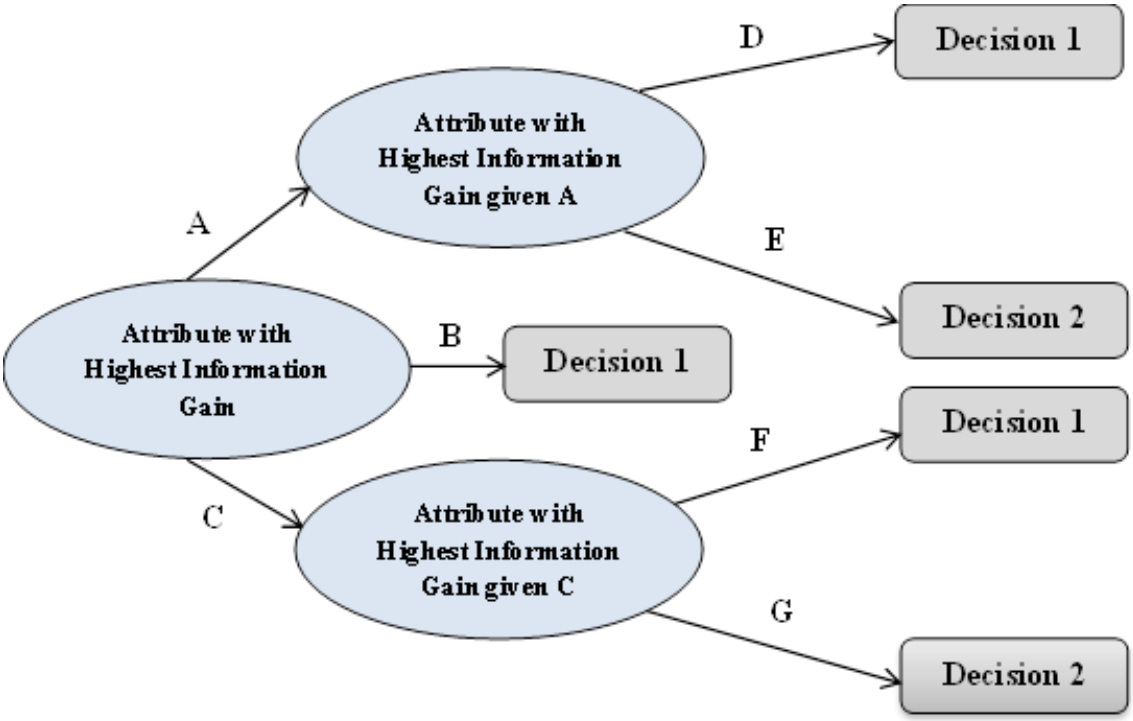

Figure 2. 14 ID3 diagram [117]

- **Random Forest (RF)**

Random forest is a collection of decision trees used to solve classification and regression issues. Frequently, decision trees suffer from overfitting. Combining numerous decision trees and their contributions to the final decision reduces this issue in RF. Decision tree (or classification tree) is a basic algorithm, represented by a tree-like network, in which each node performs the classification job into a specific number of groups based on a preset criteria.

This procedure divides the data into smaller groups in a hierarchical fashion. These criteria are evaluated during learning based on the knowledge gained after the split. For a given sample, the tree leaves indicate a probability distribution across the classes. Combining the distribution of every tree in the forest determines the final class, see Figure 2.15. All trees are trained using random selections of training samples or features, for example. The benefit of RF is the ability to examine the relevance of a feature, since the most essential characteristics are used most often in the initial layers. The less significant characteristics may then be eliminated. In recent years, random forest has been regularly used to the challenge of segmenting brain tumors as well as other segmentation tasks. The benefits of utilizing RF in medical image analysis include their effectiveness in dealing with high-dimensional feature spaces, their capacity to handle multi-label issues, and their generalizability [118].

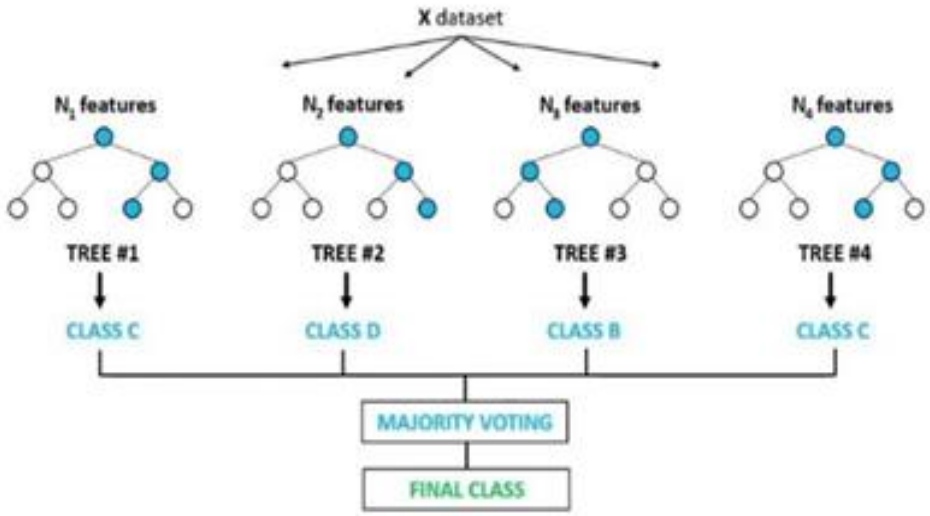

Figure 2. 15 Random Forest [119]

- **K-means Clustering**

Clustering is a concept that divides pixels or data points into clusters with related characteristics. There are two types of clustering (hard and soft clustering), the former of which determines if a sample or pixel is a member of a cluster or not and, as a result, prevents cluster overlap [120]. Contrarily, the latter indicates that the sample or pixel must belong to a cluster, and as a result, overlapping is feasible. Clustering involves discovering a structure or pattern in an unlabeled dataset collection. Clustering technique organizes a given dataset into K clusters such that data points within each cluster are comparable and data points from other clusters are distinct [121]. Commonly, K-means clustering is used to separate an area of interest from the remainder of a picture. K-means has been thoroughly evaluated for its accuracy in the segmentation of brain tumors [64]. K-means is unsupervised clustering that is simple but requires more processing time due to a large number of iterations. Choosing the right number of clusters (i.e., K) leads to accurate segmentation, otherwise, the results may be false [121]. In real-time clustering, the parameter K could be unknown and therefore the algorithm needs to be rerun several times by choosing different values for K. Moreover, in each iteration, the distance between data points and the nearest cluster is computed. Therefore, this adds more computations and time.

2.6 Evaluation Metrics

In any research project, it is an essential to evaluate a performance of a proposed machine learning model according on different metrics. For instance, evaluating a model based on one metric such as accuracy could lead to unreliable model when it compares with other metrics such as precision and confusion matrix. Therefore, evaluating a proposed system must rely on different metrics. In this section, various metrics will be discussed [58].

2.6.1 Confusion Matrix

The confusion matrix is a specialized table that presents a performance of a classifier. A confusion matrix is commonly called as the error matrix in the subject of machine learning. Based on the data type, an image region is considered to be positive or negative. A judgment for the observed result can also be correct (true) or incorrect (false). As a result, one of four options will be considered: true positive (TP), true negative (TN), false positive (FP), and false negative (FN). The diagonal of the confusion matrix is the correct decision [122]. The confusion matrix for two classification classes is shown in Table 2.1. The descriptions inside the table are explained as follows:

- True positive (TP): correctly classified as the class of interest
- True negative (TN): correctly classified as not the class of interest
- False positive (FP): incorrectly classified as the class of interest
- False negative (FN): incorrectly classified as not the class of interest

Table 2. 1 A confusion matrix

Predicted	**True**		
	Positive	True positive	False positive
	Negative	False negative	True negative

2.6.2 Area under the Curve (AUC)

AUC is the area under the ROC curve, and this metric indicates how well the probabilities from the positive classes are separated from the negative classes. By obtaining probabilities from a classifier, different values for thresholds can be used to draw sensitivity and 1- specificity on a curve and the result is ROC curve shown in Figure 2.16. The ROC curves can be used based on a threshold value, and the latter could be chosen depending on a classifier that is intended to

be used [123]. The threshold should not be as high as 0.5 for cancer classification applications. You would categorize a patient as 1 even if he had a 0.3 chance of getting cancer. In any other application for lowering credit card limits, the threshold should not be less than 0.5. Negative effects could have a negative impact on customer satisfaction limits.

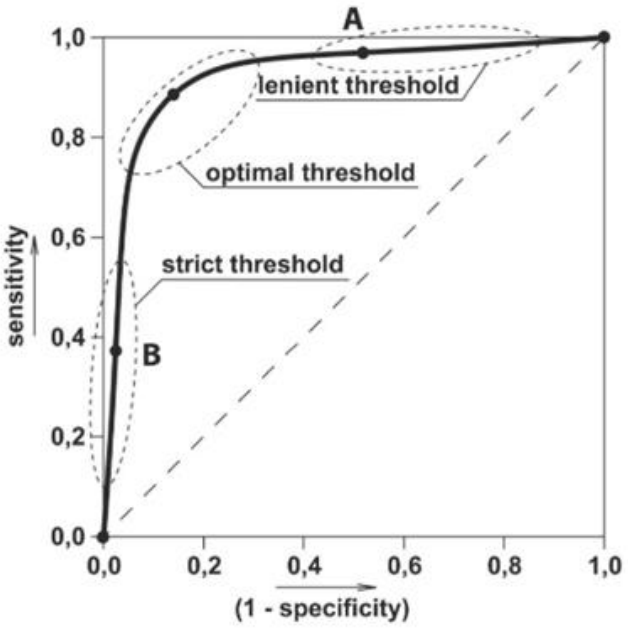

Figure 2. 16 The ROC curve [124]

2.6.3 Other Evaluation Metrics

Accuracy: The accuracy of a classifier's prediction is the measure of how accurate it is. It is a proportion of true positive and true negative predictions divided by the total number of forecasts is the accuracy. It specifies the classifier's overall performance capability [122]. The accuracy is defined as in Eq.2.21.

$$\text{Accuracy} = \frac{TP+TN}{TP+TN+FP+FN} \tag{2.21}$$

Precision: The precision is the proportion of true positive divided by true positive and false positive. When we want to be absolutely certain of our forecast, precision is a good statistic to use. Its equation is as follow:

$$\text{Precision} = \frac{TP}{TP+FP} \quad (2.22)$$

Recall or Sensitivity: The recall is the proportion of true positive divided by true positive and false negative. When we aim to collect as many positives as possible, recall is a good option for assessment statistics. Its equation is as follow:

$$\text{Recall} = \frac{TP}{TP+FN} \quad (2.23)$$

Specificity: The number of correct negative predictions (TN) divided by the total number of negatives yields the Specificity. The highest specificity is 1.0, while the lowest is 0.0. Its formula is presented in Eq. 2.24 [125].

$$\text{Specificity} = \frac{TN}{TN+FP} \quad (2.24)$$

Error Rate (ERR): The error rate (ERR) is derived by dividing the total number of inaccurate predictions by the total number of predictions in the dataset. The ideal error rate is zero, whereas the worst is one. Based on the confusion matrix, the formula of prediction error rate is shown in (Eq. 2.25).

$$error\ rate = 1 - accuracy \quad (2.25)$$

2.7 Datasets

There are various datasets regarding medical images, but the most popular datasets are the following:

2.7.1 Harvard Medical Dataset

This dataset is named the Harvard Medical School Database, which represents a big source for different MRI brain slice images. The images in this dataset are in different sizes. The dataset consists of normal and abnormal brain MRI

images. The abnormal brain MR images in the dataset consist of the following diseases: acute stroke, Alzheimer's disease, cerebral toxoplasmosis, carcinoma, multiple sclerosis, sub-acute stroke, chronic subdural hematoma, hypertensive encephalopathy, Lyme encephalopathy, metastatic bronchogenic disease, multiple embolic infarctions, fatal stroke, motor neuron disease, Pick's disease, and herpes encephalitis [126]. This dataset is web-based and gathers information from several sources for diverse classes of MRI, which is fetched from the whole brain atlas site [127].

2.7.2 Open Access Series of Imaging Studies (OASIS) Dataset

The OASIS means Open Access Series of Imaging Studies database which is an open-access database of neuroimaging [128]. This dataset contains extensive imaging data that can be used in neuroimaging, clinical, and psychological studies of normal aging and cognitive decline. This dataset is available and can be accessed by using a web-link [129]. The most recent version of the OASIS neuroimaging dataset is OASIS-3 that is publicly available to the research community in order to foster future discoveries in fundamental and clinical neuroscience. For normal aging and Alzheimer's disease, OASIS-3 is a longitudinal neuroimaging, clinical, and biomarker dataset. OASIS-3 is a collection of information and data for over 1000 members obtained over the course of 30 years by the Washington University in St. Louis (WUSTL) Knight Alzheimer Disease Research Center (ADRC) through a series of projects.

2.7.3 Figshare Dataset

The Figshare dataset is a larger and more difficult dataset for brain tumor detection. It includes 3064 brain MRI pictures from 233 people with three different forms of tumors: meningioma, glioma, and pituitary tumors. In particular, the Figshare database comprises 930 photos from the Pituitary class, 708 images from the Meningioma class, and 1426 samples from the Glioma tumor type. The matrix size of all photos in this dataset is 512 × 512 pixels. The

Figshare database is accessible via the Internet and includes images that are challenging in terms of textural complexity, color fluctuations, noise, capturing technologies, and bias field-effect, among other factors [76]. T1-weighted contrast-enhanced samples are also included in the collection since T1-weighted MRI images show a greater difference between the healthy and affected brain regions [128].

Chapter Three

Methodology

3.1 Introduction

As stated in chapter two, classification of brain tumor using MRI image is a crucial step in the diagnosis of a tumor in the brain. Therefore, many researchers have proposed several algorithms to identify the type and/or the grade of brain tumor. In fact, computers can separate various portions of an image using a great variety of techniques. Currently, several algorithms are utilized to extract abnormal regions and other malformations from medical images, these regions are referred to as regions of interest ROI.

This chapter aims to contribute to the medical image analysis domain, specifically to the field of brain tumor detection and segmentation in MR images. Two proposed methods are described:

- A hybrid feature extraction method based on discrete wavelet transform (DWT) and principal component analysis (PCA).
- An effective method for automatically segmenting brain tumors using the proposed optimized thresholded difference (OTD) and rough set theory (RST).

3.2 Representation of MR Images

MRI T2-w images are denoted as a two-dimensional matrix representation. Assuming a function g for the two independent variables m and n, the function of the image can be considered as $g(m, n)$. The function g is also known as the intensity. The independent variables m and n represents the row and column of pixels in an image, respectively. The function $g(m, n)$ in this notation represents the intensity of light for the pixel at the position defined by the row m and column n in an image.

Figure 3.1 presents the intensity convention which is the used representation in this research. Based on this notation, the MRI represented in the form of a matrix as follows:

$$g(m,n) = \begin{bmatrix} g(1,1) & \cdots & g(1,N) \\ \vdots & \ddots & \vdots \\ g(M,1) & \cdots & g(M,N) \end{bmatrix} \quad (3.1)$$

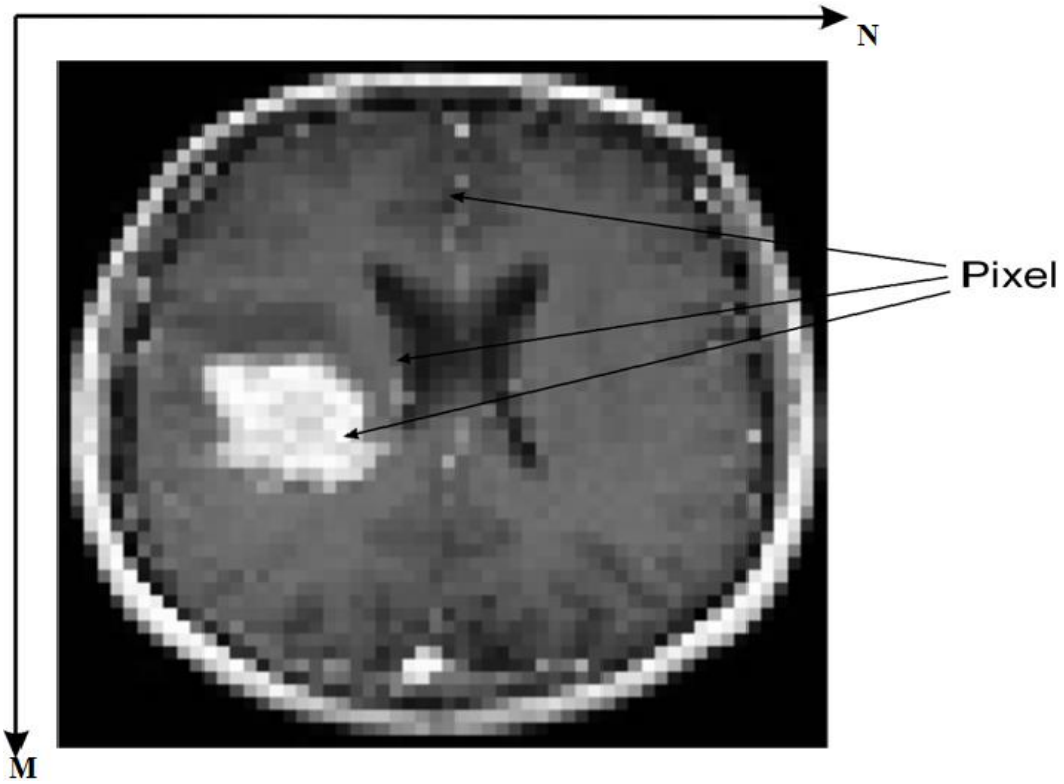

Figure 3. 1 A representation of MR image

In the above described image, the image consists of *M* rows and *N* columns; the numbers *M* and *N* correspond to the size of the image in pixels. Generally, the image size is described in pixels instead of distance like centimeters. The image that has a size of 256×256 pixels is an image that has 256×256 different intensity values within it.

In MRI T2-w images, the intensity values are affected by the image's representation. The image intensity in computers is a closed interval with a minimum and maximum value for the image intensity. In practice, the intensity range for an image is chosen based on the image processing goal. The brighter pixels in an image are often assigned a greater intensity value. White or bright

colors have higher intensity values, while dark pixels have lower intensity values.

3.3 Proposed method 1: Hybrid Feature Extraction Method Based on DWT and PCA

This chapter introduces the first proposed method of this dissertation. To extract image characteristics, the suggested approach used preprocessing to enhance and dedicate the region of interest (ROI) image. Then 3 levels of discrete wavelet transform (DWT) are applied. After that, the principle component analysis (PCA) is used to decrease the size of correlated features. In this model T2-w images with axial view have been utilized to identify brain anomalies. Wavelet transform is an effective method for extracting features from MR brain images because its multi-resolution analytic property enables image analysis at different resolution levels. On the other hand, the principal component analysis (PCA) is used to scale back the feature vector dimensions and to increase the discriminative power. PCA is attractive because it effectually decreases the dimensions of the data, thus reducing the cost of computing new data analysis. Finally, a random forest classifier (RF) with a selection of identification features was used. The approach consists of six stages:

1. Data Acquisition
2. Preprocessing including:
   - Resizing MR images.
   - Brain region segmentation
   - Apply k-means clustering.
3. Segmentation.
4. Transformation and Reduction (including applying 3L DWT and PCA).
5. Feature Extraction.

6. Random forest training, apply new MRI brains to the trained random forest and perform the prediction.

In Figure 3.2, the detailed processes of the proposed model are demonstrated.

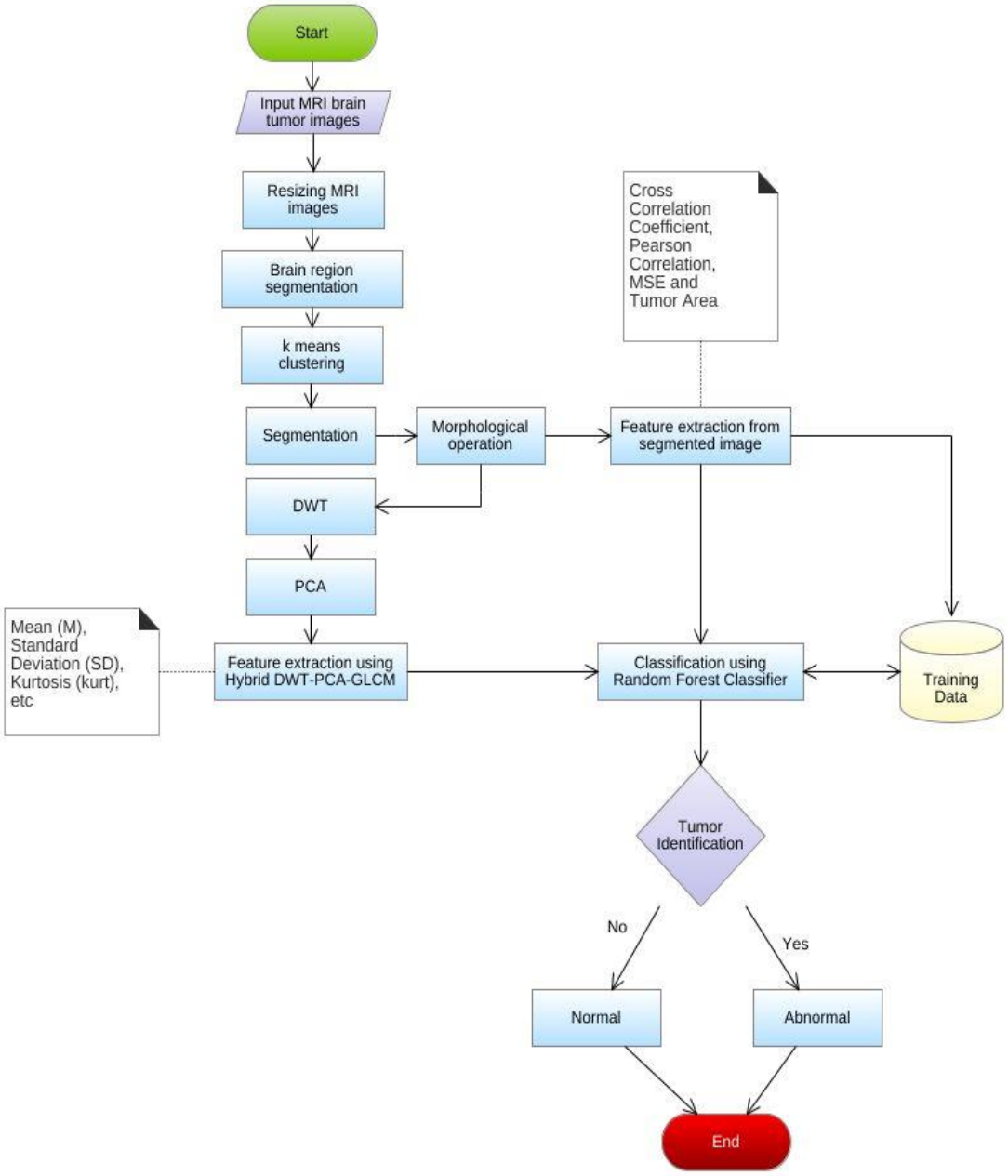

Figure 3. 2 The workflow of the proposed method

3.3.1 Data acquisition

The datasets consist of axial plane T2-weighted MRI brain images of resolution 256×256 in-plane. 181 images are retrieved from the Harvard Medical School dataset and the OASIS dataset. Since T2 images, compared to T1 modalities, are of greater contrast and better vision, we selected the T2 model.

3.3.2 Preprocessing

The most significant and difficult step in computer-aided segmentation is preprocessing. Every image must be preprocessed before applying any algorithm on it. Preprocessing is the most important step in tumor detection since it ensures that the segmentation algorithm works perfectly. As a result, image quality should be increased before the segmentation.

3.3.2.1 Resizing the Dimensions of MR images

The provided MRI brain slices are collected from different scanners with different spatial resolutions. To enable the utilization of the complete set disinterestedly, the dimensions of the magnetic resonance imaging are changed using the nearest neighbor interpolation approach which is probably the simplest image scaling method. Every output pixel is replaced by its nearest pixel in the input. In 2D, a pixel with coordinates (x, y) in the output image has coordinate $(x/\text{scale}\_x, y/\text{scale}\_y)$ in the input image. Since these coordinates do not always exist (if they have a decimal part), for that we will round the coordinates to the nearest integer, thus rounding to the nearest neighbor. As shown in Figure 3.3, the green pixel is approximated by its nearest neighbor, so that the width or height doesn't exceed 256 pixels while preserving the ratio of the image when changing its size.

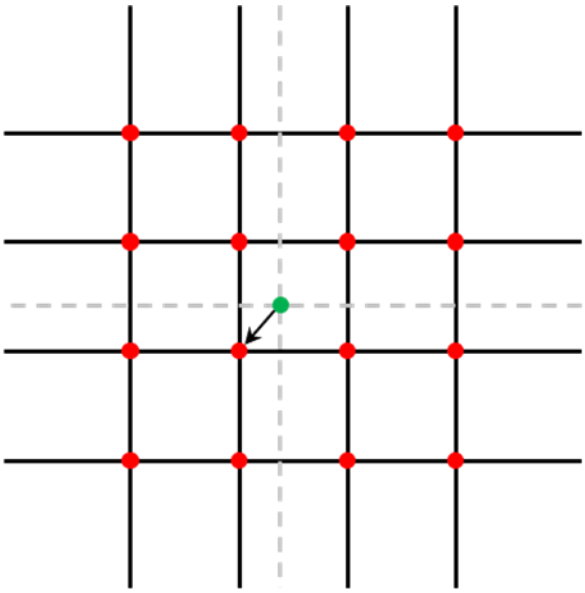

Figure 3. 3 Pixel rounding in nearest neighbor interpolation approach

3.3.2.2 Brain region segmentation

Brain region segmentation used to remove the bones of the skull and extract the brain region only to obtain a brain region that does not contain the bones of the skull, so as not to affect later in the process of tumor segmentation as shown in Figure 3.4. The proposed removal method consists of three levels:

- Converting the MRI to a grayscale image and applying the preprocessing operation.
- The second is the use of the threshold with the value = 80 on an MRI image that results in a binary image containing the bones of the skull and some areas affected by the process of applying the threshold. Then, a completed ring built, where the outer edges in the image are adopted after applying the threshold, which represents the edges of the skull resulting from the thresholding process and the generation of a closed ring depending on the values of these edges, which represents the skull ring.
- Third, the resulting skull ring adopted as a mask to apply to the original brain image. Where the areas corresponding to the extracted ring neglected, and

only the area confined in the original image left inside the extracted ring, which represents the brain region.

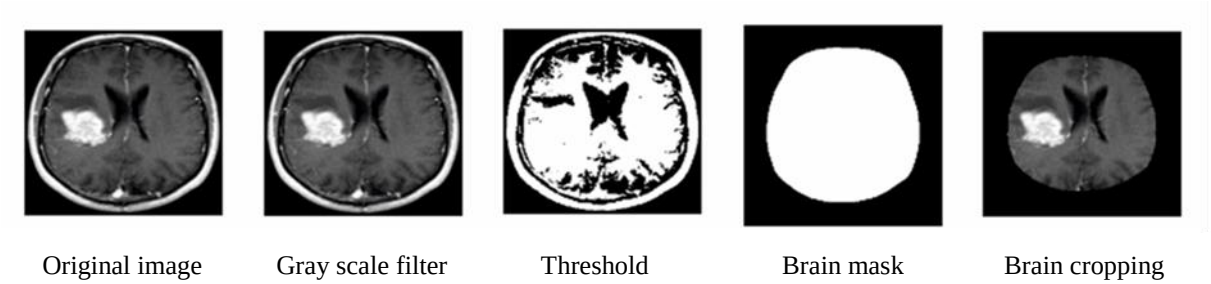

Figure 3. 4 Skull-removing steps

3.3.2.3 K-means clustering

The interest area is isolated from the background using K-means clustering approach. It divides a given set of data into *k* distinct clusters. The K-means algorithm is divided into two phases. In the first phase, it computes the *k* centroid, and in the second phase, it assigns each data point to the cluster with the closest centroid to it. The Euclidean distance is one of the most commonly used methods for determining the distance to the nearest centroid. Once the grouping is complete, it recalculates the new centroid of each cluster and, based on that centroid, calculates a new Euclidean distance between each center and each data point, and assigns the cluster points with the shortest Euclidean distance. The centroid of each cluster is the place at which the summation of distances from all objects in that cluster is smallest. So, over all clusters, K-means is an iterative algorithm that minimizes the sum of distances from each object to its cluster centroid.

Let us consider an image with resolution of x×y and the image has to be cluster into *k* number of cluster. Let $p(x, y)$ be an input pixels to be cluster and c_j be the cluster centers. The algorithm for k-means clustering is explained in the below steps:

Step 1 Initialize number of cluster k = 9 and center.

Step 2 For each pixel of an image, calculate the Euclidean distance d, between the center and each pixel of an image using the relation given below.

$$d = ||p(x, y) - c_j||^2 \quad (3.2)$$

Step 3 Assign all the pixels to the nearest center based on distance d.

Step 4 After all pixels have been assigned, recalculate new position of the center using the relation given below.

$$(c_j) = \frac{1}{k}\sum_{x=1}^{cj}\sum_{y=1}^{cj} p(x, y) \quad (3.3)$$

Step 5 Repeat the process until it satisfies the tolerance or error value.

Step 6 Reshape the cluster pixels into image.

3.3.3 Segmentation

Segmentation is a mechanism in which the MRI is broken into distinct regions. Let the entire area of the image be stated by A. The method of segmentation can be seen as a partition of A into n sub-regions such as A1, A2, and A3 … An. As the segmentation must be intact, some requirements must be fulfilled; that is, every pixel should be within the region, every point should be linked in some way within the regions, regions should be disjointed, etc.

Dilation and erosion are the essential operations used here. Dilation attaches the pixels to the boundary region, while erosion deletes the pixels from the object boundary region. Based on the structuring components also known as kernel (3×3), which specify the precise effect of the erosion and dilation on the input image, these operations were conducted by comparing all the values of pixels in the neighborhood of the input image defined by the structuring element, dilation selects the highest value, and during erosion, the rock bottom value is chosen by comparing all the pixel values in the input image region.

Figure 3.5 shows the ROI operations (thresholding, erosion and dilation). By making a binary mask, we define an ROI, which is a binary image of the same size as the image we want to process, with pixels representing the ROI set to 1 and all other pixels set to 0. The segmentation of the affected brain MRI regions is accomplished by two steps:

- Transformed the preprocessed brain MR image into a binary image with a cut-off threshold of 150 chosen in the initiative. Pixel values greater than 150 are mapped as white, and the others are marked as black.
- In the second phase, an erosion method of morphology was used to remove sporadic white pixels. Dilation anchors the segmented region. As a result, the tumor area remains without any abnormalities.

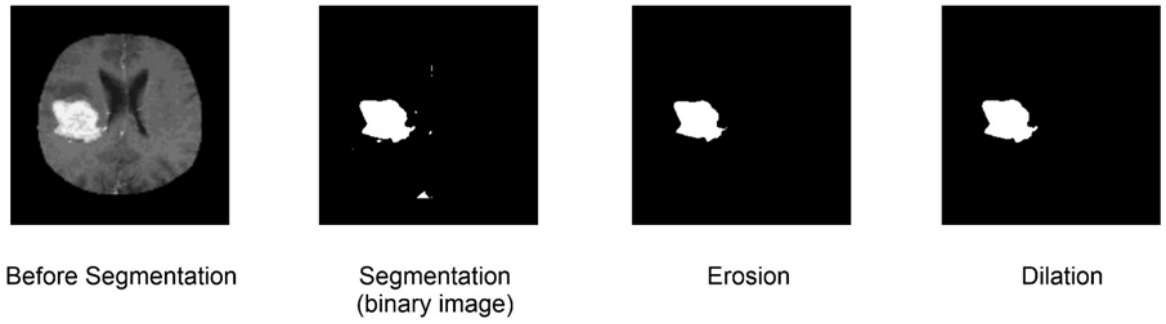

Figure 3. 5 ROI Segmentation

3.3.4 Transformation and Reduction

In this section, we used three levels of (DWT) for extracting wavelet coefficients, followed by (PCA) to reduce the feature vector dimensions and increase the discriminative ability.

3.3.4.1 Image Transformation

The DWT are added separately to every dimension in the case of two-dimension images. As a result, each scale has four sub-bands (LL, LH, HH, and HL). For the next two-dimension DWT, the sub-band LL is hired. The LL sub-

band is often considered the image's approximation component, while the detailed components of the image can be considered the LH, HL, and HH sub-bands. Therefore, to interpret the image detail, wavelets provide an easy hierarchical structure. Three-level decomposition of Haar wavelet was used in our proposed model.

Applying DWT to 2-D images is equivalent to processing the image with 2-D filters in each dimension. The filters separate the input image into four non-overlapping multiresolution sub bands: LL, LH, HL, and HH. The coarse-scale DWT coefficients are represented by the LL sub-band, while the fine-scale DWT coefficients are represented by the LH, HL, and HH sub-bands. The LL sub-band is further processed to generate the next coarser scale of wavelet coefficients until some final scale N is achieved. Figure 3.6 shows the wavelet decomposition when the scale N equals 3.

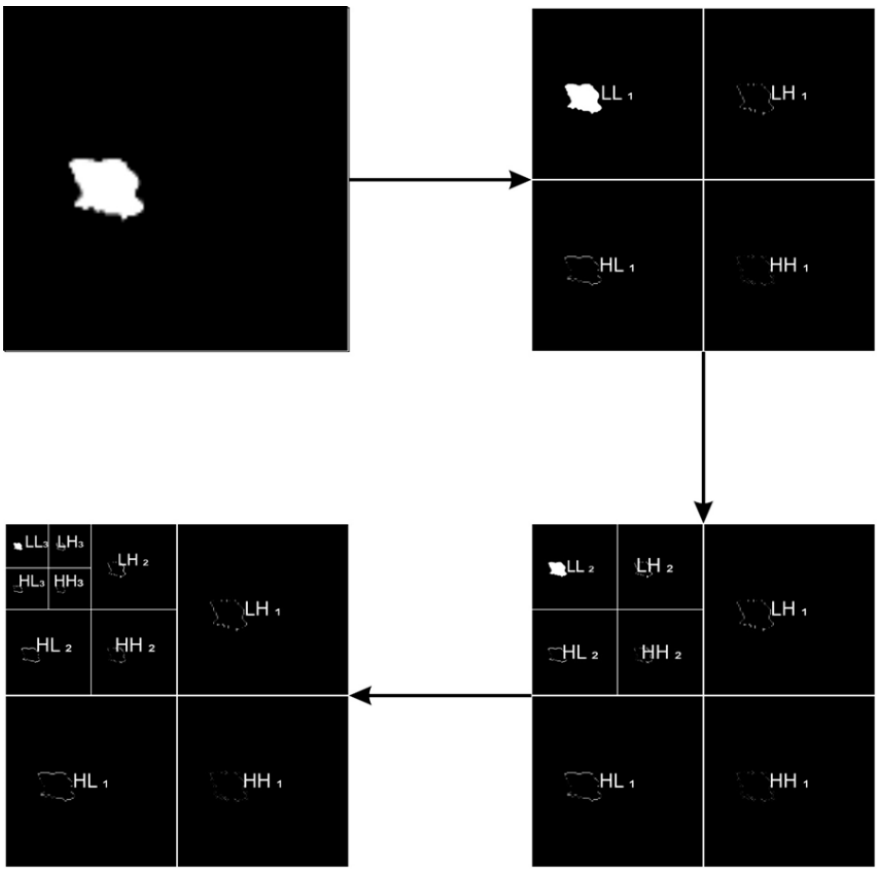

Figure 3. 6 The procedures of 3-level DWT

3.3.4.2 Principal Component Analysis (PCA)

PCA is an important method to scale down the dimension of a data set composed of an over-sized number of interrelated variables while preserving many of the variants. It is done by converting the data set into a completely new set of ordered variables aligned with their variances or significance.

PCA is a dimensionality reduction that identifies important relationships in our data, transforms the existing data based on these relationships, and then quantifies the importance of these relationships so we can keep the most important and drop the others. The PCA applied to the LL sub-band of the three-level wavelet decomposition of size 32×32. As showing in Figure 3.7 PCA implemented in the following procedure:

Step 1 Convert LL sub-bands of the three-level wavelet decomposition to 32×32 array.

Step 2 Compute the mean of the array.

Step 3 Subtract the mean from the array (data adjust).

Step 4 Calculate the Covariance Matrix.

Step 5 Calculate the Eigenvectors of the Covariance Matrix.

Step 6 Choosing components and formatting a feature vector (select only the first eigenvector).

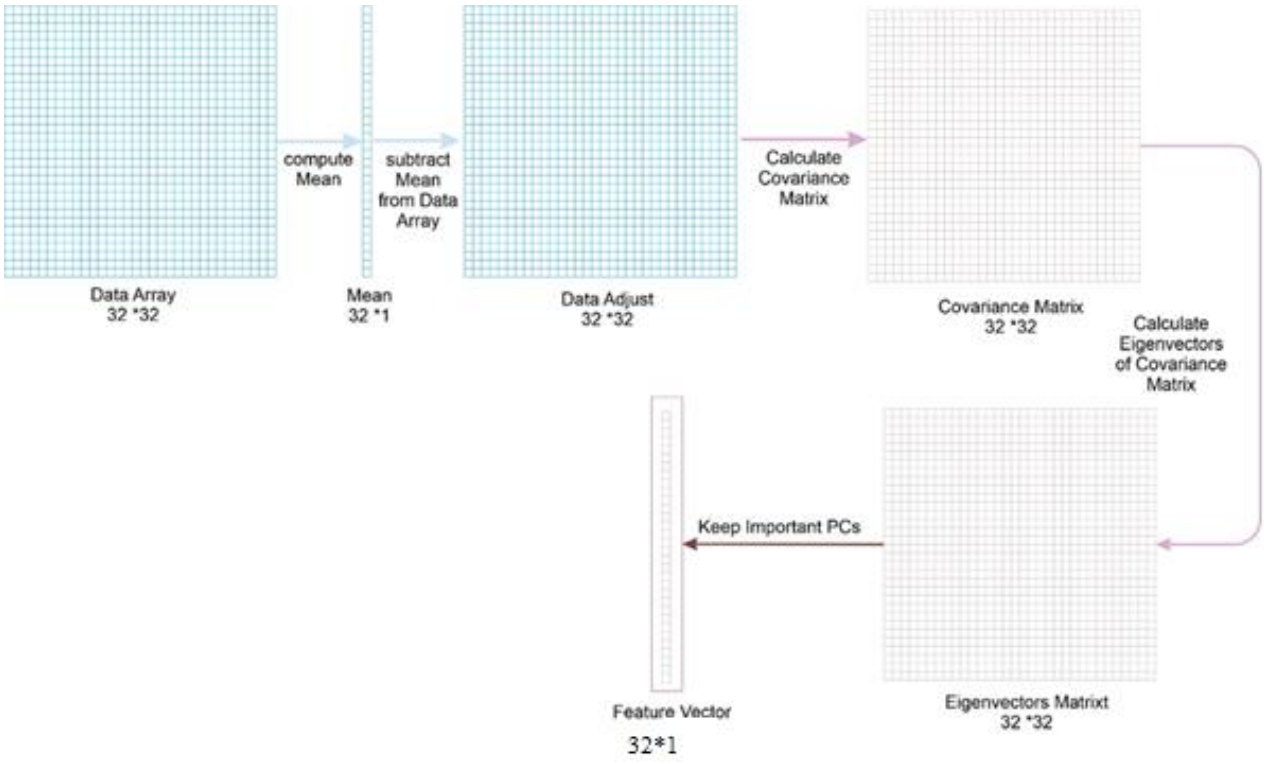

Figure 3. 7 PCA implementation procedures

3.3.5 Features Extraction

The analysis of texture effectively distinguishes natural and irregular tissues for human beholding and machine learning. It offers differences between normal and malignant tissues that cannot be observed by the human eye. It improves early diagnosis efficacy by selecting effective quantitative features.

In the initiative, statistical textural analysis features including cross-correlation coefficient, Pearson correlation, MSE, and tumor area are extracted from the segmented image intensities. In the next step, textural features are obtained from the PCA components acquired from the LL sub-bands of the first three-level wavelet decomposition.

3.3.5.1 Feature Extraction from the Segmented Image

In this method, four features (cross-correlation coefficient, Pearson correlation, MSE, and tumor area) are obtained from the segmented image. The textural features extracted are listed below:

- **Cross-Correlation Coefficient:** It is a measure of the similarity of two series as a function of their displacement from one another. The cross-correlation coefficients are less sensitive to variations in illumination than the MSE.

$$\text{Cross-Correlation Coefficient} = \frac{\sum_{i=1}^{n}(x_i - \bar{x})(y_i - \bar{y})}{\sqrt{\sum_{i=1}^{n}(x_i - \bar{x})^2}} \quad (3.4)$$

Where,

n: is sample size

x_i , y_i: are the individual sample points indexed with i

$\bar{x} = \frac{1}{n}\sum_{i=1}^{n} x_i$: (the sample mean); and analogously for $\bar{y}$

- **Pearson Correlation Coefficient:** is the product of the standard deviations of the two variables divided by their covariance [4].

$$\text{Pearson Correlation Coefficient} = \frac{\sum_{i=1}^{n}(x_i - \bar{x})(y_i - \bar{y})}{\sqrt{\sum_{i=1}^{n}(x_i - \bar{x})^2}\sqrt{\sum_{i=1}^{n}(y - \bar{y})^2}} \quad (3.5)$$

Where,

n: is sample size

x_i , y_i: are the individual sample points indexed with i

$\bar{x} = \frac{1}{n}\sum_{i=1}^{n} x_i$: (the sample mean); and analogously for $\bar{y}$

- **Mean Square Error (MSE):** It used by providing quantitative or similarity scores to compare two images and defined as [130]:

$$\text{MSE} = \frac{1}{m*n} \sum_{x=0}^{m-1} \sum_{y=0}^{n-1} (f(x,y) - \bar{f}(x,y))^2 \quad (3.6)$$

Where,

f, $\bar{f}$: are the original and segmented image alternately

- **Tumor area:** it is the area of the segmented region (the summation of white pixels in the white region of the segmented binary image).

3.3.5.2 Feature Extraction using Hybrid DWT-PCA-GLCM

Texture analyses distinguish normal and abnormal tissues easily for machine learning and human visual perception. It also gives variation between malignant and normal tissues, which may not be visual to human eye. It improves the accuracy by choosing efficient quantitative features for early diagnosis. Gray level co-occurrence matrix (GLCM) is one of the most commonly used in image-processing implementations and texture function and has been developed by Haralick et al. [131]. The hybrid DWT-PCA-GLCM is a DWT-PCA-based GLCM feature extraction method that combines the DWT and PCA method with GLCM. In this method, the three-wavelet decomposition levels significantly reduce the size of the input image, as shown in Figure 3.6.

The wavelet coefficients image's top left corner denotes the level-3 approximation coefficients, the value of which is just 32 × 32 = 1024. The quantity of extracted features was reduced to 1024, as mentioned above. Nonetheless, it is also too big for estimation. PCA is utilized to further minimize the size of features to an optimum degree. Then nine features are extracted using the GLCM algorithm from the PCA components. The statistics formulas for the features are listed below:

- **Mean (μ):** The image mean is determined by summing all the image pixel values divided by the total count of image pixels.

$$\mu = \frac{1}{m*n}\sum_{x=0}^{m-1}\sum_{y=0}^{n-1} f(x,y) \quad (3.7)$$

- **Standard Deviation (SD):** The second central moment is the standard deviation that defines the distribution of the probability of an observed population and can function as an inhomogeneity metric. A higher value implies a higher level of intensity and high contrast between an image's edges.

$$\mathrm{SD} = \sqrt{\frac{1}{m*n}\sum_{x=0}^{m-1}\sum_{y=0}^{n-1}(f(x,y)-\mu)^2} \quad (3.8)$$

- **Kurtosis (Kurt):** The shape of the probability distribution of a random variable is defined as Kurtosis. It denoted as $K_{\text{urt}}(X)$ for the random variable X and it defined as:

$$K_{\text{urt}}(X) = \frac{\mu^4}{\sigma^4} \quad (3.9)$$

Where

μ: is the fourth central moment

σ: is the standard deviation

- **Energy (En):** The quantifiable quantity of the degree of pixel pair repetitions is described as energy. It is defined as.

$$\text{En} = \sqrt{\sum_{x=0}^{m-1}\sum_{y=0}^{n-1} f(x,y)^2} \quad (3.10)$$

- **Coarseness (Cness):** Coarseness is the textural analysis of an image as an indicator of roughness.

$$\text{Coarseness} = \frac{1}{2^{m+n}}\sum_{x=0}^{m-1}\sum_{y=0}^{n-1} f(x,y) \quad (3.11)$$

- **Homogeneity:** evaluates the closeness of the elements distribution in the GLCM to the GLCM diagonal. It is defined as:

$$\sum_{x=0}^{m-1}\sum_{y=0}^{n-1} \frac{1}{1+(i-y)^2}.f(x,y) \quad (3.12)$$

- **Variance:** Measures the dispersion (with regard to the mean) of the gray level distribution. It is defined as:

$$\frac{\sum_{x=0}^{m-1}\sum_{y=0}^{n-1}(f(x,y)-M)^2}{m*n} \quad (3.13)$$

- **Auto Correlation Predictor:** It is defined as:

$$\sum_{x=0}^{m-1}\sum_{y=0}^{n-1} (x*y).f(x,y) \quad (3.14)$$

- **Dissimilarity:** is a measure of distance between pairs of objects (pixels) in the region of interest. It is defined as:

$$\sum_{x=0}^{m-1}\sum_{y=0}^{n-1} |x-y|.f(x,y) \quad (3.15)$$

3.3.6 Random Forest Classifier

Classification methods are used to obtain the classification of tumor based on the extracted features. We employed random forest classifiers in the proposed work. The number of trees depends on the dataset rows number. The rows in our dataset are 181, number of trees considered in our model are 10. We used 5-fold cross-validation instead of holdout partitioning, since it is straightforward, easy, and uses all data for training and validation. We have considered the average accuracy obtained from the 5-folds. The Steps involved in random forest classifier as follows:

Step 1 Select random K data points from the training set.

Step 2 Build the decision trees associated with the selected data points (Subsets).

Step 3 Choose the number N for decision trees that you want to build.

Step 4 Repeat Step 1 & 2.

Step 5 For new data points, find the predictions of each decision tree, and assign the new data points to the category that wins the majority votes.

To train the classification models, Stratified 5-fold cross-validation was used (80 % for training and 20% for testing), where each fold has almost an equal class distribution. The pseudocode of the random forest classifier is as follows:

Algorithm 3.1 Random Forest Classifier

Input: Dataset **D**

Output: Confusion Matrix, Validation

Step 1 (Divide the dataset into training and testing)
Training ← Split (**D**, size = 0.8)

Testing ← Split (**D**, size = 0.2)

Step 2 (Algorithm training)
Teacher = new RandomForestLearning()

```
{
    NumberOfTrees = 10, // use 10 trees in the forest
};
```

Step 3 (Brain tumor prediction for the testing dataset)
Forest = **Teacher**.Learn(**Training**, **Training_Output**)
Prediction = **Forest**.Decide(**Testing**)

Step 4 (Extract classification results)
Calculate **Scores**(**Prediction, Testing_output**)
Compute **Confusion Matrix**(**Prediction, Testing_output**)

Step 5 (Evaluation of results)
Validate Model

3.4 Proposed Method 2: Optimized Thresholded Difference (OTD) and Rough Set Theory (RST)

Usually, when dealing with tumor segmentation in a brain tumor dataset, the tumors are an area of higher density than the rest of the image, so the segmentation process when using thresholding algorithms in the first phase is to split the pixels that have a higher density than the rest of the image. But it is different in the Figshare dataset which also contains brain images in which the tumors have a lower density than the rest of the image, so the segmentation process when using thresholding algorithms in the second phase is to divide the pixels that are less dense than the rest of the pixels in the image.

In this model, an optimized thresholded difference (OTD) algorithm proposed to solve the segmentation problem. The proposed technique begins by creating an overlay image (a uniform intensity gray image that is the average intensity of all the pixels in the brain image to be segmented), and then extracting the tumor

areas using the threshold difference between the brain image and the overlay image.

The Figshare brain tumor dataset that used in this model contains contrast-enhanced images with T1 weighting in which the tumor region is in both of the above cases (high and low intensity). Because of the convergence of pixel intensities across all brain regions and the lack of high contrast between background and foreground, making use of automatic thresholding for segmentation is unhelpful for such a data set.

The proposed brain tumor segmentation can be defined in seven steps. The process is as follows:

1. Data acquisition
2. Pre-processing
3. Skull identification and brain region segmentation
4. Tumor segmentation
5. Feature extraction
6. Feature selection (RST)
7. Classification.

As seen in Figure 3.8. The first and second stage is the data acquisition and pre-processing. The third and fourth stage is skull identification and brain region segmentation. To improve the segmentation process, it has been proposed to segment the brain region and separate the skull from it due to its closeness to the intensity of the affected areas in the MRI images. The proposed OTD method utilized for the segmentation of the affected part from the brain region image.

The gray level co-occurrence matrix (GLCM) approach is utilized in the fifth step to extract the features. The selection of features is the next step. From the retrieved features, the RST approach is suggested for selecting the most relevant

features. Finally, the classifier was used to classify the types of tumor as meningioma, glioblastoma, and pituitary gland using the ID3 machine learning mechanism. The details of the method are given in the next sections.

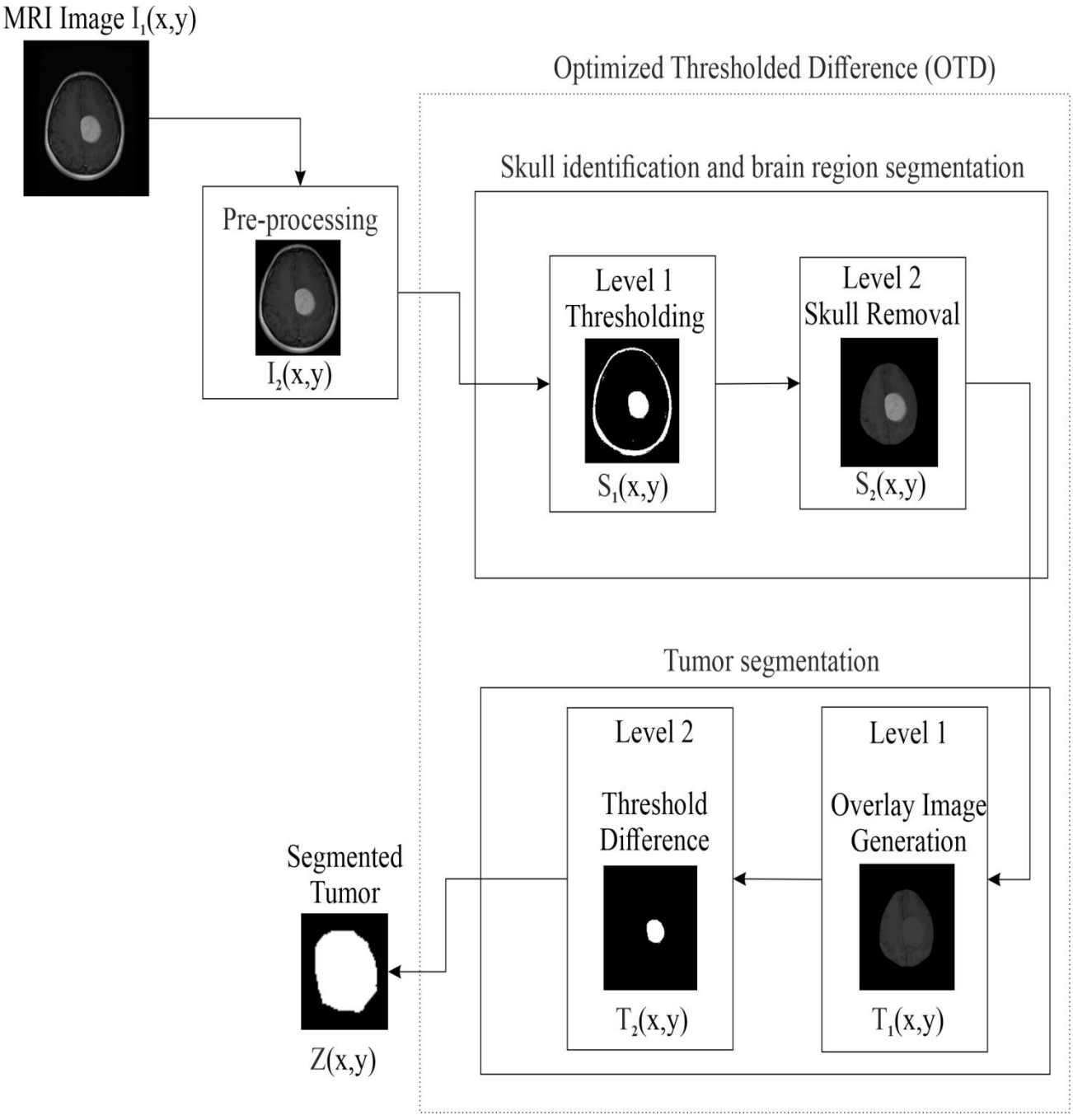

Figure 3. 8 Block diagram of the proposed MRI segmentation method

3.4.1 Data Acquisition

The Figshare brain tumor dataset contains 3064 T1-weighted contrast-enhanced images from 233 patients with three kinds of brain tumor: meningioma (708 slices), glioma (1426 slices), and pituitary tumor (930 slices). Each image contained an original size of 512 × 512 in pixels. The dataset contain axial, coronal and sagittal of brain slices, only images with an axial view used in this research with three types of brain tumors: meningioma (93 slices), glioma (105 slices), and pituitary tumor (56 slices).

3.4.2 Pre-processing

Background minimization tries to reduce non-tumors region information while preserving tumor-specific features. Here, the background removed and the brain region selected using two levels of operations: the first is to determine the starting points for the brain region of the four sides of the image (top, bottom, right, and left). In the second step, the area between the extracted points is truncated and a padding of 25 pixels is added around the extracted brain region on all four sides. This is used for the segmentation process as shown in Figure 3.9.

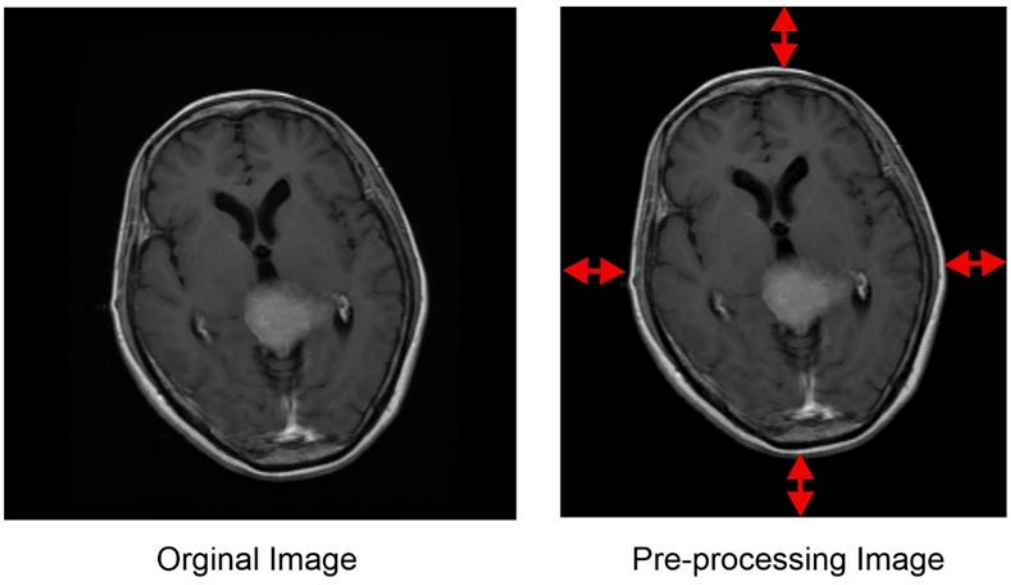

Figure 3. 9 Background minimization

3.4.3 Skull Identification and Brain Region Segmentation

Thresholding is a segmentation technique that compares the intensity of a pixel to one or more intensity thresholds. Regarding brain MRI image processing, when using segmentation methods that rely on thresholding methods, the skull bone presents a major challenge in this case. Moreover, it greatly affects the quality of the segmentation process because it has a high intensity comparable to the intensity of the tumor areas in the gray images. Therefore, a method was proposed to remove the bones of the skull and extract the brain region only to obtain a brain region that does not contain the bones of the skull, so as not to affect later in the process of tumor segmentation, as shown in Figure 3.10. The proposed removal method consists of two levels:

- The first is the use of the threshold algorithm on an MRI image with a thresholding value of 80, which results in a binary image (black and white) containing the bones of the skull and certain areas affected by the thresholding process. Then, a completed ring is produced, in which the outer edges of the image are adopted after applying the threshold, representing the edges of the skull arising from the thresholding process, and a closed ring is generated based on the values of these edges, representing the skull ring.
- Second, emptying the contents of the resulting ring (in this step we ensure that the process of neglecting the bones of the skull is not accompanied by any neglect of the tumor areas in the brain). The resulting skull ring is adopted as a mask to be applied to the original brain image. Where the areas corresponding to the extracted ring are neglected, any areas in the original image outside the extracted ring are neglected, and only the area confined in the original image is left inside the extracted ring, which represents the brain region.

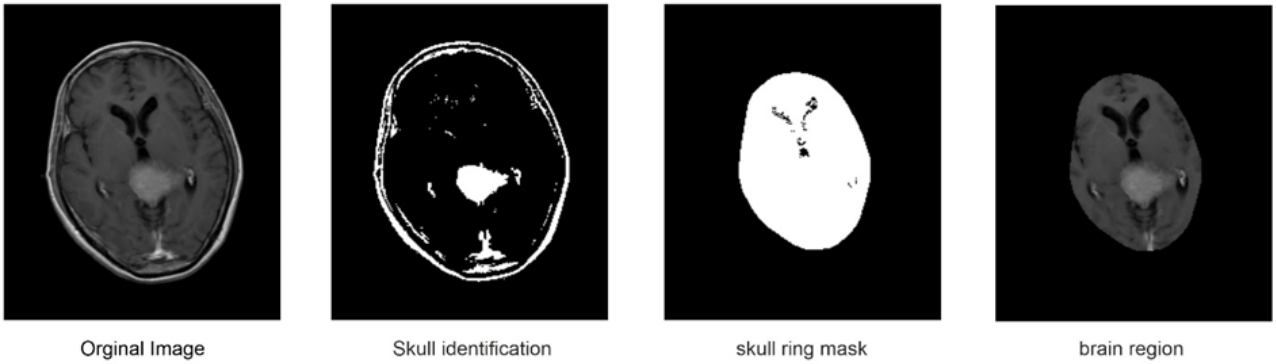

Figure 3. 10 Skull identification and brain region segmentation

3.4.4 Tumor Segmentation

The proposed optimized thresholded difference (OTD) algorithm consists of two levels of operation. In the first level, the brain image resulting from the previous stage (skull identification and brain region segmentation) is used, where an overlay image is generated that is a gray image with one intensity, which is the average intensity of all pixels in the brain image. In other words, the sum of the intensity of each pixel is divided by the total of the pixels in the image. As a result one intensity value is obtained that applies to all pixel intensities except the dark regions of the image. This image is used as an overlay image for the threshold difference process in the second level of the tumor segmentation process.

In the second level, the threshold difference process (difference value = 60) is applied between the previously segmented brain image and the resulting overlay image from the previous (first level) of the segmentation process. There are several segmented regions in OTD's segmented output. The correct border can be determined by selecting the region with the greatest area. As a result, all regions' perimeters are evaluated, and the region with the largest area is selected as the accurate region. Figure 3.11 shows the tumor segmentation steps.

Figure 3. 11 Tumor segmentation process

3.4.5 Features Extraction

The GLCM technique is used to extract features from segmented images. It extracts statistical texture features by evaluating the relationship between *i* and *j* pixels. A set of eight textural features extracted from each co-occurrence gray level matrix are presented in this model:

- **Entropy:**

$$Entropy = \sum_i^M \sum_j^N S_{Img}(i,j)\log(S_{Img}(i,j)) \quad (3.16)$$

Where $S_{Img}(i,j)$ is a segmented image

- **Energy:**

$$Energy = \sum_i^M \sum_j^N S_{Img}(\mathrm{i},\mathrm{j})^2 \quad (3.17)$$

- **Contrast:**

$$Contrast = \sum_i^M \sum_j^N |i-j|^2 S_{Img}(i,j) \quad (3.18)$$

- **Correlation:**

$$Correlation = \frac{\sum_i^M \sum_j^N (i-\mu_i)(j-\mu_j)}{\sigma_i \sigma_j} \quad (3.19)$$

The mean and variance are defined by μ and σ respectively.

- **Homogeneity**:

$$\text{Homogeneity} = \sum_i^M \sum_j^N \frac{1}{1+(i-j)^2} S_{Img}(i,j) \quad (3.20)$$

- **Variance:**

$$Variance = \sum_i^M \sum_j^N (i-j)^2 \, S_{Img}(i,j) \quad (3.21)$$

- **Inverse Difference Moment (IDM):**

$$\text{IDM} = \sum_{I,j}^{M,N} \frac{S_{Img}(i,j)}{1+|i-j|} \quad (3.22)$$

- **Sum of Square Variance:**

$$Sum\ of Square\ Variance = \sum_i^M \sum_j^N |i-\mu|^2 S_{Img}(i,j) \quad (3.23)$$

3.4.6 Feature Selection

Feature selection has been used to decrease the time of prediction and ignore the features that lead to a false prediction. The rough set theory is utilized to select features in this research.

Feature selection using rough set theory has been widely used in data analysis. The selected subset of attributes, which has the same equivalence relation of entire attribute, referred to as reduct (Red (R)). In this work, rough set theory indiscernibility relation method used for feature selection. Here, we will discuss some preliminaries of RST[109].

Information System Table: It can be presented as IST = (U, Att ∪ C) where U is a finite set of objects, Att is a set of an attribute, and C is the decision (class label).

Indiscernibility Relation (IND (B)): It is an equivalence relation. Let $a \in A$tt, B ⊆ Att; indiscernibility relation is defined as:

$$\text{IND (B)} = \{(x, y) \in U \times U : \forall a \in \text{B}, a(x) = a(y)\} \quad (3.24)$$

Upper approximation of a collection M ($\bar{R}$ (M)) contains all information system table objects that may belong to class M.

The lower approximation of set N ($\underline{R}$ (N)) is the collection of information system table objects that belong to class M.

The positive region refers to the collection of all objects that belong to the lower approximation (Pos(N)).

The boundary region refers to the difference between the upper and lower approximation sets (Bnd(M)).

Equations (3.25)–(3.28) show the mathematical formula for ($\bar{R}$ (M)), ($\underline{R}$ (N)), (Bnd(M)), and (Pos_R(N)):

$$\bar{R}\ (\mathrm{M}) = \{x \in U: R\ (X) \cap x \neq \emptyset\} \tag{3.25}$$

$$\underline{R}\ (\mathrm{N}) = \{x \in U: R\ (X) \subseteq x\} \tag{3.26}$$

$$\mathrm{Bnd}_R\ (\mathrm{M}) = \bar{R}\ (\mathrm{M}) - \underline{R}\ (\mathrm{N}) \tag{3.27}$$

$$\mathrm{Pos}_R\ (\mathrm{N}) = \bigcup_{\mathrm{x} \in \frac{\mathrm{U}}{\mathrm{IND(B)}}} \underline{R}\ (\mathrm{N}) \tag{3.28}$$

The reduct (Red (R)) is the smallest subset of attributes with the same characteristic as the entire attribute. The overpass of the attributes of reducts is called core (C). The overall number of least subsets of features (S) contending for the reducts becomes

$$S = 2^n - 2 \tag{3.29}$$

Where n stands for the total number of attributes

The number of least subset of attributes produced in every number of attributes (S_i) can be calculated by the rule of combination (C). It becomes

$$S_i = C_{\mathrm{n}_i}^N \tag{3.30}$$

Where n_i is the number of attributes in the minimal subset

The following are the processes of choosing the reduct:

Step 1 Find upper approximation of each class utilizing (3.25).

Step 2 Find a lower approximation of each class by utilizing (3.26).

Step 3 Compute the positive region of the universe by utilizing (3.28).

Step 4 Using (3.29) and (3.30), determine the number of minimum subsets of attributes.

Step 5 Find indiscernibility of each subset of attributes of a positive region utilizing (3.24).

Step 6 Compare the indiscernibility of each subset to the attribute's overall indiscernibility.

Step 7 Then choose equivalent indiscernibility as reduct (Red (R)).

Based on the given steps in the above algorithm, the reduct of Table 3.1 is computed as shown in the following:

Table 3. 1 Data sample example

U	A			**D**
	Att_1	Att_2	Att_3	**Class**
P_1	2	0	3	1
P_2	1	2	1	0
P_3	3	2	3	1
P_4	2	0	0	0
P_5	3	0	0	0
P_6	3	0	0	1

Step 1

$\bar{R}$ $(D = 1) = \{P\ 1, P3, P5, P6\}$ $(D = 0) = \{P\ 2, P4, P5, P6\}$

Step 2

$\underline{R}$ $(D = 1) = \{P\ 1, P3\}$ $(D = 0) = \{P\ 2, P4\}$

Step 3

$\text{Pos}(x) = \{P1, P2, P3, P4\}$

Step 4

$S = 2^3 - 2 = 6$ $S_1 = C_1^3 = 3$ $S_2 = C_2^3 = 3$

Step 5

$\text{IND}(\text{att}_1) = \{\{P1, P4\}, \{P2\}, \{P3\}\}$ $\text{IND}(\text{att}_2) = \{\{P1, P4\}, \{P2, P3\}\}$

$\text{IND}(\text{att}_3) = \{\{P1, P3\}, \{P2\}, \{P4\}\}$ $\text{IND}(\text{att}_1, \text{att}_2) = \{\{P1, P4\}, \{P2\}, \{P3\}\}$

$\text{IND}(\text{att}_1, \text{att}_3) = \{\{P1\}, \{P2\}, \{P3\}, \{P4\}\}$ $\text{IND}(\text{att}_2, \text{att}_3) = \{\{P1\}, \{P2\}, \{P3\}, \{P4\}\}$

$\text{IND}(C) = \text{IND}(\text{att}_1, \text{att}_2, \text{att}_3) = \{\{P1\}, \{P2\}, \{P3\}, \{P4\}\}$

Step 6

$\text{IND}(\text{att}_1) \neq \text{IND}(C)$ $\text{IND}(\text{att}_2) \neq \text{IND}(C)$

$\text{IND}(\text{att}_3) \neq \text{IND}(C)$ $\text{IND}(\text{att}_1, \text{att}_2) \neq \text{IND}(C)$

$\text{IND}(\text{att}_1, \text{att}_3) = \text{IND}(C)$ $\text{IND}(\text{att}_2, \text{att}_3) = \text{IND}(C)$

$\text{IND}(C) = \text{IND}(\text{att}_1, \text{att}_2, \text{att}_3) = \{\{P1\}, \{P2\}, \{P3\}, \{P4\}\}$

Step 7

$\text{Red}(C) = \{\{\text{att}_1, \text{att}_3\}, \{\text{att}_2, \text{att}_3\}\}$ $\text{Core}(C) = \{\text{att}_3\}$

3.4.7 Classification

Iterative Dichotomiser 3 (ID3) is a top-down greedy approach to building a decision tree. It was invented by Ross Quinlan. In simple terms, the top-down strategy indicates that we build trees from the top-down, whereas the greedy approach means that we choose the best features at the moment to produce a node at each iteration [132].

Testing and evaluation of the proposed model followed a fivefold cross-validation procedure. The ID3 model has been trained using the features chosen from the training images, as well as their class labels. The trained ID3 is then given the features derived from testing images. The predicted classes for the testing data are obtained as output from the ID3. The performance of the classifier is assessed by comparing predicted classes with true class labels. The Pseudocode of the ID3 classifier is as follows:

Algorithm 3.2 The ID3 classifier

Input: Dataset **D**

Output: Confusion Matrix, Validation

Step 1 (Divide the dataset into training and testing)
Training ← Split (**D**, size = 0.8)

Testing ← Split (**D**, size = 0.2)

Step 2 (Algorithm training)

Teacher = new ID3Learning()

Id3 = **Teacher**.Learn(**Training**, **Training_Output**)

Step 3 (Brain tumor prediction for the testing dataset)

Prediction = **Id3**.Decide(**Testing**)

Step 4 (Extract classification results)
Calculate **Scores**(**Prediction, Testing_output**)

Compute **Confusion Matrix**(**Prediction, Testing_output**)

Step 5 (Evaluation of results)

Validate Model

Chapter Four

Results and Discussion

4.1 Introduction

This chapter illustrates how the experiments have been set to test the proposed algorithms, and then the preliminary results are presented. The methodology and techniques discussed in the previous chapter have been applied on two datasets with different tumor types, and their performance has been measured and compared using different parameters. The first proposed model is a hybrid DWT+PCA+GLCM identifier system developed to classify the normal and abnormal MRIs of the brain tumor based on hybrid techniques such as DWT and PCA with RF. The second model is automatically segmenting brain tumors using the proposed optimized thresholded difference (OTD) and rough set theory (RST).

All practical results of the application of the two proposed models are presented and discussed in this chapter. Different experiments were carried out under different parameters and image processing characteristics. The results are tabulated, discussed, and evaluated in this chapter. The results tabulated, discussed, and evaluated in this chapter. All the experimentations are performed on a computer with these attributes: Manufacturer: Sony Vaio E Series, Windows 10 Pro 64-bit, Intel(R) Core(TM) i5-2450M CPU @ 2.50 GHz, (8.00 GB RAM). The proposed methods were implemented in Visual Studio.Net framework 2019 using C# language, and the detailed figures of the proposed models are located in the appendices A, and B.

4.2 Performance Evaluation Metrics

Measuring the performance of the proposed algorithm is based on the performance of the classifier model that is determined using the labels given in the database. This can be done by applying a set of examples to the classifier and measuring the number of errors the classifier has made. There are four fundamental outcomes that are used to test the classifier:

- True Positive (TP): the classifier recognizes the positive example correctly.
- True Negative (TN): the classifier recognizes the negative example correctly.
- False Positive (FP): the classifier incorrectly recognizes the negative example as positive.
- False Negative (FN): the classifier incorrectly recognizes the positive example as negative.

In this work, we will calculate the accuracy, sensitivity, and specificity of the proposed method given in the model using Eqs. (4.1, 4.2, and 4.3), the classification quality can be calculated as follows:

- Sensitivity: is the probability that a positive example will be identified properly by the classifier and its formula is:

$$\text{Sensitivity} = \frac{TP}{TP+FN} \quad (4.1)$$

- Specificity: is the probability that a negative example will be identified properly by the classifier and its formula is:

$$\text{Specificity} = \frac{TN}{TN+FP} \quad (4.2)$$

- Accuracy: is the frequency of correctly classified samples made by the classifier over a given set of examples, and it is computed as:

$$\text{Accuracy} = \frac{\text{TP+TN}}{\text{TP+TN+FP+FN}} \quad (4.3)$$

Receiver Operating Characteristics (ROC) curve: It is defined as trade-off visualization between a pair of criteria such as sensitivity and specificity, in the plane spanned by the two measures. As a result, a diagnostic test with adequate accuracy should have a ROC curve in the top left triangle.

4.3 K-Fold Cross-Validation

The K-fold cross-validation is implemented and uses all the data for training and validation. The method is to make the whole dataset a 5-fold partition, repeat 5 times for training using 4 folds and a left fold for validation, and eventually average the error rates of the 5 experiments as shown in Figure 4.1.

Table 4.1 demonstrates the setting of the training images and the validation images, as 5-fold cross-validation was used for both proposed models.

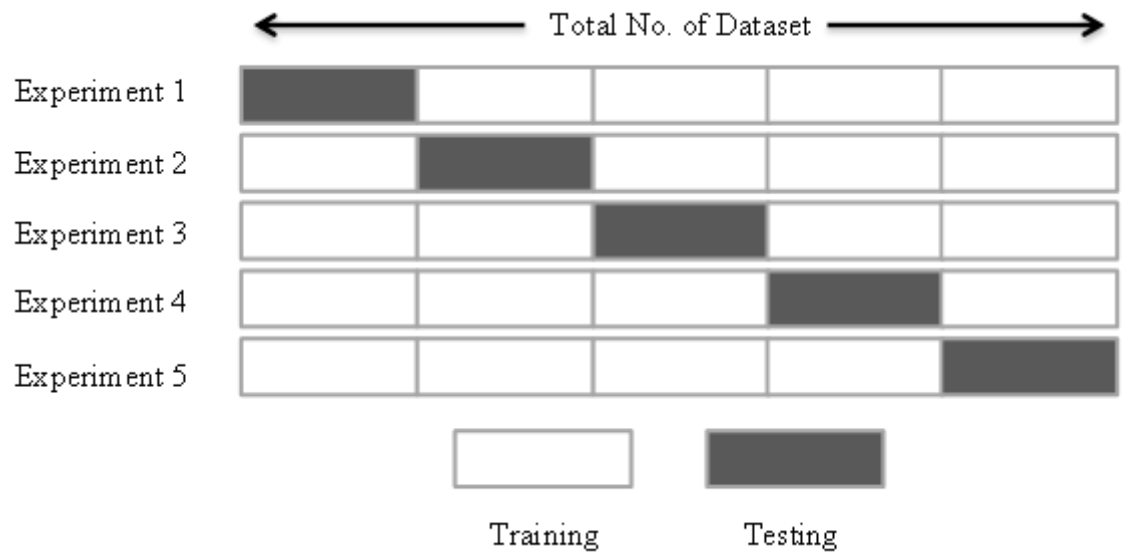

Figure 4. 1 A 5-fold cross-validation

Table 4. 1 The configuration (cross-validation) of training and validation images for both proposed models

The proposed model	**Total No.**	**Training (145)**		**Validation (36)**	
		Normal	**Abnormal**	**Normal**	**Abnormal**
First model	181	65	80	16	20
The proposed model	**Total No.**	**Training (203)**			**Validation (51)**		
		Meningioma	**Glioma**	**Pituitary tumor**	**Meningioma**	**Glioma**	**Pituitary tumor**
Second model	254	74	84	45	19	21	11

4.4 Results of the First Proposed Model (Hybrid Feature Extraction Method Based on DWT and PCA)

4.4.1 Dataset

The datasets consist of axial plane T2-weighted MR brain images, retrieved from the Harvard Medical School website and the OASIS dataset. Since T2 images, compared to T1 and PET modalities, are of greater contrast and better vision, we selected the T2 model. Consisting of 81 normal and 100 abnormal brain images, 181 images were chosen.

4.4.2 Pre-processing Results

Regarding brain MR image processing, when using segmentation methods that rely on thresholding methods, the skull bone presents a major challenge in this case. Moreover, it greatly affects the quality of the segmentation process because it has a high intensity comparable to the intensity of the tumor areas in the gray images. Therefore, a method was proposed to remove the bones of the skull and extract the brain region only to obtain a brain region that does not contain the bones of the skull, so as not to affect later in the process of tumor segmentation. The proposed removal method showing in Figure 4.2 (b, c and d) consist of the following steps:

- Converting the MRI to a grayscale image and the preprocessing operation.
- Transformed the preprocessed brain MR image into a binary image with a cut-off threshold of 80 chosen in the initiative.
- Remove the bones of the skull and extract the brain region only to obtain a brain region that does not contain the bones of the skull.

4.4.3 Segmentation Results

The preprocessing step is followed by a segmentation step and this can be done manually or automatically. Segmentation is applied for two purposes: to remove the skull and other tissues like fat and skin and to retain the brain tissue.

This purpose is also known as brain extraction. The other purpose of segmentation is to extract the tumor region to make the image analysis easier. The segmentation of the affected brain MRI regions accomplished by the following steps:

- Appling K means clustering on the extracted brain region.
- Pixel values greater than 150 are mapped as white, the others are marked as black.

In the last step, an erosion method of morphology is used to remove sporadic white pixels. Dilation anchors the segmented region As a result, the tumor area remains without any abnormalities. Figure 4.2 (e and f) shows the results and effect of segmentation steps on brain tumor images.

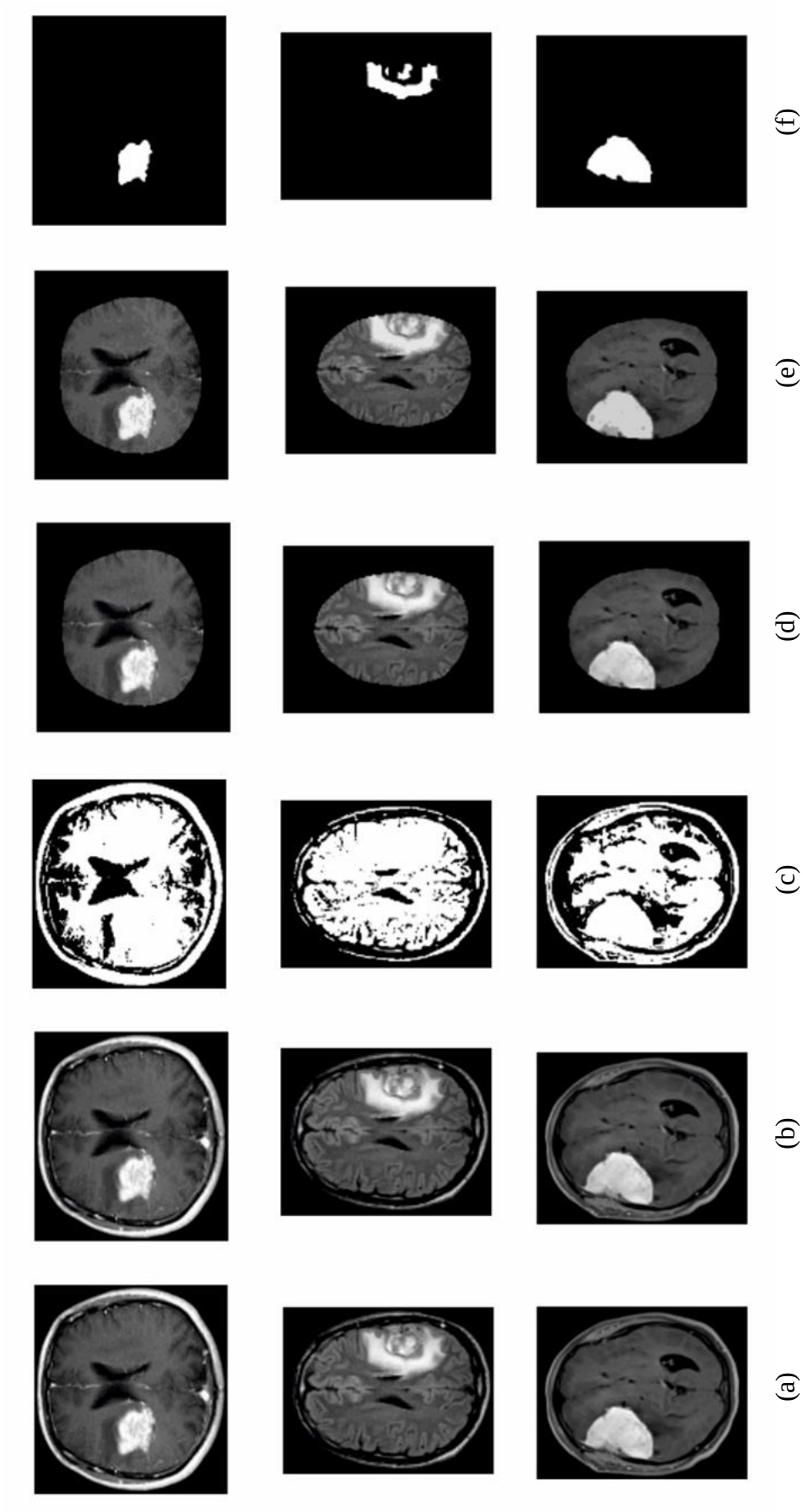

Figure 4. 2 The pre-processing and segmentation of tumor regions outputs: a) Original image, b) Grayscale filter, c) Thresholding, d) Skull removal, e) K means clustering, f) Segmented tumor

4.4.4 Classification Performance

The results of the proposed system are obtained by using actual MRI brain images. Since MRI scan visual diagnosis is subjective and based on the radiologist's experience, texture analysis has been thoroughly researched to enhance the diagnosis of brain MRI scans. First, during this study, the k-means clustering algorithm and thresholding accompanied by morphological operations have been combined, and then applying DWT and PCA with the extraction of GLCM features, then assessed by a classifier tool with RF. After testing the classifier model over all images in the dataset, the metric values (TP, TN, FP, and FN) are achieved as mentioned in section 4.2. The diagonal numbers (TP and TN) represent how many times the algorithm worked properly and made the correct diagnosis. However, the values that are not on the diagonal (FP and FN) indicate the number of instances that the model incorrectly identified normal and abnormal cases. Table 4.2 shows the confusion matrix of the proposed method.

Table 4. 2 Confusion matrix for the proposed method

Predicted	**Actual**		
	Positive	TP = 98	FP = 2
	Negative	FN = 1	TN = 80

According to Eqs. (4.1, 4.2, and 4.3) as described in Section 4.2, which represent some formulas, the sensitivity, specificity, and accuracy, are computed to measure the efficiency of the proposed method as shown in Table 4.3.

Table 4. 3 Results of the proposed method

Sensitivity	**Specificity**	**Accuracy**
99%	97.6%	98.3%

The research focuses on the extraction of segmented area features in order to detect and distinguish medical brain MR images of normal and abnormal tumor cells. Performance of the classification is measured in terms of accuracy, sensitivity, specificity, and ROC curve as shown in Figure 4.3.

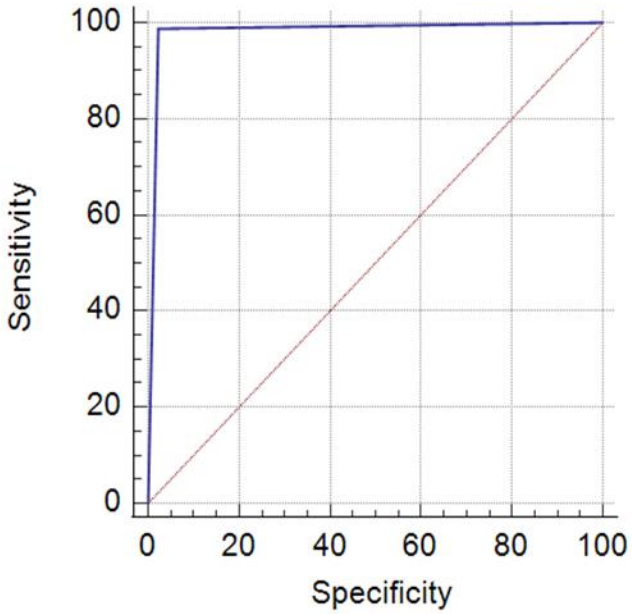

Figure 4. 3 ROC curve of the classification results

As shown in Table 4.4 and Figure 4.4, we examined the proposed method in various ways to improve the experimental results. Firstly, we utilized k-means, 2DWT, and PCA. Secondly, we applied 3DWT and PCA. Finally, k-means and 2DWT are utilized. As a result, the proposed method (3DWT, PCA, and K-means) outperformed the other examined techniques when compared in terms of accuracy, sensitivity, and specificity.

Table 4. 4 Comparison of experimental results for the proposed method

Model 1	**K-Means, 3DWT, PCA**	**K-Means, 2DWT, PCA**	**3DWT, PCA**	**K-Means, 2DWT**
Accuracy	98.30	97.20	97.80	97.70
Sensitivity	99.00	97.00	99.00	98.00
Specificity	97.60	97.50	96.40	97.60

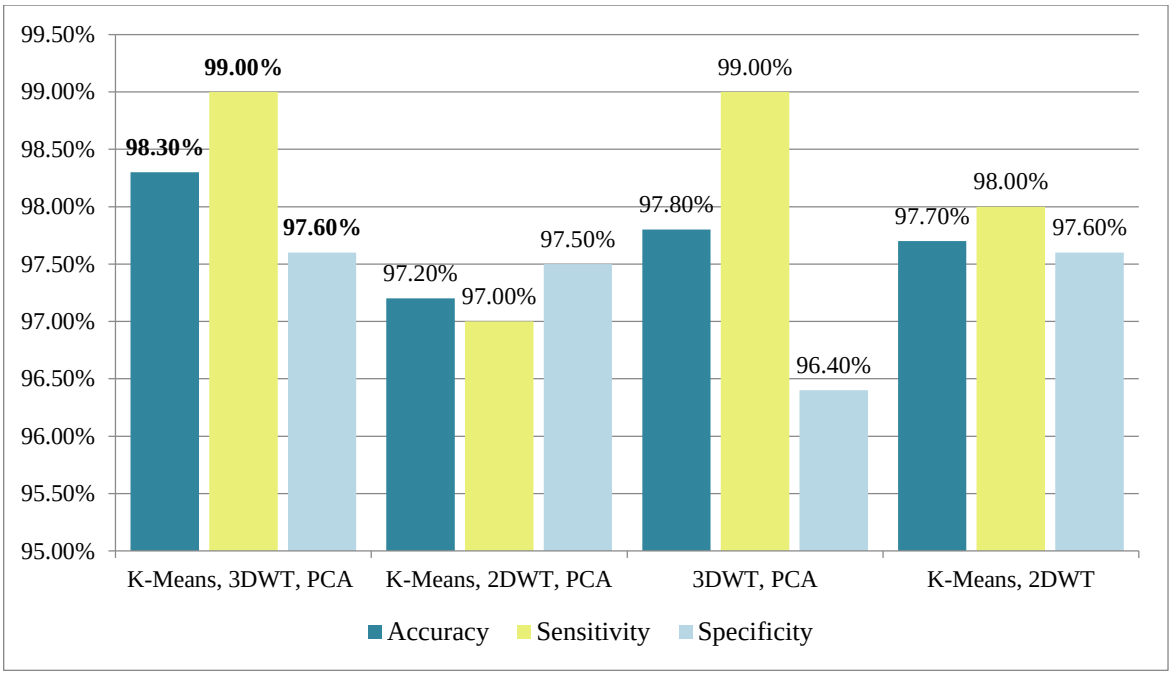

Figure 4. 4 Comparison of the experimental results for the proposed method

As seen in Table 4.5. The proposed algorithm's experimental results are compared to previous studies. Compared with other techniques, we exceeded the performance of the work by Siddiqui et al. [8] that only achieved an accuracy of 95.70% using DWT with RF. On the other hand, we also outperformed the work of Naser et al. [24] that reported an accuracy of 86.5%. Moreover, the highest accuracy of 96.6% was reported by Siddiqi et al. [28] using Symlet wavelet transform with LR. The proposed system As a result, it is possible for clinical experts to decide and diagnose based on the proposed model.

Table 4. 5 Comparison of the proposed method with the existing techniques

Reference	Dataset	Features	Classifier	Accuracy
Siddiqui et al. [8]	Harvard + OASIS	DWT	RF	95.70%
Naser et al. [24]	Harvard + OASIS	GLCM	SVM	86.5%
Siddiqi et al. [27]	Harvard + OASIS	partial Z-test	SVM	96.4%
Siddiqi et al. [28]	Harvard + OASIS	Symlet wavelet transform	LR	96.6%
Proposed System	**Harvard + OASIS**	**Hybrid DWT-PCA-GLCM**	**RF**	**98.3%**

The proposed system is designed to classify and identify the brain MR image into normal and abnormal tumors. Figure 4.5 show that the proposed method outperformed other popular methods in recent literature in terms of accuracy. The accuracy of the system was achieved at 98.3% for the tested dataset. Due to the statistical textural features being extracted from the PCA component of LL sub-bands 3-level wavelet decomposition. The results that have been achieved concluded that the proposed method outperformed and clearly distinguishes between normal and abnormal tumors, enabling clinical experts to make accurate diagnosis decisions.

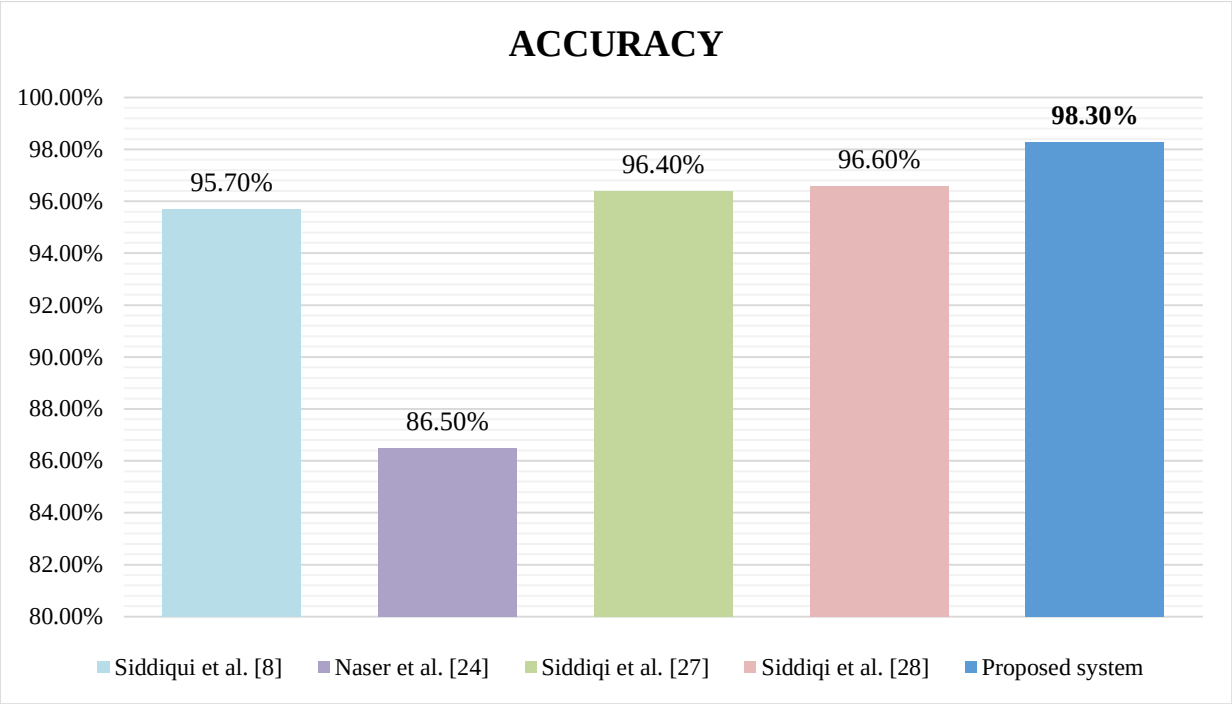

Figure 4. 5 Comparison of the existing techniques with the proposed system

4.4.5 Computational Cost Analysis

Another important factor in classifier evaluation is computation time. The period for RF training is not taken into account because the RF parameters remain unchanged after training. We input all 181 images into the classifier, measured the corresponding computation time, computed the average value, and presented the consumed time in Figure 4.6.

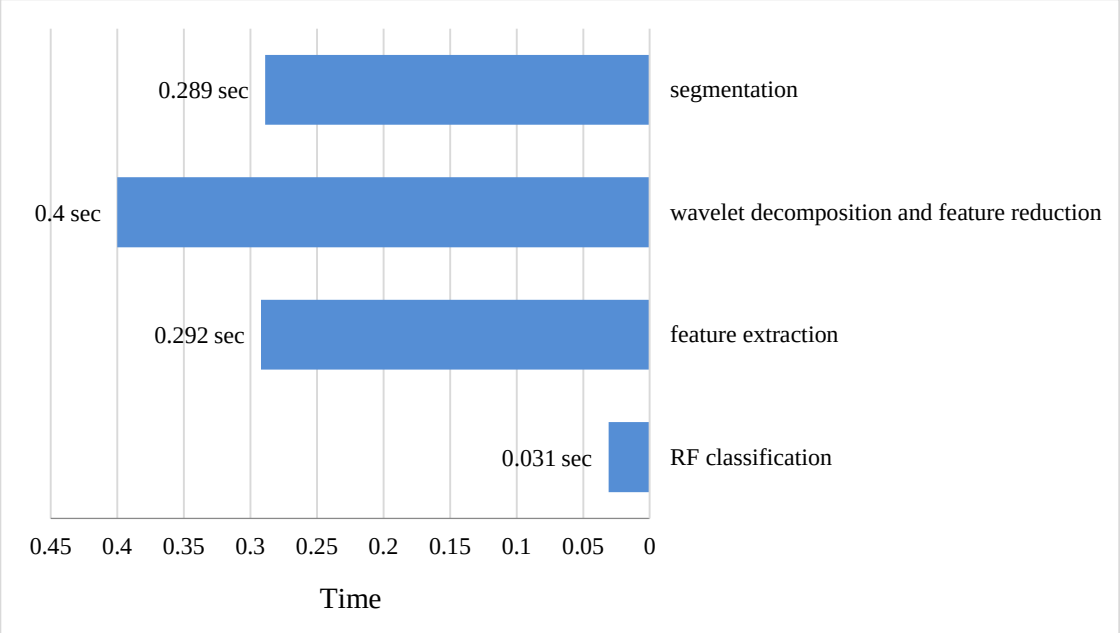

Figure 4. 6 Computation times at different stages

For each 256 × 256 image, the averaged computation time on segmentation, (wavelet decomposition and feature reduction), feature extraction, and RF classification is 0.289 s, 0.4 s, 0.292 s, and 0.031 s, respectively. The feature extraction stage is the most time-consuming at 0.292 s. The feature reduction costs 0.4 s. The RF classification costs the least time only 0.031 s. The total computation time for each 256 × 256 size image is about 1.012 s, which is rapid enough for a real-time diagnosis.

4.5 Results of the Second Proposed Model (Optimized Thresholded Difference (OTD) and Rough Set Theory (RST))

This section contains a comparison of results as well as a discussion of the second proposed method. The classifier's performance assessed and compared to that of related works. The experimental results for the proposed segmentation method are shown in this section.

4.5.1 Data Set

The data comes from a T1-weighted contrast-enhanced image Figshare database with size 512 ×512 pixels. As indicated in Table 4.6, images with an axial view used in this research with three types of brain tumors: meningioma, glioma, and pituitary tumor.

Table 4. 6 Description of Figshare dataset

Type	No of slices
Meningioma	93
Glioma	105
Pituitary tumor	56

4.5.2 Pre-processing Results

Here, the background removed and the brain region selected using two levels of operations: the first is to determine the starting points of the brain region from the four sides of the image (top, bottom, right, and left). In the second step, the region between the extracted points cut off while keeping five pixels around the brain from the background on all sides and used in the segmentation process. Figure 4.7.b shows the output images obtained during preprocessing (background elimination).

4.5.3 Brain Region Segmentation

A method proposed to remove the skull bone and extract the brain region only to obtain a brain region that does not contain the skull bone, so as not to later affect the tumor segmentation process. The proposed removal method as shown in Figure 4.7(c and d) consists of two levels:

- Construction of a completed ring representing the skull, depending on the segmented skull bone regions in the thresholding process.
- The resulting skull ring adopted as a mask to apply to the original brain image. Where the regions corresponding to the extracted ring neglected, as are the regions outside it.

4.5.4 Tumor Segmentation

The proposed optimized difference OTD algorithm consists of two levels of operations. At the first level, an overlay image is generated, which is a gray image with a single intensity, and it is the average intensity of all pixels in the brain image. At the second level, a threshold difference process applied between the pre-segmented brain image and the resulting overlay image from the previous step of the segmentation process. Figure 4.7 (e and f) shows the results of the tumor segmentation steps.

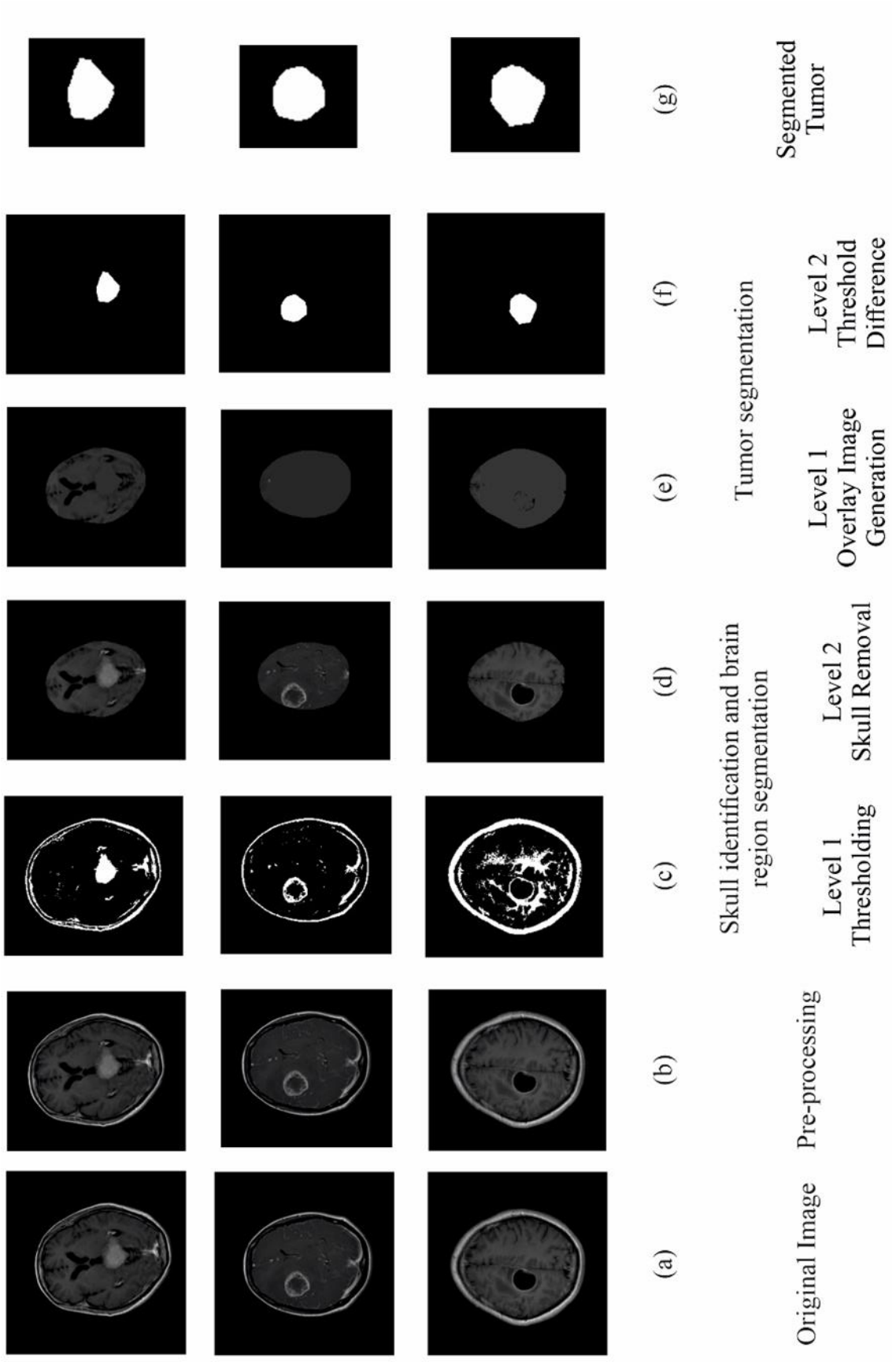

Figure 4. 7 The segmentation of tumor regions outputs: a) Original image, b) Pre-processing, c) Thresholding, d) Skull removal, e) Overlay image generation, f) threshold difference, g) Segmented tumor

4.5.5 Comparison with Related Works in Terms of Accuracy

Accuracy is expressed as a proportion of true predictions generated by the classifier. All previous works on this specific classification challenge is compared to the proposed method. There are two reasons why classification accuracy is employed as a comparative statistic. In the beginning, it is the standard measure utilized in all related research. Second, the same dataset is used to evaluate the related research. Table 4.7 summarizes the proposed model performances and gives a performance comparison.

Table 4. 7 Comparison table of the proposed model with other works

Work/ Year	Dataset	Techniques	Accuracy (%)
Ismael *et al.* [10]	Figshare	DWT, Gabor, NN	91.90
Pashaei *et al.* [14]	Figshare	CNN, ELM	93.68
Swati *et al.* [21]	Figshare	CNN (TL)	94.80
Deepak *et al.* [16]	Figshare	DCNN, KNN	98.0
Deepak *et al.* [22]	Figshare	CNN, SVM	95.82
The proposed model	**Figshare**	**GLCM, ID3**	**98.9**

As seen in Table 4.7, the experimental results of the proposed algorithm are contrasted with prior research studies. Compared with other techniques, we exceeded the performance of the work by Swati et al. [21] that only achieved an accuracy of 94.80% using CNN (TL). On the other hand, we also outperformed the work of Deepak et al. [22] that reported an accuracy of 95.82%. Moreover, the highest accuracy of 98.0 % was reported by Deepak et al. [16] using DCNN

and KNN. The proposed system result leads to the conclusion that it makes as possible for clinical experts to decide and diagnose.

As shown in Figure 4.8 the obtained results showing the proposed method is more reliable than other approaches described in the literature and leads to a result that allows clinical experts to decide and diagnose.

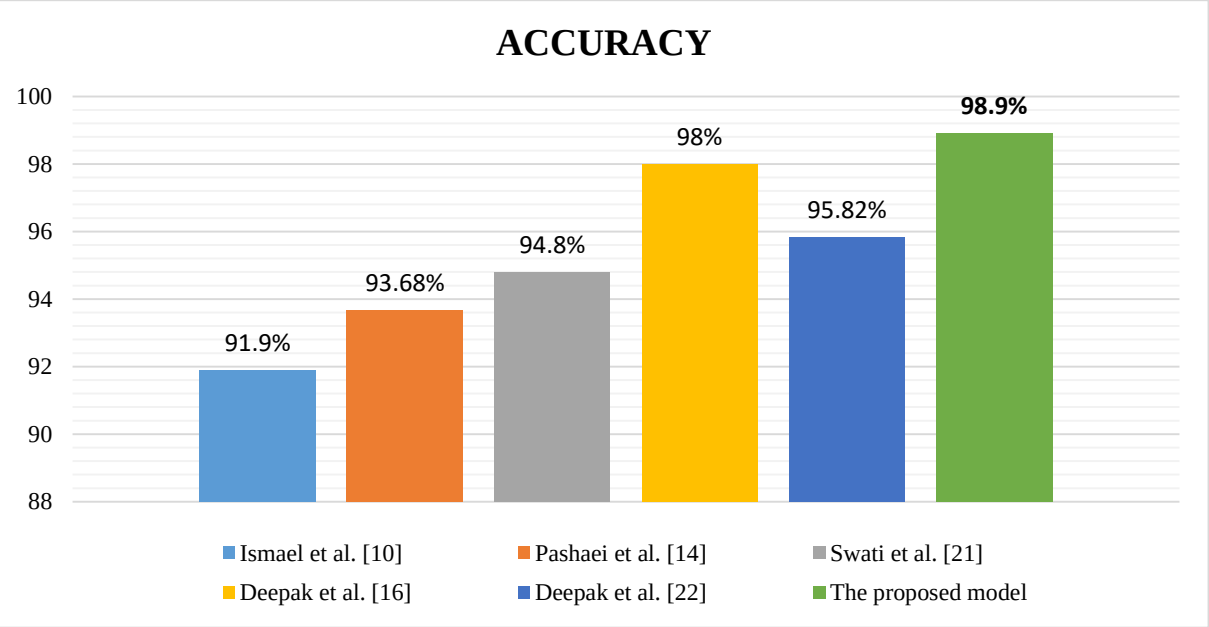

Figure 4. 8 Comparison of the existing techniques with the proposed system

4.5.6 Other Performance Metrics

We use a confusion matrix to evaluate the results. The confusion matrix obtained for the experiment shown in Table 4.8.

Table 4. 8 Confusion matrix of the achieved results

Actual class				
Predicted class		**M**	**G**	**P**
	M: Meningioma	92	1	0
	G: Glioma	0	104	1
	P: Pituitary	1	0	55

To explain the above confusion matrix, the sum of all the numbers in the confusion matrix equal the total number of test samples (93 + 105 + 56 = 254 samples). The diagonal numbers show the number of samples that are correctly classified while the other numbers are the misclassified samples.

For each class, the following key evaluation metrics produced using the confusion matrix. Figure 4.9 shows the performance measures for each tumor class. The proposed model is exceptional in terms of specificity across all classes. Because it shows the proportion of samples free of a specific tumor class, specificity is an essential statistic in disease categorization. In terms of sensitivity, the classifier is a high-performance model. In addition, the ROC curve of the three types of tumors used to assess the classification's efficiency in the proposed method, as shown in Figures 4.10, 4.11, and 4.12.

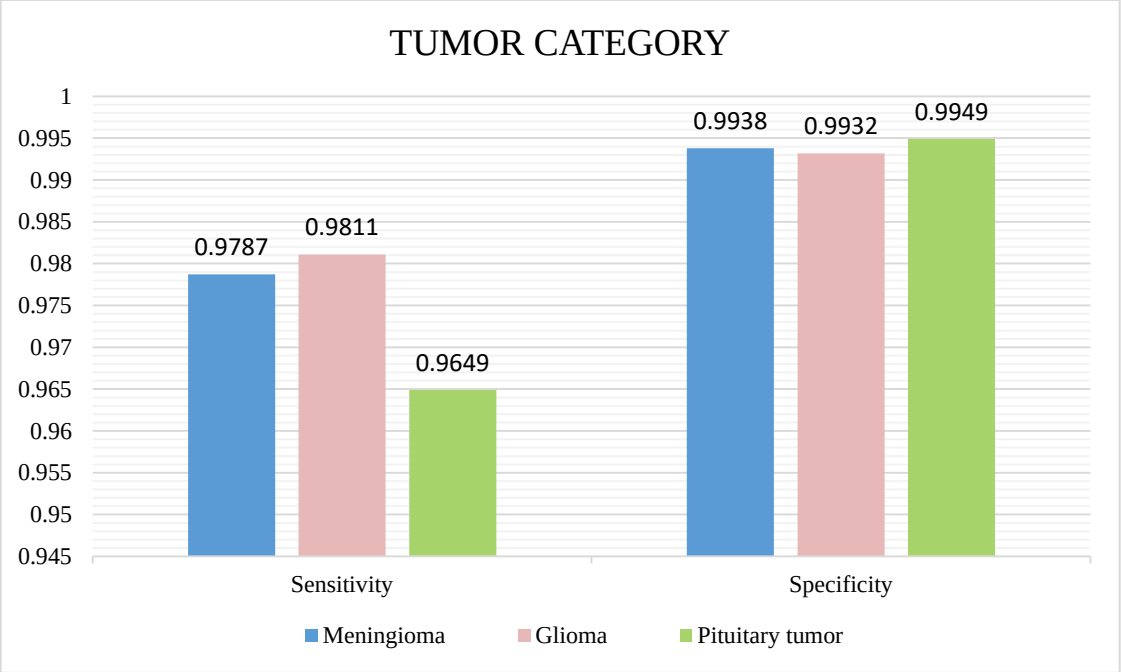

Figure 4. 9 Performance measures for the proposed method

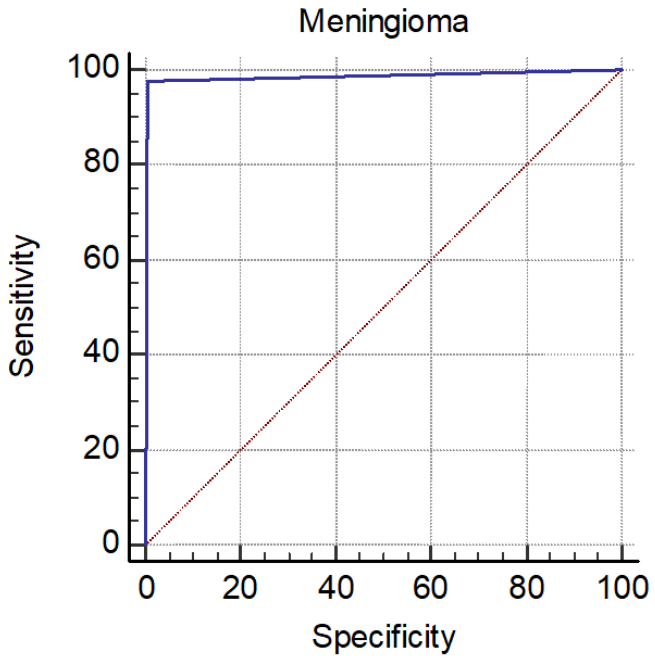

Figure 4. 10 ROC curve of the (Meningioma) classification results

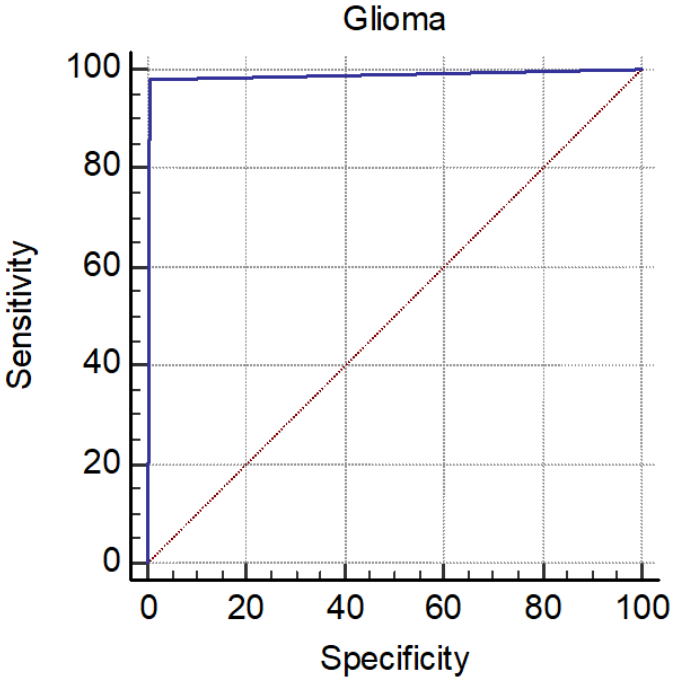

Figure 4. 11 ROC curve of the (Glioma) classification results

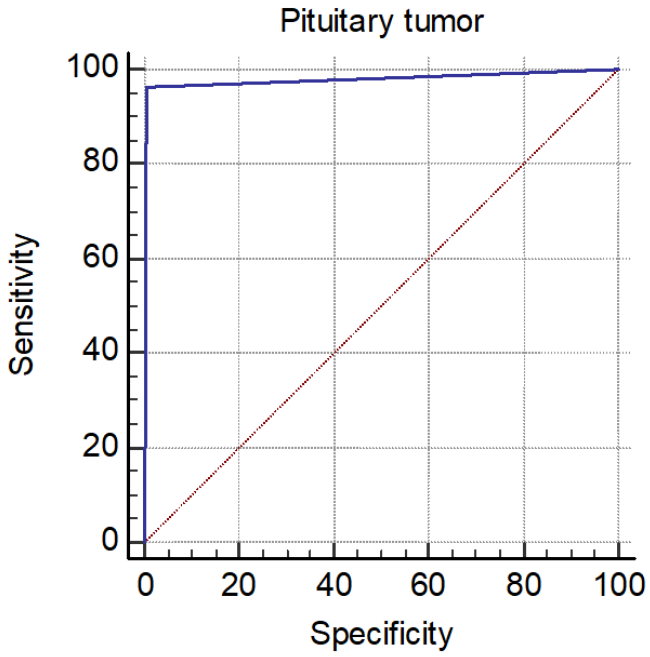

Figure 4. 12 ROC curve of the (Pituitary tumor) classification results

Chapter Five

Conclusions and Future Works

5.1 Conclusions

A brain tumor is a disease that affects the human brain system at different ages. Radiologists often use either invasive or noninvasive procedures or both to diagnose a brain tumor. Noninvasive diagnosis is mostly based on the use of MRI. An intelligent assistant can improve the radiologist's diagnosis, allowing for better diagnoses. This prompted several academic works to suggest a variety of strategies for detecting and classifying tumors in MRI brain images using image processing and machine learning techniques. In this dissertation, we used these techniques for automatic brain tumor identification by proposing two methods. The findings of the proposed models have led to the following conclusions:

- The first proposed technique is a hybrid feature extraction submitted to enhance the classification results and consists of three stages. The first stage uses a 3-level discrete wavelet transform (DWT) to extract image characteristics. In the second stage, the principal component analysis (PCA) is applied to reduce the size of the dimension, resulting in 32 principal components (from 1024 coefficients). In the third stage, nine features were extracted using the gray-level co-occurrence matrix (GLCM) from the PCA components, and four statistical textural analysis features were extracted from the segmented image intensities. Finally, a random forest classifier (RF) was used with feature selection for identification. For the evaluation of this scheme, 181 MRI brain images (81 normal and 100 abnormal) were collected and retrieved from the Harvard Medical School website and the OASIS dataset [127] [129], distinguishing normal and abnormal tissues. The experimental results obtained an accuracy of 98.3%, a sensitivity of 99%, and a specificity of 97.6% and showed the effectiveness of the proposed technique compared with the similar literature. The results demonstrate that the proposed 3L-DWT+PCA+RF method achieves high classification accuracy

while its computational complexity is not too high. The proposed model could apply to the brain MRI sphere classification, which will help doctors diagnose a tumor if it is normal or abnormal to certain degrees.

- The second model proposed an improved segmentation algorithm based on the optimized threshold difference (OTD) method to solve the problem of segmenting tumor regions with high or low intensity, which cannot be segmented using traditional thresholding algorithms. The OTD method consists of two stages. The first stage is skull identification and brain region segmentation, and in the second stage, the tumor segmentation from the brain region image was performed in two levels. At the first level, an overlay image was generated, and then the threshold difference process was applied between the segmented brain image and the overlay image. A set of eight textural features were then obtained from the segmented region by applying GLCM using RST to select the most important features and ignoring the features that lead to false predictions. A Figshare database with 233 patient images was utilized for the evaluation, which is a T1-weighted contrast-enhanced image. Only images with an axial view were used in this work with three types of brain tumors: meningiomas (93 slices), gliomas (105 slices), and pituitary tumors (56 slices). Finally, ID3 was utilized to perform the classification, and the experimental results obtained an accuracy of 98.9%. In terms of accuracy, specificity, and sensitivity, the obtained results demonstrate that the proposed algorithm exceeds the reference methods. The higher performance of the proposed algorithm is mainly due to the accurate segmentation policy in the proposed segmentation step. Any errors in the segmentation step are propagated to the next steps of the system. Based on the results obtained in diagnosing the type of brain tumor, the proposed segmentation technique can be considered a successful method for diagnosing brain tumors using MRI images in other systems as well.

5.2 Future Works

There are different areas of future work that could be carried out to further advance the findings of this research. The details of the suggestion are listed below:

- Proposing a segmentation method based on advanced architectures such as deeply supervised networks.
- Implementing methods based on deep learning may enhance classifier performance for the detection of tumors.
- In this dissertation, the two proposed models utilized an axial view of the MR images. In the future, additional MRI datasets can be gathered with other brain tumor views such as sagittal (Lateral Plane) and coronal (Frontal Plane) for classification.
- Measuring the size and location of the tumor in the brain will be helpful for the neurosurgeons for analysis and detecting the tumor from MRI scans. This strategy makes accurate decisions about treatment and applies the right tests for the patient.
- Adding normal brain images to the dataset may aid in differentiating tumor classification further.
- Brain tumor detection can be more accurately done using real data through utilizing different image acquisition methods (modalities). Handcrafted and deep features can be combined to improve the classification results.

Publications

(Scopus)

1. Dalia M. T., Ali M. S. and, Hadi V. “Brain Tumor Segmentation from Magnetic Resonance Image using Optimized Thresholded Difference Algorithm and Rough Set.”, *TEM Journal.* Vol. 11, No.2, pp. 631-638, ISSN 2217-8309, DOI: 10.18421/TEM112-17, May 2022.

(Scopus)

2. Dalia M. T., Ali M. S., and Hadi V., "Brain tumor identification with a hybrid feature extraction method based on discrete wavelet transform and principle component analysis.", Bulletin of Electrical Engineering and Informatics, Vol. 10, No. 5, pp. 2588–2597, October 2021.

(Scopus)

3. Dalia M. T., Ali M. S. and, Hadi V. “A Review on Brain Tumor Classification in MRI Images.”, *Turkish Journal of Computer and Mathematics Education*, Vol.12, No.14 (2021), 1958- 1969.

References

[1] Schipmann S, Brix T, Varghese J, Warneke N, Schwake M, Brokinkel B, Ewelt C, Dugas M, Stummer W. Adverse events in brain tumor surgery: incidence, type, and impact on current quality metrics. Acta neurochirurgica. 2019 Feb;161(2):287-306.

[2] Nazir M, Khan MA, Saba T, Rehman A. Brain tumor detection from MRI images using multi-level wavelets. In2019 international conference on Computer and Information Sciences (ICCIS) 2019 Apr 3 (pp. 1-5). IEEE.

[3] Tiwari A, Srivastava S, Pant M. Brain tumor segmentation and classification from magnetic resonance images: Review of selected methods from 2014 to 2019. Pattern Recognition Letters. 2020 Mar 1;131:244-60.

[4] Dvorak P, Kropatsch WG, Bartusek K. Automatic brain tumor detection in T2-weighted magnetic resonance images. Measurement Science Review. 2013 Jan 1;13(5):223-30.

[5] Nabizadeh N, Kubat M. Brain tumors detection and segmentation in MR images: Gabor wavelet vs. statistical features. Computers & Electrical Engineering. 2015 Jul 1;45:286-301.

[6] Cheng J, Huang W, Cao S, Yang R, Yang W, Yun Z, Wang Z, Feng Q. Enhanced performance of brain tumor classification via tumor region augmentation and partition. PloS one. 2015 Oct 8;10(10):e0140381.

[7] Hasan AM, Meziane F. Automated screening of MRI brain scanning using grey level statistics. Computers & Electrical Engineering. 2016 Jul 1;53:276-91.

[8] Siddiqui MF, Mujtaba G, Reza AW, Shuib L. Multi-class disease classification in brain MRIs using a computer-aided diagnostic system. Symmetry. 2017;9(3):37.

[9] Mohsen H, El-Dahshan E-SA, El-Horbaty E-SM, Salem A-BM. Classification using deep learning neural networks for brain tumors. Future Computing and Informatics Journal. 2018;3(1):68-71.

[10] Ismael MR, Abdel-Qader I. Brain tumor classification via statistical features and back-propagation neural network. In2018 IEEE international conference on electro/information technology (EIT) 2018 May 3 (pp. 0252-0257). IEEE.

[11] Sharif M, Tanvir U, Munir EU, Khan MA, Yasmin M. Brain tumor segmentation and classification by improved binomial thresholding and multi-features selection. Journal of ambient intelligence and humanized computing. 2018 Oct 10:1-20.

[12] Varuna Shree N, Kumar TN. Identification and classification of brain tumor MRI images with feature extraction using DWT and probabilistic neural network. Brain informatics. 2018 Mar;5(1):23-30.

[13] Byale H, Lingaraju GM, Sivasubramanian S. Automatic segmentation and classification of brain tumor using machine learning techniques. International Journal of Applied Engineering Research. 2018;13(14):11686-92.

[14] Pashaei A, Sajedi H, Jazayeri N. Brain tumor classification via convolutional neural network and extreme learning machines. In2018 8th International conference on computer and knowledge engineering (ICCKE) 2018 Oct 25 (pp. 314-319). IEEE.

[15] Hussain L, Saeed S, Awan IA, Idris A, Nadeem MS, Chaudhry QU. Detecting brain tumor using machines learning techniques based on different features extracting strategies. Current Medical Imaging. 2019 Jul 1;15(6):595-606.

[16] Deepak S, Ameer PM. Brain tumor classification using deep CNN features via transfer learning. Computers in biology and medicine. 2019 Aug 1;111:103345.

[17] Khan MA, Lali IU, Rehman A, Ishaq M, Sharif M, Saba T, Zahoor S, Akram T. Brain tumor detection and classification: A framework of marker-based watershed algorithm and multilevel priority features selection. Microscopy research and technique. 2019 Jun;82(6):909-22.

[18] Gumaei A, Hassan MM, Hassan MR, Alelaiwi A, Fortino G. A hybrid feature extraction method with regularized extreme learning machine for brain tumor classification. IEEE Access. 2019 Mar 11;7:36266-73.

[19] Cheng J, Yang W, Huang M, Huang W, Jiang J, Zhou Y, Yang R, Zhao J, Feng Y, Feng Q, Chen W. Retrieval of brain tumors by adaptive spatial pooling and fisher vector representation. PloS one. 2016 Jun 6;11(6):e0157112.

[20] Mohammed M, Nalluru SS, Tadi S, Samineni R. Brain tumor image classification using convolutional neural networks. International Journal of Advanced Science and Technology. 2019;29(5):928-34.

[21] Swati ZN, Zhao Q, Kabir M, Ali F, Ali Z, Ahmed S, Lu J. Brain tumor classification for MR images using transfer learning and fine-tuning. Computerized Medical Imaging and Graphics. 2019 Jul 1;75:34-46.

[22] Deepak S, Ameer PM. Automated categorization of brain tumor from mri using cnn features and svm. Journal of Ambient Intelligence and Humanized Computing. 2021 Aug;12(8):8357-69.

[23] Bandyopadhyay S, Dutta S. Adaptive neuro fuzzy inference system used to classify the five major types of brain tumors. 2020.

[24] Naser WAK, Kadim EA, Abbas SH. SVM Kernels comparison for brain tumor diagnosis using MRI. Global Journal of Engineering and Technology Advances. 2021;7(2):026-36.

[25] Niharika N, Patel S, Bharath KP, Subramanian B, Kumar R. Brain Tumor Detection and Classification Based on Histogram Equalization Using Machine Learning. InHandbook of Research on Deep Learning-Based Image Analysis Under Constrained and Unconstrained Environments 2021 (pp. 23-43). IGI Global.

[26] Sathi KA, Islam S. Multi-classification of Brain Tumor Images Based on Hybrid Feature Extraction Method. InInternational Conference on Intelligent Computing & Optimization 2020 Dec 17 (pp. 989-999). Springer, Cham.

[27] Siddiqi MH, Alsayat A, Alhwaiti Y, Azad M, Alruwaili M, Alanazi S, et al. A Precise Medical Imaging Approach for Brain MRI Image Classification. Computational Intelligence and Neuroscience. 2022;2022.

[28] Siddiqi MH, Azad M, Alhwaiti Y. An Enhanced Machine Learning Approach for Brain MRI Classification. Diagnostics. 2022;12(11):2791.

[29] Fabelo H, Ortega S, Szolna A, Bulters D, Piñeiro JF, Kabwama S, JO'Shanahan A, Bulstrode H, Bisshopp S, Kiran BR, Ravi D. In-vivo hyperspectral human brain image database for brain cancer detection. IEEE Access. 2019 Mar 14;7:39098-116.

[30] Tomasila G, Emanuel AW. MRI image processing method on brain tumors: A review. InAIP Conference Proceedings 2020 Nov 16 (Vol. 2296, No. 1, p. 020023). AIP Publishing LLC.

[31] Norouzi A, Rahim MS, Altameem A, Saba T, Rad AE, Rehman A, Uddin M. Medical image segmentation methods, algorithms, and applications. IETE Technical Review. 2014 May 4;31(3):199-213.

[32] Kamil MY. Brain tumor area calculation in CT-scan image using morphological operations. IOSR Journal of Computer Engineering. 2015 Mar;17(2):125-8.

[33] Khan HA, Jue W, Mushtaq M, Mushtaq MU. Brain tumor classification in MRI image using convolutional neural network. Math. Biosci. Eng. 2020 Sep 1;17(5):6203-16.

[34] Lewis T. Human Brain: Facts, Functions & Anatomy [Internet]. Live Science. Live Science; 2018. [cited 2022 Mar 6]. Available from: https://www.livescience.com/29365-human-brain.html

[35] Javed, K., Reddy, V. and Lui, F., 2019. Neuroanatomy, cerebral cortex.

[36] Boly M, Massimini M, Tsuchiya N, Postle BR, Koch C, Tononi G. Are the neural correlates of consciousness in the front or in the back of the cerebral cortex? Clinical and neuroimaging evidence. Journal of Neuroscience. 2017 Oct 4;37(40):9603-13.

[37] Lights V. Brain Tumor: Types, Risk Factors, and Symptoms [Internet]. Healthline. 2012. [cited 2022 Mar 8]. Available from: https://www.healthline.com/health/brain-tumor

[38] Ansell P, Johnston T, Simpson J, Crouch S, Roman E, Picton S. Brain tumor signs and symptoms: analysis of primary health care records from the UKCCS. Pediatrics. 2010 Jan;125(1):112-9.

[39] Charles NA, Holland EC, Gilbertson R, Glass R, Kettenmann H. The brain tumor microenvironment. Glia. 2012 Mar;60(3):502-14.

[40] Amulya C, Prathibha G. Mri brain tumor classification using surf and sift features. International Journal for Modern Trends in Science and Technology. 2016 Jul;2(7):123-7.

[41] Sultan HH, Salem NM, Al-Atabany W. Multi-classification of brain tumor images using deep neural network. IEEE access. 2019 May 27;7:69215-25.

[42] DeAngelis LM. Brain tumors. New England journal of medicine. 2001 Jan 11;344(2):114-23.

[43] Müller HL. Craniopharyngioma. InHandbook of Clinical Neurology 2014 Jan 1 (Vol. 124, pp. 235-253). Elsevier.

[44] Stamm AC, Vellutini E, Balsalobre L. Craniopharyngioma. Otolaryngologic Clinics of North America. 2011 Aug 1;44(4):937-52.

[45] Goldbrunner R, Minniti G, Preusser M, Jenkinson MD, Sallabanda K, Houdart E, von Deimling A, Stavrinou P, Lefranc F, Lund-Johansen M, Moyal EC. EANO guidelines for the diagnosis and treatment of meningiomas. The Lancet Oncology. 2016 Sep 1;17(9):e383-91.

[46] Melmed S. Pathogenesis of pituitary tumors. Nature Reviews Endocrinology. 2011 May;7(5):257-66.

[47] Molitch ME. Diagnosis and treatment of pituitary adenomas: a review. Jama. 2017 Feb 7;317(5):516-24.

[48] Weller M, Wick W, Aldape K, Brada M, Berger M, Pfister SM, Nishikawa R, Rosenthal M, Wen PY, Stupp R, Reifenberger G. Glioma. Nature reviews Disease primers. 2015 Jul 16;1(1):1-8.

[49] Astrocytoma Tumors – Symptoms, Diagnosis and Treatments [Internet]. www.aans.org. [cited 2022 Mar 28]. Available from: https://www.aans.org/Patients/Neurosurgical-Conditions-and-Treatments/Astrocytoma-Tumors/

[50] Sathornsumetee S, Rich JN, Reardon DA. Diagnosis and treatment of high-grade astrocytoma. Neurologic clinics. 2007 Nov 1;25(4):1111-39.

[51] Stages of Cancer [Internet]. Cancer.net. 2010 [cited 2022 Mar 6]. Available from: https://www.cancer.net/navigating-cancer-care/diagnosing-cancer/stages-cancer/

[52] Huben RP, Mounzer AM, Murphy GP. Tumor grade and stage as prognostic variables in upper tract urothelial tumors. Cancer. 1988 Nov 1;62(9):2016-20.

[53] Urbańska K, Sokołowska J, Szmidt M, Sysa P. Glioblastoma multiforme–an overview. Contemporary Oncology/Współczesna Onkologia. 2014 May;18(5):307-12.

[54] Jalalian A, Mashohor S, Mahmud R, Karasfi B, Saripan MI, Ramli AR. Foundation and methodologies in computer-aided diagnosis systems for breast cancer detection. EXCLI journal. 2017;16:113.

[55] Litjens G, Kooi T, Bejnordi BE, Setio AA, Ciompi F, Ghafoorian M, Van Der Laak JA, Van Ginneken B, Sánchez CI. A survey on deep learning in medical image analysis. Medical image analysis. 2017 Dec 1;42:60-88.

[56] Wadhwa A, Bhardwaj A, Verma VS. A review on brain tumor segmentation of MRI images. Magnetic resonance imaging. 2019 Sep 1;61:247-59.

[57] Jibon FA. An Improved Classification Method of Brain MRI Image for Abnormality Detection 2019.

[58] Mohsen H, El-Dahshan E, El-Horbaty E, Salem A. Brain tumor type classification based on support vector machine in magnetic resonance images. Annals Of "Dunarea De Jos" University Of Galati, Mathematics, Physics, Theoretical mechanics, Fascicle II, Year IX (XL). 2017 Jan 1(1).

[59] Tahir MN. Classification and characterization of brain tumor MRI by using gray scaled segmentation and DNN. 2018.

[60] Elsayed AS. Region of interest based image classification: a study in MRI brain scan categorization. The University of Liverpool (United Kingdom); 2011.

[61] Ismael MR. Hybrid Model-Statistical Features and Deep Neural Network for Brain Tumor Classification in MRI Images. 2018.

[62] Pedapati P, Tannedi RV. Brain tumour detection using hog by svm. 2018.

[63] Fleischmann D, Boas FE. Computed tomography—old ideas and new technology. European radiology. 2011 Mar;21(3):510-7.

[64] Biratu ES, Schwenker F, Ayano YM, Debelee TG. A survey of brain tumor segmentation and classification algorithms. Journal of Imaging. 2021 Sep 6;7(9):179.

[65] Kumar K. Positron Emission Tomography (PET)/Computed Tomography (CT) Guided Diffuse Optical Tomography (DOT) for Breast Cancer Imaging. University of California, Merced; 2018.

[66] Jerusalem G, Hustinx R, Beguin Y, Fillet G. PET scan imaging in oncology. European journal of cancer. 2003 Jul 1;39(11):1525-34.

[67] Das AK, Ghosh S, Thunder S, Dutta R, Agarwal S, Chakrabarti A. Automatic COVID-19 detection from X-ray images using ensemble learning with convolutional neural network. Pattern Analysis and Applications. 2021 Aug;24(3):1111-24.

[68] Jahanavi MS, Kurup S. A novel approach to detect brain tumour in MRI images using hybrid technique with SVM classifiers. In2016 IEEE International Conference on Recent Trends in Electronics, Information & Communication Technology (RTEICT) 2016 May 20 (pp. 546-549). IEEE.

[69] Gonzalez RC, Woods RE. Digital image processing second edition. Beijing: Publishing House of Electronics Industry. 2008;455.

[70] Lone AH, Siddiqui AN. Noise models in digital image processing. Global Sci-Tech. 2018;10(2):63-6.

[71] Gonzalez RC, Woods RE. Digital image processing third edition. Beijing: Publishing House of Electronics Industry. 2008;455.

[72] Mokhomo M. *Automatic detection and segmentation of brain lesions from 3D MR and CT images* (Master's thesis, University of Cape Town). 2014.

[73] Shantta K, Basir O. Brain Tumor Detection and Segmentation: A Survey. IRA-International Journal of Technology & Engineering (ISSN 2455-4480). 2018;10(4):55-61.

[74] Rehman A, Naz S, Razzak MI, Akram F, Imran M. A deep learning-based framework for automatic brain tumors classification using transfer learning. Circuits, Systems, and Signal Processing. 2020 Feb;39(2):757-75.

[75] Rezaee K, Haddadnia J. Designing an algorithm for cancerous tissue segmentation using adaptive k-means cluttering and discrete wavelet transform. Journal of Biomedical Physics & Engineering. 2013 Sep;3(3):93.

[76] brain tumor dataset. figshare [Internet]. [cited 2022 May 9]. Available from: https://figshare.com/articles/brain_tumor_dataset/1512427/5

[77] Clark K, Vendt B, Smith K, Freymann J, Kirby J, Koppel P, Moore S, Phillips S, Maffitt D, Pringle M, Tarbox L. The Cancer Imaging Archive (TCIA): maintaining and operating a public information repository. Journal of digital imaging. 2013 Dec;26(6):1045-57.

[78] Poliovirus treatment helped patients with deadly brain tumors live longer [Internet]. Science News. 2018. [cited 2022 May 23]. Available from: https://www.sciencenews.org/article/poliovirus-treatment-helped-patients-deadly-brain-tumors-live-longer/

[79] Vadmal V, Junno G, Badve C, Huang W, Waite KA, Barnholtz-Sloan JS. MRI image analysis methods and applications: an algorithmic perspective using brain tumors as an exemplar. Neuro-Oncology Advances. 2020 Jan;2(1):vdaa049.

[80] Sheela VK, Babu SS. Pre-processing Technique For Brain Tumor Detection and Segmentation. International research journal of engineering and technology (IRJET). 2015 Jun;2(3).

[81] Isra'a Abdul-Ameer Abdul-Jabbar. Image processing for face recognition rate enhancement. International Journal of Advanced Science and Technology. 2014 Mar 30;64:1-0.

[82] Tomasila G, Emanuel AW. MRI image processing method on brain tumors: A review. InAIP Conference Proceedings 2020 Nov 16 (Vol. 2296, No. 1, p. 020023). AIP Publishing LLC.

[83] Mateen M, Wen J, Song S, Huang Z. Fundus image classification using VGG-19 architecture with PCA and SVD. Symmetry. 2018 Dec 20;11(1):1.

[84] Shantta K, Basir O. Brain Tumor Detection and Segmentation: A Survey. IRA-International Journal of Technology & Engineering (ISSN 2455-4480). 2018;10(4):55-61.

[85] Ciecholewski M. Malignant and benign mass segmentation in mammograms using active contour methods. Symmetry. 2017 Nov 16;9(11):277.

[86] Babu KR, Nagajaneyulu PV, Prasad KS. Brain tumor segmentation of T1w MRI images based on clustering using dimensionality reduction random projection technique. Current Medical Imaging. 2021 Mar 1;17(3):331-41.

[87] Varuna Shree N, Kumar TN. Identification and classification of brain tumor MRI images with feature extraction using DWT and probabilistic neural network. Brain informatics. 2018 Mar;5(1):23-30.

[88] Vyas A, Yu S, Paik J. Fundamentals of digital image processing. InMultiscale Transforms with Application to Image Processing 2018 (pp. 3-11). Springer, Singapore.

[89] Al-Waeli AM. An automated system for the classification and segmentation of brain tumours in MRI images based on the modified grey level co-occurrence matrix. University of Salford (United Kingdom); 2017.

[90] Rathi VP, Palani S. Brain tumor MRI image classification with feature selection and extraction using linear discriminant analysis. arXiv preprint arXiv:1208.2128. 2012 Aug 10.

[91] Handayani HH. Digital Image Matching Method Using Normalized Cross-Correlation (Ncc). Geoid. 2010 Aug 1;6(1):001-5.

[92] Benesty J, Chen J, Huang Y, Cohen I. Pearson correlation coefficient. InNoise reduction in speech processing 2009 (pp. 1-4). Springer, Berlin, Heidelberg.

[93] Mohanaiah P, Sathyanarayana P, GuruKumar L. Image texture feature extraction using GLCM approach. International journal of scientific and research publications. 2013 May;3(5):1-5.

[94] Indra Z, Jusman Y. Performance of GLCM algorithm for extracting features to differentiate normal and abnormal brain images. InIOP Conference Series: Materials Science and Engineering 2021 Feb 1 (Vol. 1082, No. 1, p. 012011). IOP Publishing.

[95] Zhang J, Ong SH, Le TM. Kurtosis-based no-reference quality assessment of JPEG2000 images. Signal Processing: Image Communication. 2011 Jan 1;26(1):13-23.

[96] Jain S. Brain cancer classification using GLCM based feature extraction in artificial neural network. International Journal of Computer Science & Engineering Technology. 2013 Jul 7;4(7):966-70.

[97] Singh S, Srivastava D, Agarwal S. GLCM and its application in pattern recognition. In2017 5th International Symposium on Computational and Business Intelligence (ISCBI) 2017 Aug 11 (pp. 20-25). IEEE.

[98] Mathew AR, Anto PB, Thara NK. Brain tumor segmentation and classification using DWT, Gabour wavelet and GLCM. In2017 International Conference on Intelligent Computing, Instrumentation and Control Technologies (ICICICT) 2017 Jul 6 (pp. 1744-1750). IEEE.

[99] Hasan AM, Meziane F. Automated screening of MRI brain scanning using grey level statistics. Computers & Electrical Engineering. 2016 Jul 1;53:276-91.

[100] Jain S. Brain cancer classification using GLCM based feature extraction in artificial neural network. International Journal of Computer Science & Engineering Technology. 2013 Jul 7;4(7):966-70.

[101] Davidson MW, Abramowitz M. Molecular expressions microscopy primer: Digital image processing-difference of gaussians edge enhancement algorithm. Olympus America Inc., and Florida State University. 2006.

[102] Akoglu H. User's guide to correlation coefficients. Turkish journal of emergency medicine. 2018 Sep 1;18(3):91-3.

[103] Shen F, Shen C, van den Hengel A, Tang Z. Approximate least trimmed sum of squares fitting and applications in image analysis. IEEE Transactions on Image Processing. 2013 Jan 9;22(5):1836-47.

[104] Bendjillali RI, Beladgham M, Merit K, Taleb-Ahmed A. Improved facial expression recognition based on DWT feature for deep CNN. Electronics. 2019 Mar 15;8(3):324.

[105] Tantisatirapong S. Texture analysis of multimodal magnetic resonance images in support of diagnostic classification of childhood brain tumours: University of Birmingham; 2015.

[106] Mohammed SB, Khalid A, Osman SE, Helali RG. Usage of Principal Component Analysis (PCA) in AI Applications. Int. J. Eng. Res. Technol. 2016;5(12):372-5.

[107] Devi M, Maheswaran S. An efficient method for brain tumor detection using texture features and SVM classifier in MR images. Asian Pacific journal of cancer prevention: APJCP. 2018;19(10):2789.

[108] Hadi AM, Al-Abass GJ, Hussain FF. Hybrid-Approach-Based Feature Selection for Magnetic Reverberation Imaging Brain Tumor Classification. Journal of Southwest Jiaotong University. 2020;55(2).

[109] Zhang Q, Xie Q, Wang G. A survey on rough set theory and its applications. CAAI Transactions on Intelligence Technology. 2016 Oct 1;1(4):323-33.

[110] Kourou K, Exarchos TP, Exarchos KP, Karamouzis MV, Fotiadis DI. Machine learning applications in cancer prognosis and prediction. Computational and structural biotechnology journal. 2015 Jan 1;13:8-17.

[111] Al-Azzam N, Shatnawi I. Comparing supervised and semi-supervised machine learning models on diagnosing breast cancer. Annals of Medicine and Surgery. 2021 Feb 1;62:53-64.

[112] Joseph VR, Vakayil A. Split: An optimal method for data splitting. Technometrics. 2022 Apr 3;64(2):166-76.

[113] Moocarme M, Abdolahnejad M, Bhagwat R. The Deep Learning with Keras Workshop: Learn how to define and train neural network models with just a few lines of code. Packt Publishing Ltd; 2020 Jul 29.

[114] Mahmoud MA. *Development of advanced computer methods for breast cancer image interpretation through texture and temporal evolution analysis* (Ph. D. dissertation, Universitat Rovira i Virgili). 2016.

[115] Ogheneovo EE, Nlerum PA. Iterative dichotomizer 3 (ID3) decision tree: A machine learning algorithm for data classification and predictive analysis. International Journal of Advanced Engineering Research and Science. 2020;7(4):514-21.

[116] De Ville B. Decision trees. Wiley Interdisciplinary Reviews: Computational Statistics. 2013 Nov;5(6):448-55.

[117] Bhardwaj R, Vatta S. Implementation of ID3 algorithm. International Journal of Advanced Research in Computer Science and Software Engineering. 2013 Jun;3(6).

[118] Dvořák PA. *Brain Tumor Detection and Segmentation in Multisequence MRI.* Ph. D dissertation, Electrical Engineering and Communication, Brno University of Technology, Czech Republic). 2015.

[119] Anitha R, Siva Sundhara Raja D. Development of computer-aided approach for brain tumor detection using random forest classifier. International Journal of Imaging Systems and Technology. 2018 Mar;28(1):48-53.

[120] Bradley PS, Bennett KP, Demiriz A. Constrained k-means clustering. Microsoft Research, Redmond. 2000 May.

[121] Na S, Xumin L, Yong G. Research on k-means clustering algorithm: An improved k-means clustering algorithm. In2010 Third International Symposium on intelligent information technology and security informatics 2010 Apr 2 (pp. 63-67). Ieee.

[122] Ragab DA, Sharkas M, Marshall S, Ren J. Breast cancer detection using deep convolutional neural networks and support vector machines. PeerJ. 2019 Jan 28;7:e6201.

[123] Narkhede S. Understanding auc-roc curve. Towards Data Science. 2018 Jun;26(1):220-7.

[124] Bradley AP. The use of the area under the ROC curve in the evaluation of machine learning algorithms. Pattern recognition. 1997 Jul 1;30(7):1145-59.

[125] Vujović Z. Classification model evaluation metrics. International Journal of Advanced Computer Science and Applications. 2021;12(6):599-606.

[126] Hamiane M, Saeed F. SVM classification of MRI brain images for computer-assisted diagnosis. International Journal of Electrical and Computer Engineering. 2017 Oct 1;7 (5):2555.

[127] The Whole Brain Atlas [Internet]. www.med.harvard.edu. [cited 2021 Aug 6]. Available from: https://www.med.harvard.edu/aanlib/

[128] Azam MA, Khan KB, Aqeel M, Chishti AR, Abbasi MN. Analysis of the MIDAS and OASIS biomedical databases for the application of multimodal image processing. InInternational Conference on Intelligent Technologies and Applications 2019 Nov 6 (pp. 581-592). Springer, Singapore.

[129] OASIS Brains - Open Access Series of Imaging Studies [Internet]. www.oasis-brains.org. [cited 2021 Aug 18]. Available from: https://www.oasis-brains.org/

[130] Varuna Shree N, Kumar TN. Identification and classification of brain tumor MRI images with feature extraction using DWT and probabilistic neural network. Brain informatics. 2018 Mar;5(1):23-30.

[131] Haralick RM, Shanmugam K, Dinstein IH. Textural features for image classification. IEEE Transactions on systems, man, and cybernetics. 1973(6):610-21.

[132] Quinlan JR. Induction of decision trees. Machine learning. 1986 Mar;1(1):81-106.

Appendices

Appendix A

In this appendix, the first model (identification with a hybrid feature extraction method based on discrete wavelet transform and principle component analysis) is illustrated through the following figures:

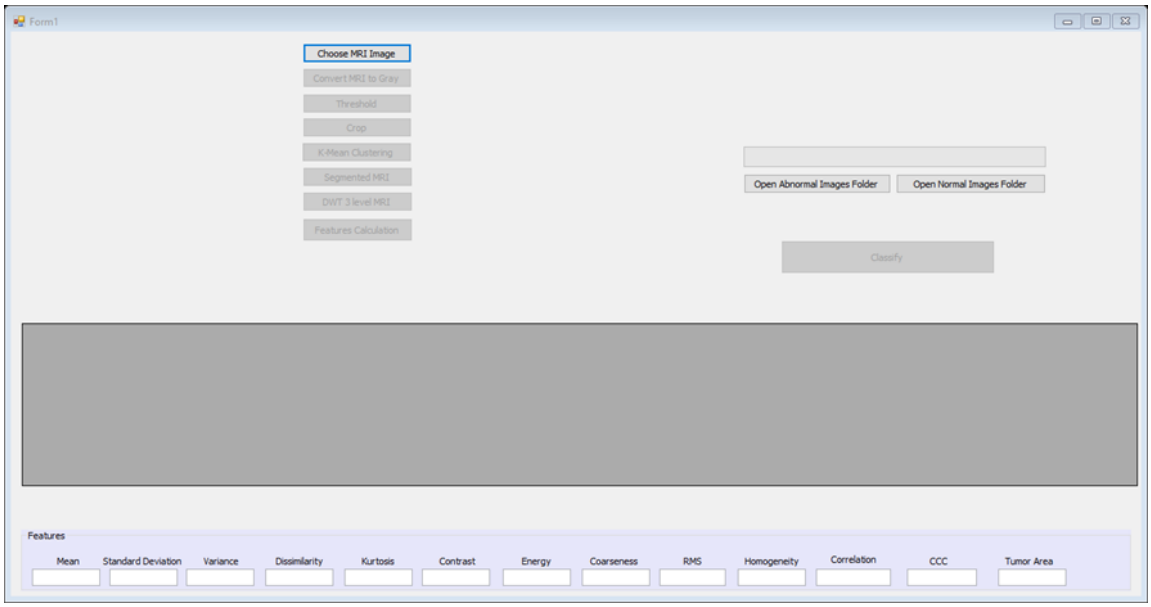

Figure A. 1 The main form of the first model

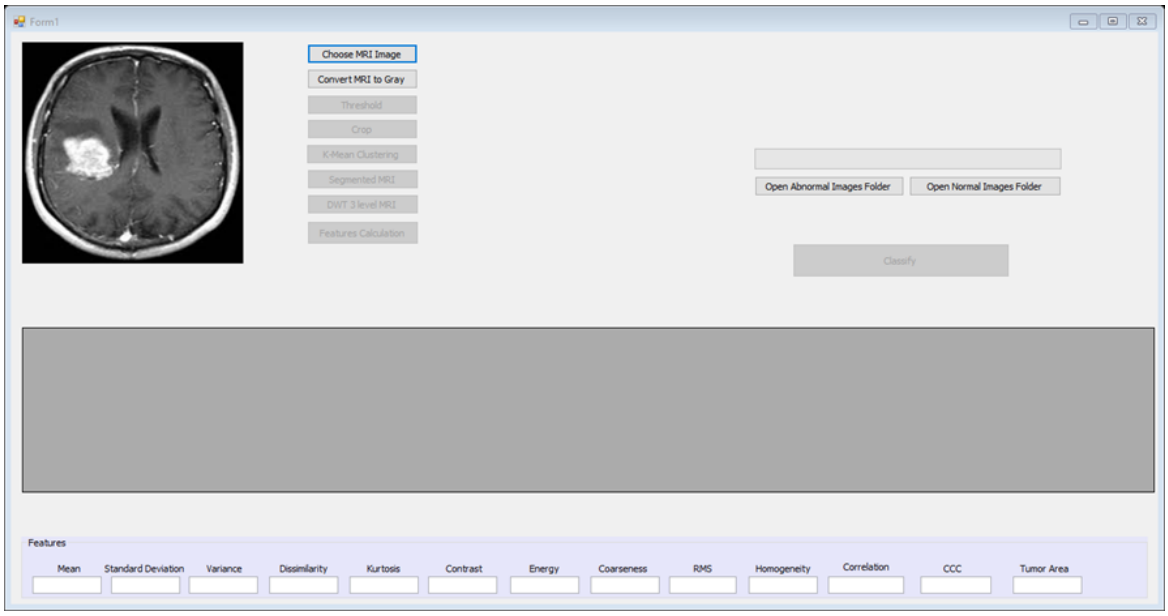

Figure A. 2 Open an MRI image

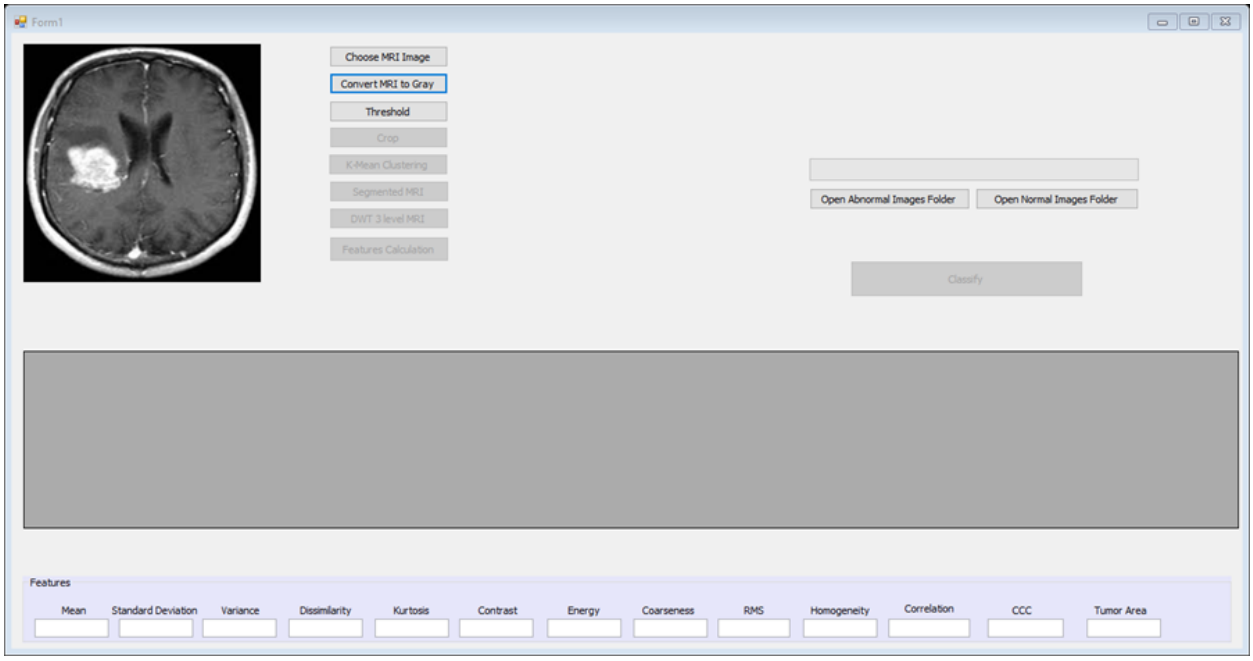

Figure A. 3 Converting MRI to gray scale image

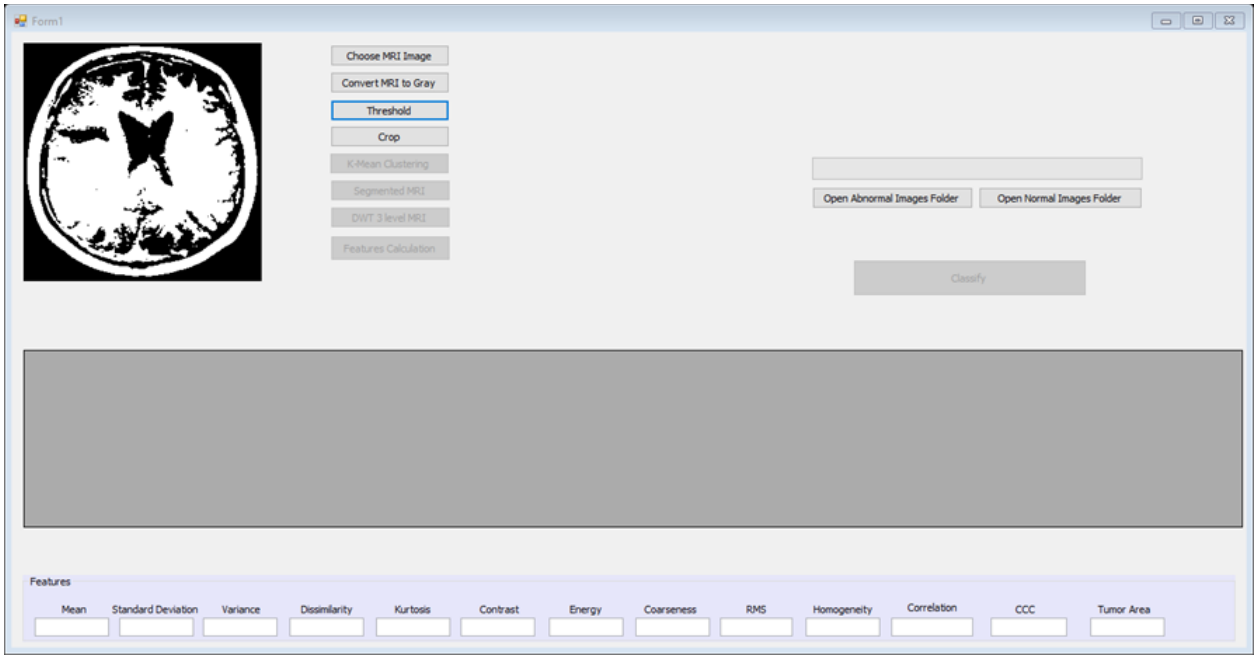

Figure A. 4 Thresholding step

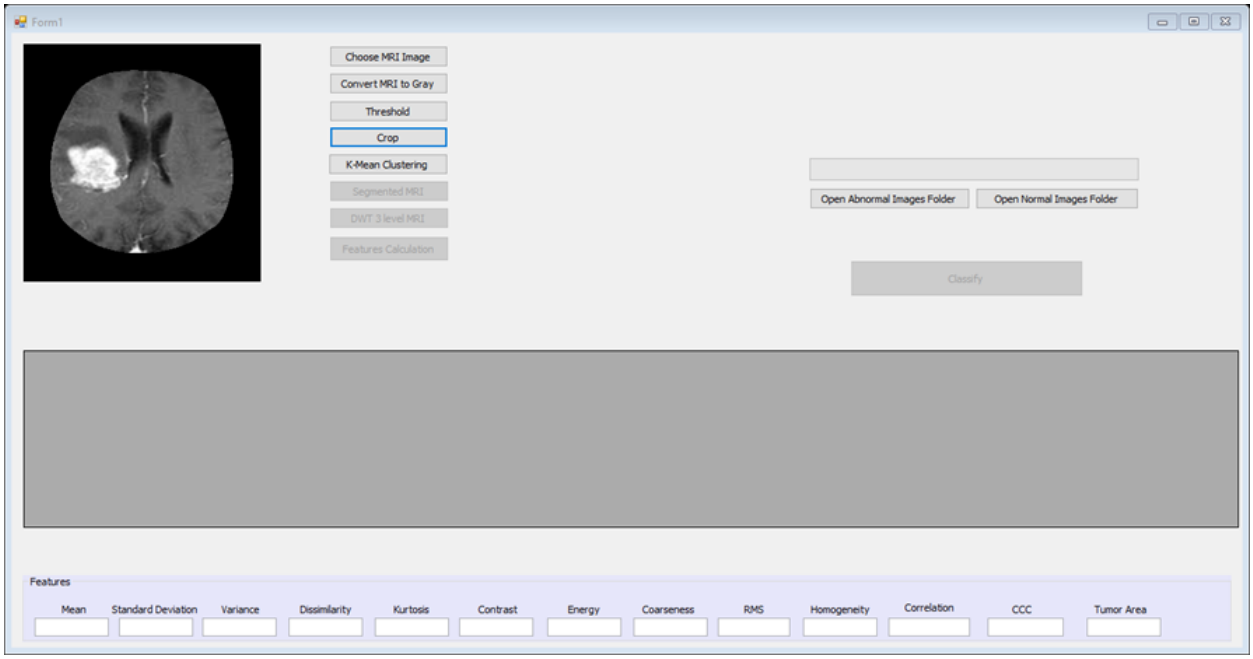

Figure A. 5 Skull removing step

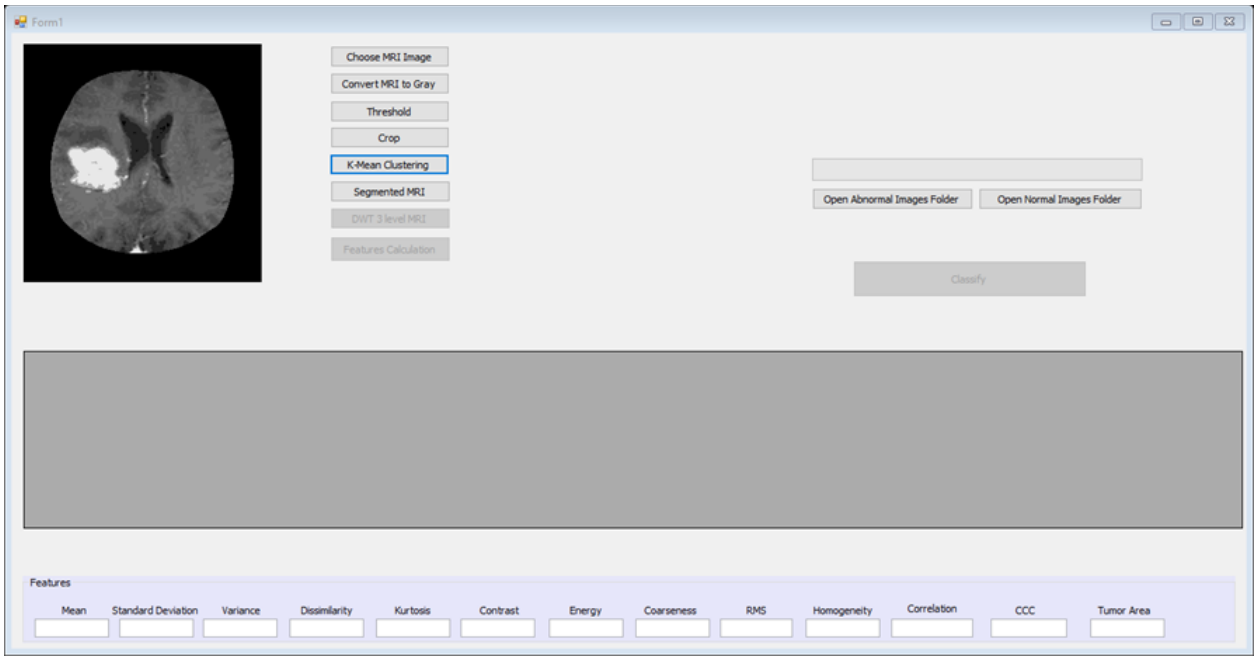

Figure A. 6 K- means step

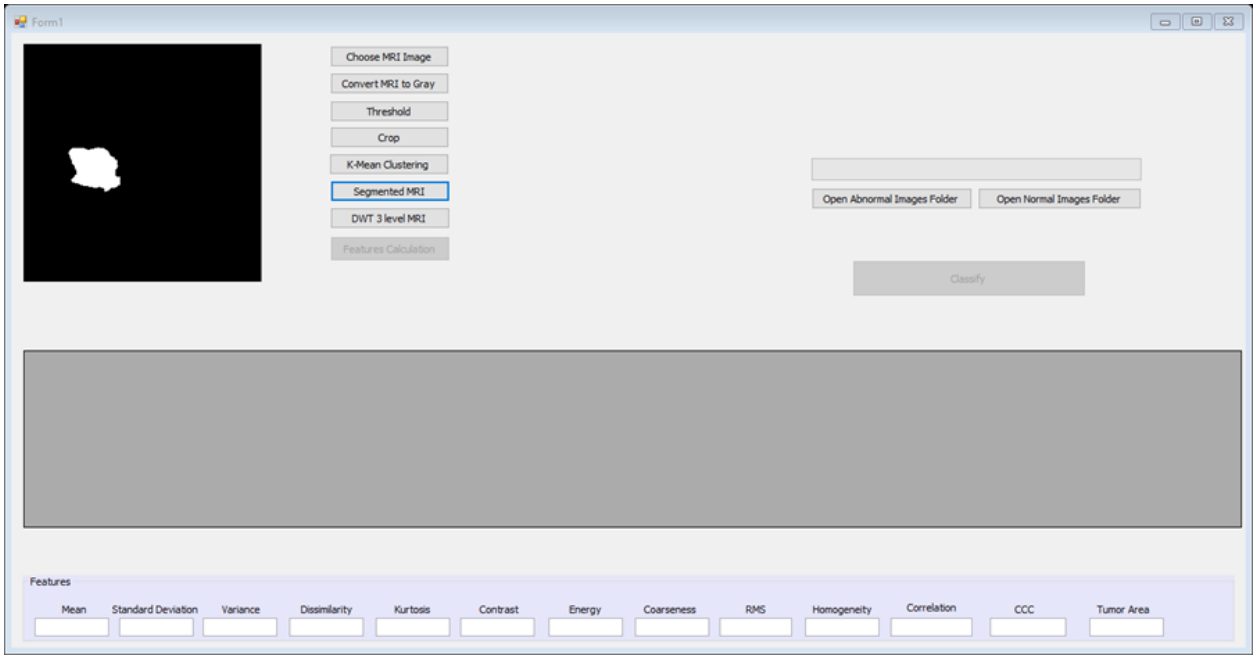

Figure A. 7 Segmentation step

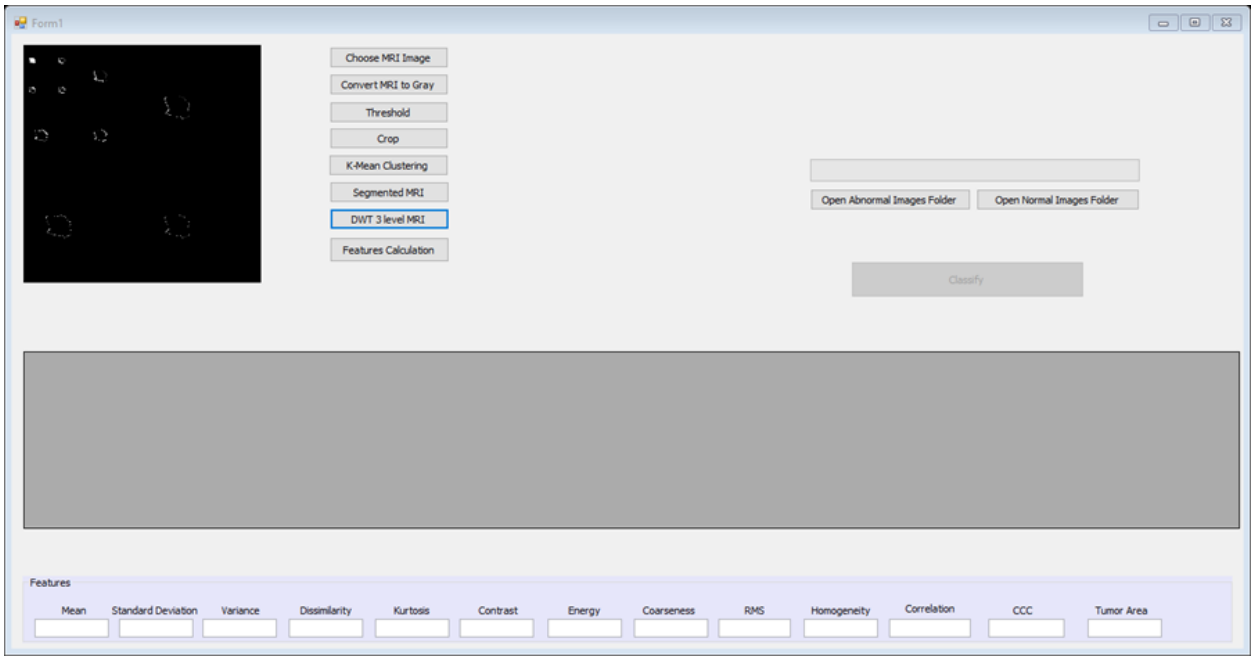

Figure A. 8 DWT step

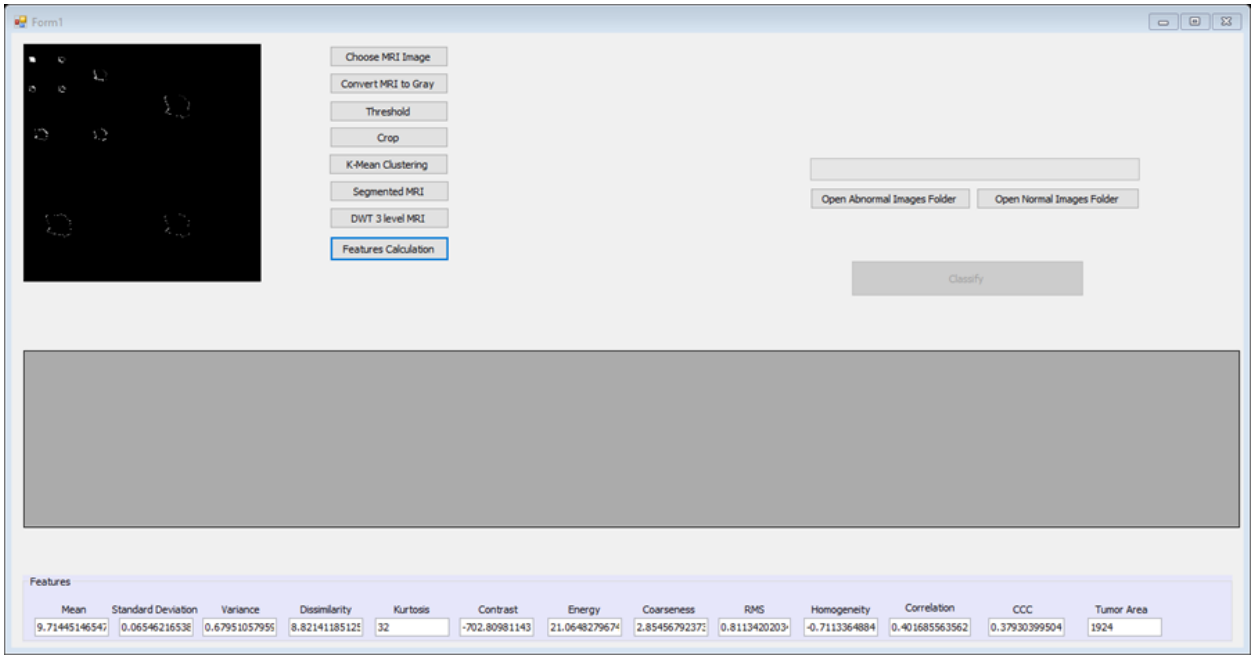

Figure A. 9 Feature extraction step for one sample

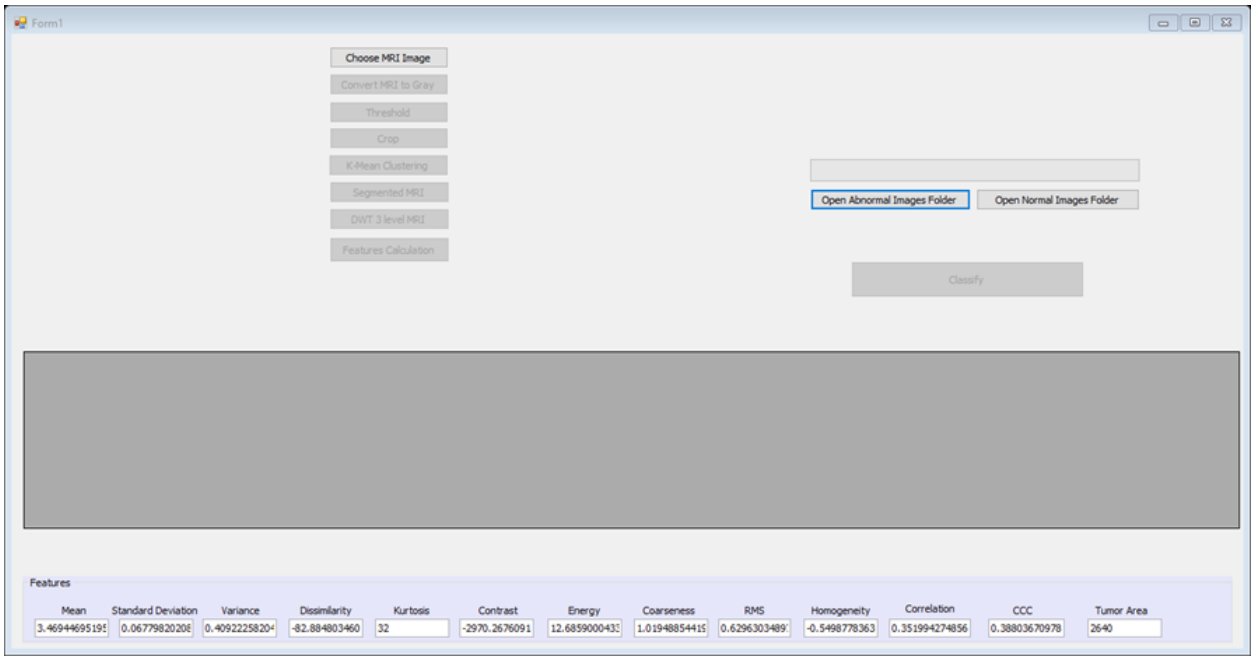

Figure A. 10 Data loading and features extraction for the dataset

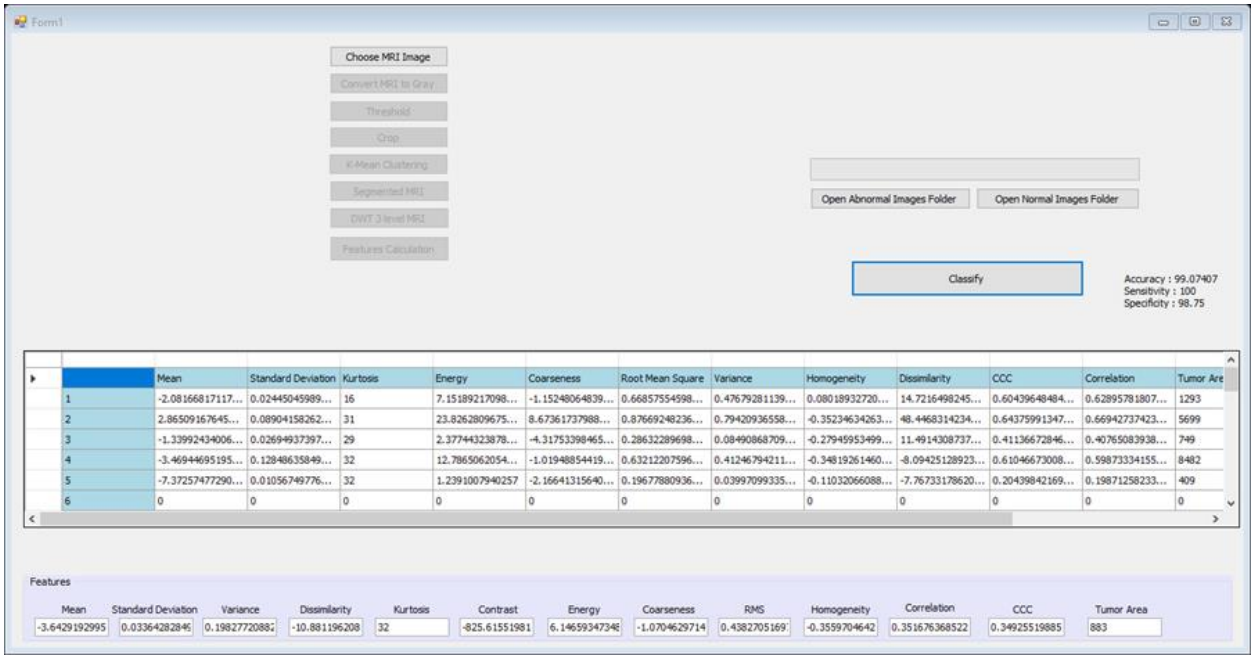

	Mean	Standard Deviation	Kurtosis	Energy	Coarseness	Root Mean Square	Variance	Homogeneity	Dissimilarity	CCC	Correlation	Tumor Are
1	-2.08166817117...	0.02445045989...	16	7.15189217098...	-1.15248064839...	0.66857554598...	0.47679281139...	0.08018932720...	14.7216498245...	0.60439648484...	0.62895781807...	1293
2	2.86509167645...	0.08904158262...	31	23.8262809675...	8.67361737988...	0.87669248236...	0.79420936558...	-0.35234634263...	48.4468314234...	0.64375991347...	0.66942737423...	5699
3	-1.33992434006...	0.02694937397...	29	2.37744323878...	-4.31753398465...	0.28632289698...	0.08490868709...	-0.27945953499...	11.4914308737...	0.41136672846...	0.40765083938...	749
4	-3.46944695195...	0.12848635849...	32	12.7865062054...	-1.01948854419...	0.63212207596...	0.41246794211...	-0.34819261460...	-8.09425128923...	0.61046673008...	0.59873334155...	8482
5	-7.37257477290...	0.01056749776...	32	1.2391007940257	-2.16641315640...	0.19677880936...	0.03997099335...	-0.11032066088...	-7.76733178620...	0.20439842169...	0.19871258233...	409
6	0	0	0	0	0	0	0	0	0	0	0	0

Mean	Standard Deviation	Variance	Dissimilarity	Kurtosis	Contrast	Energy	Coarseness	RMS	Homogeneity	Correlation	CCC	Tumor Area
-3.6429192995	0.0336428246	0.1982772088	-10.881196208	32	-825.61551981	6.1465934734E	-1.0704629714	0.4382705169	-0.3559704642	0.351676368522	0.34925519885	883

Figure A. 11 Classification step

Appendix B

In this appendix, the second model (Segmentation from magnetic resonance image using Optimized thresholded difference algorithm and Rough Set theory) is illustrated through the following figures:

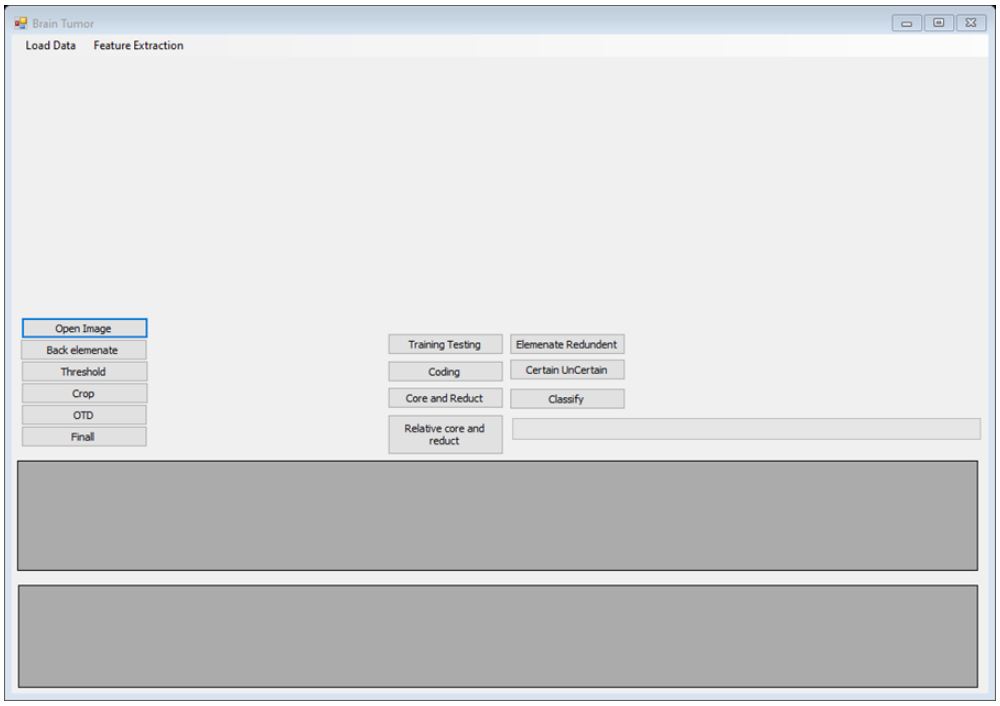

Figure B. 1 The main form of the Second model

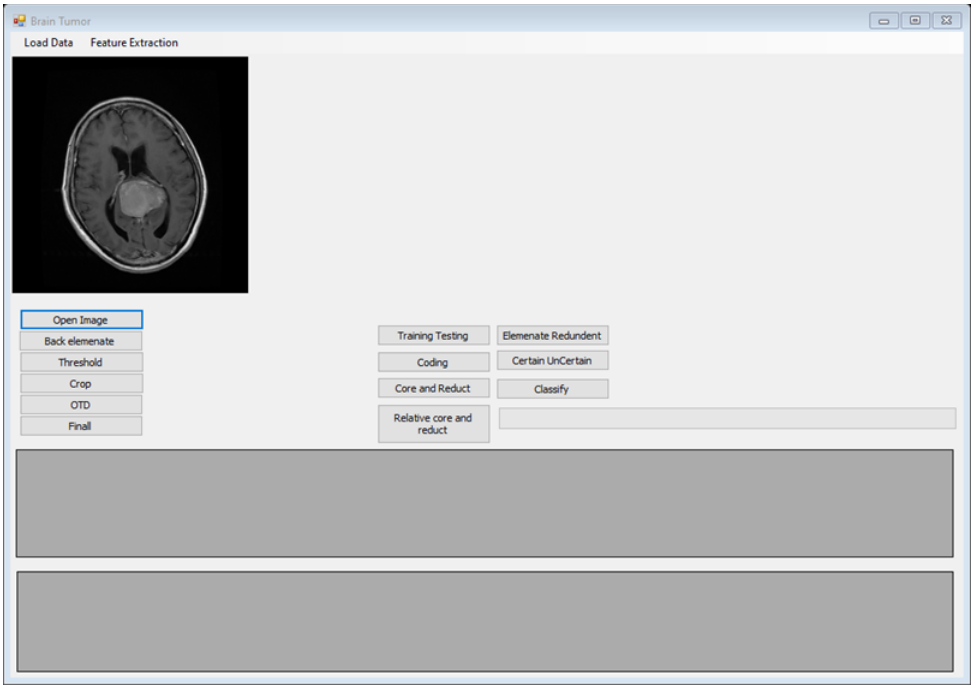

Figure B. 2 Open an MR image

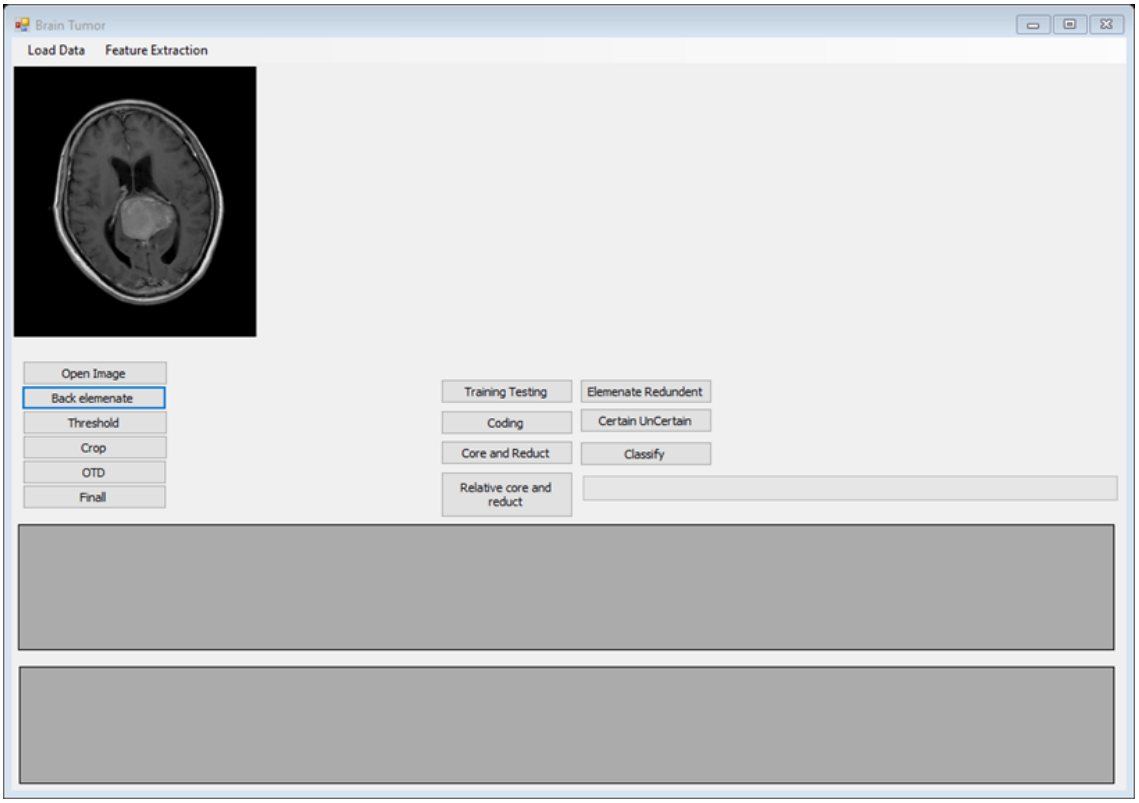

Figure B. 3 Preprocessing step (background padding)

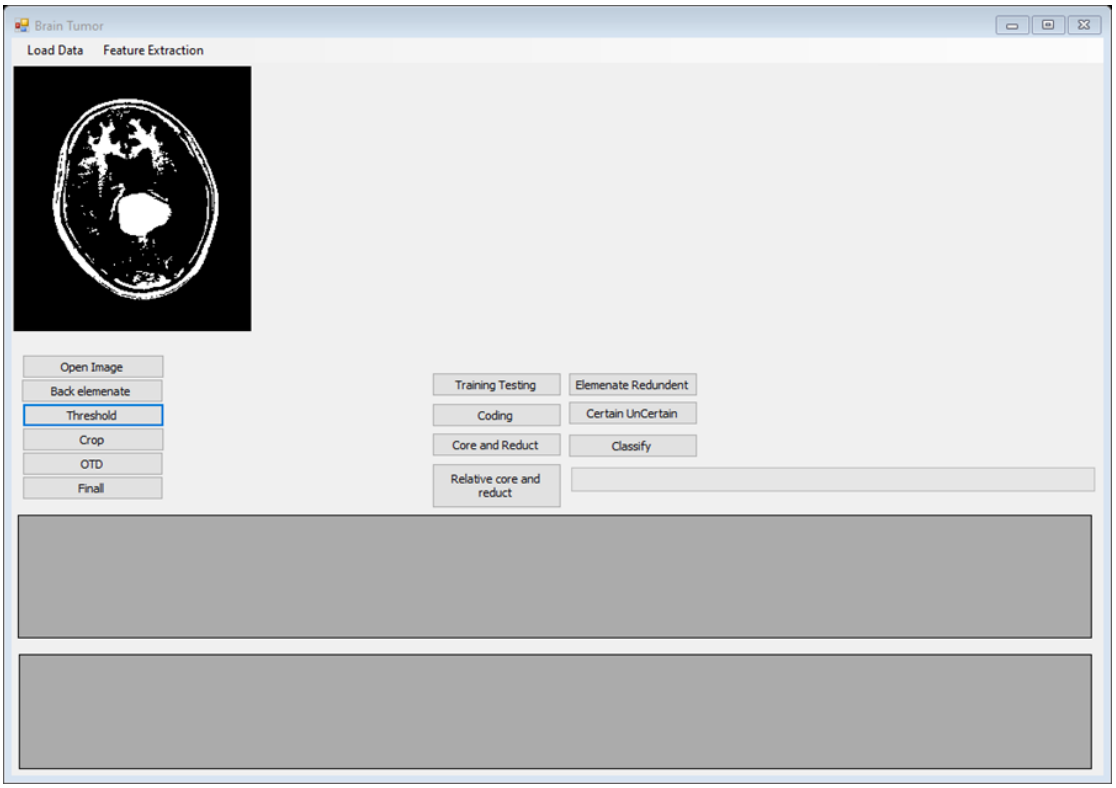

Figure B. 4 Skull identification step

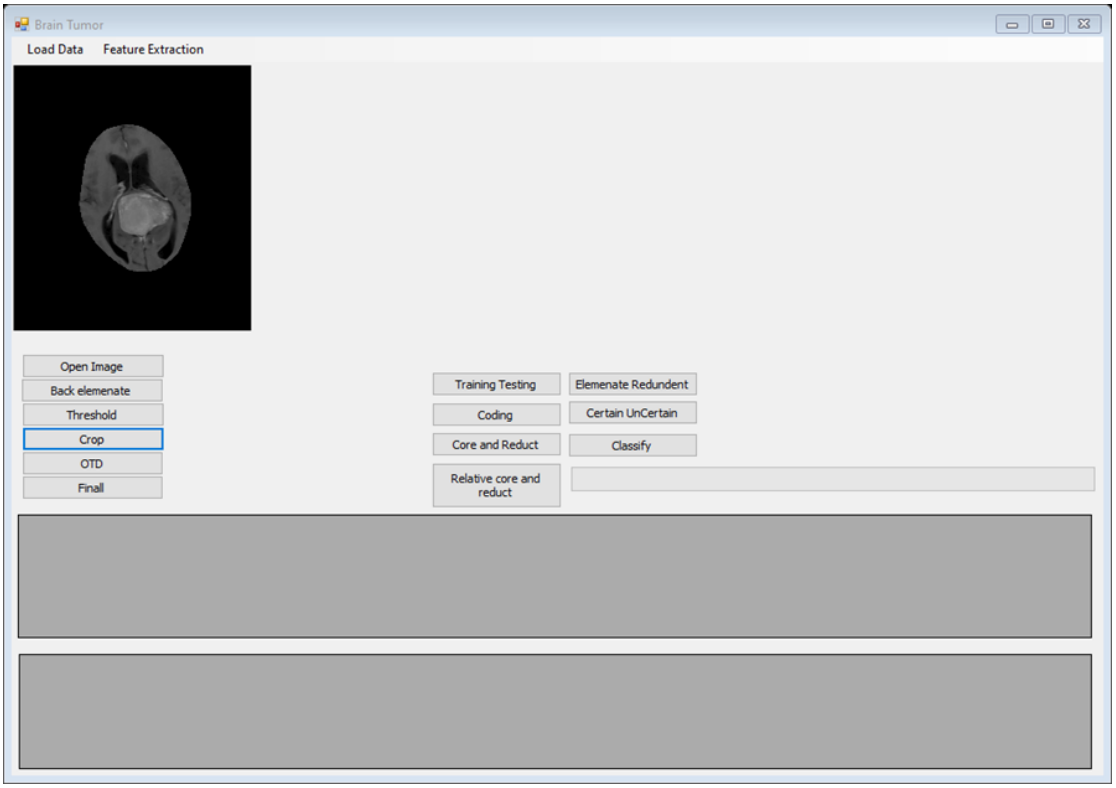

Figure B. 5 Skull removing step

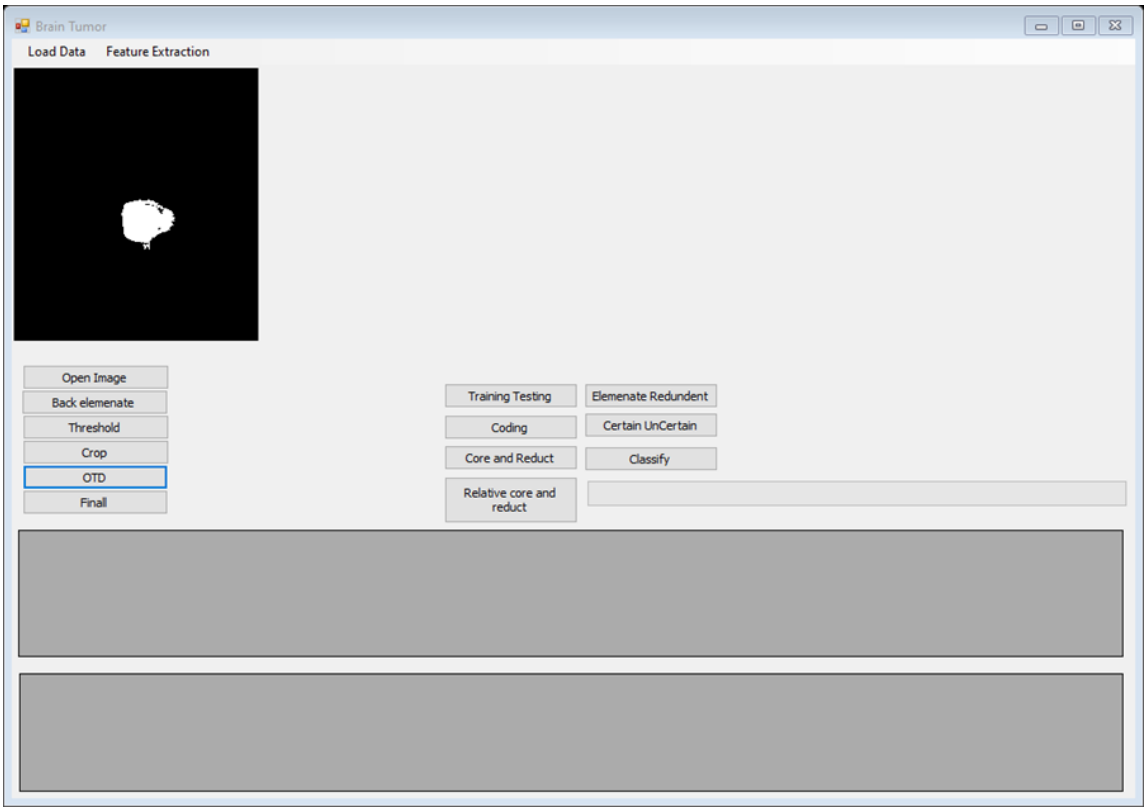

Figure B. 6 Pre segmentation step

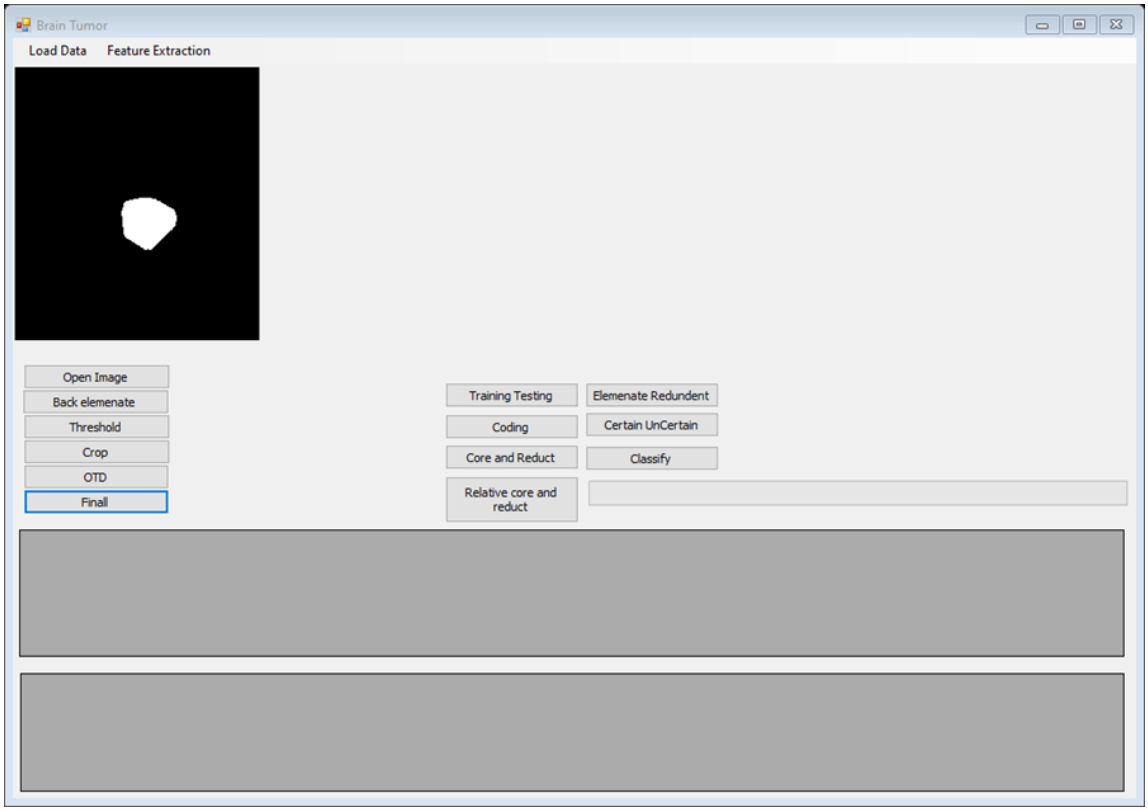

Figure B. 7 Final segmentation results

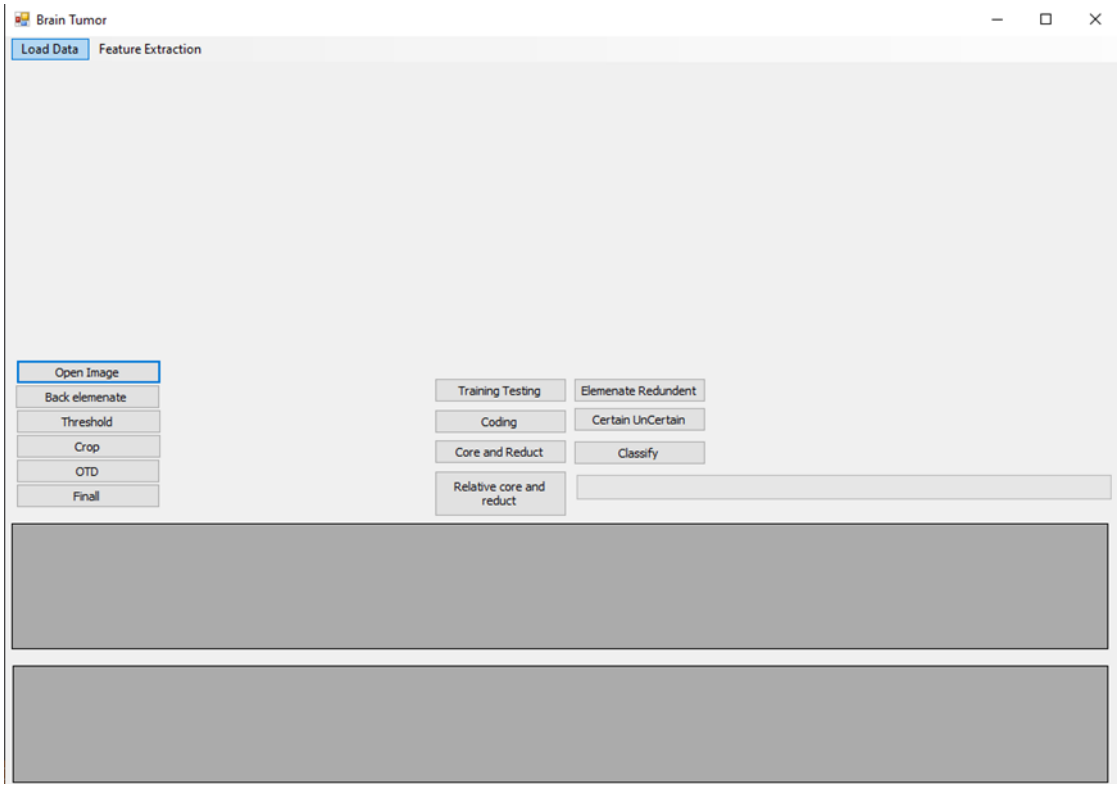

Figure B. 8 Dataset loading

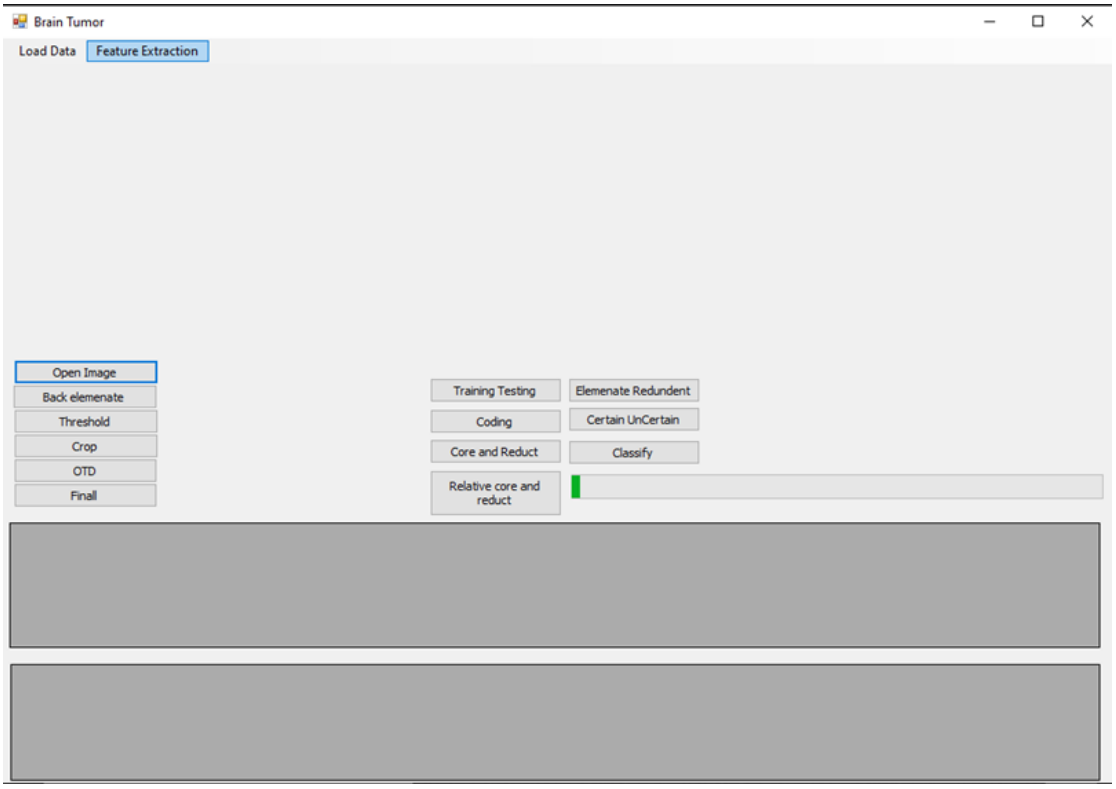

Figure B. 9 Features extraction for the loaded dataset

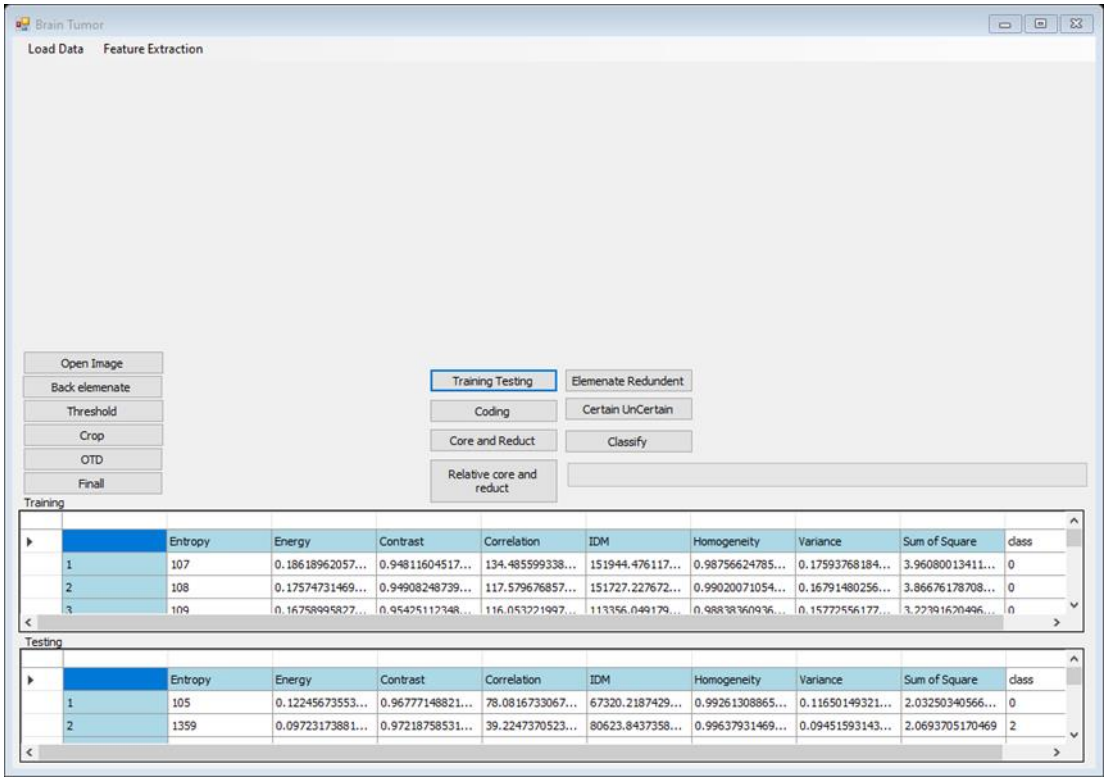

Figure B. 10 Splitting data (testing and training)

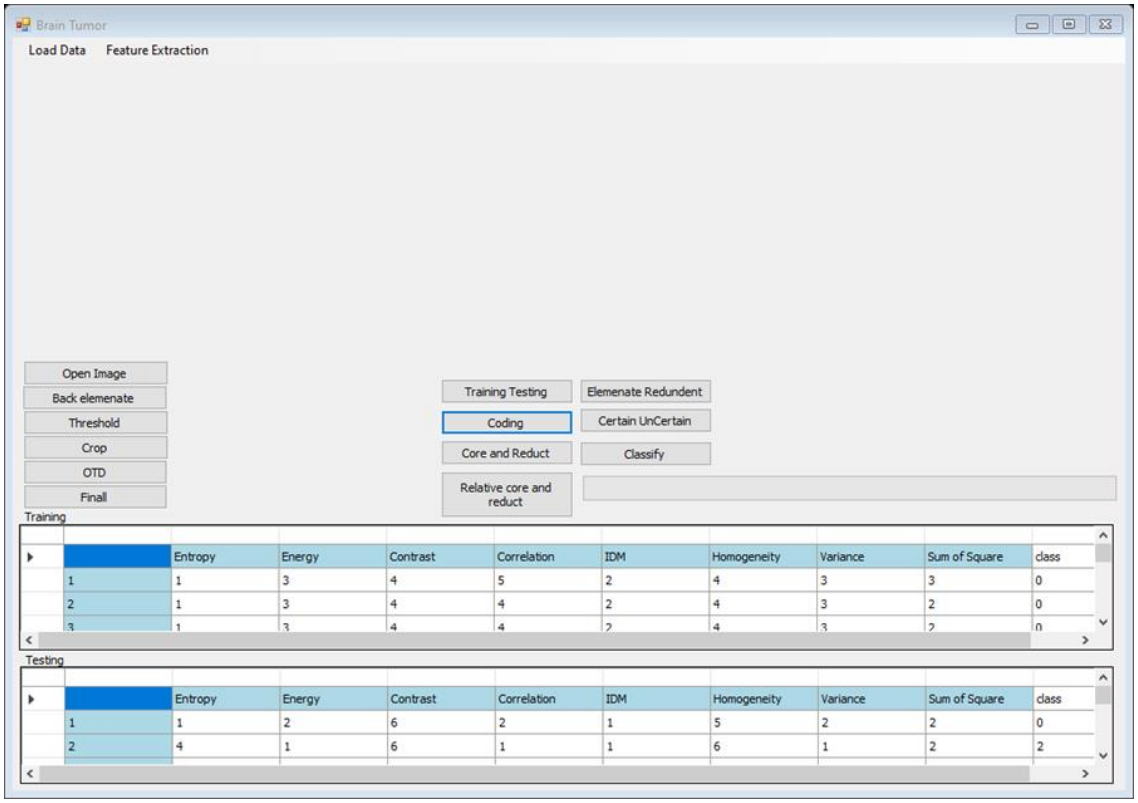

Figure B. 11 Data coding

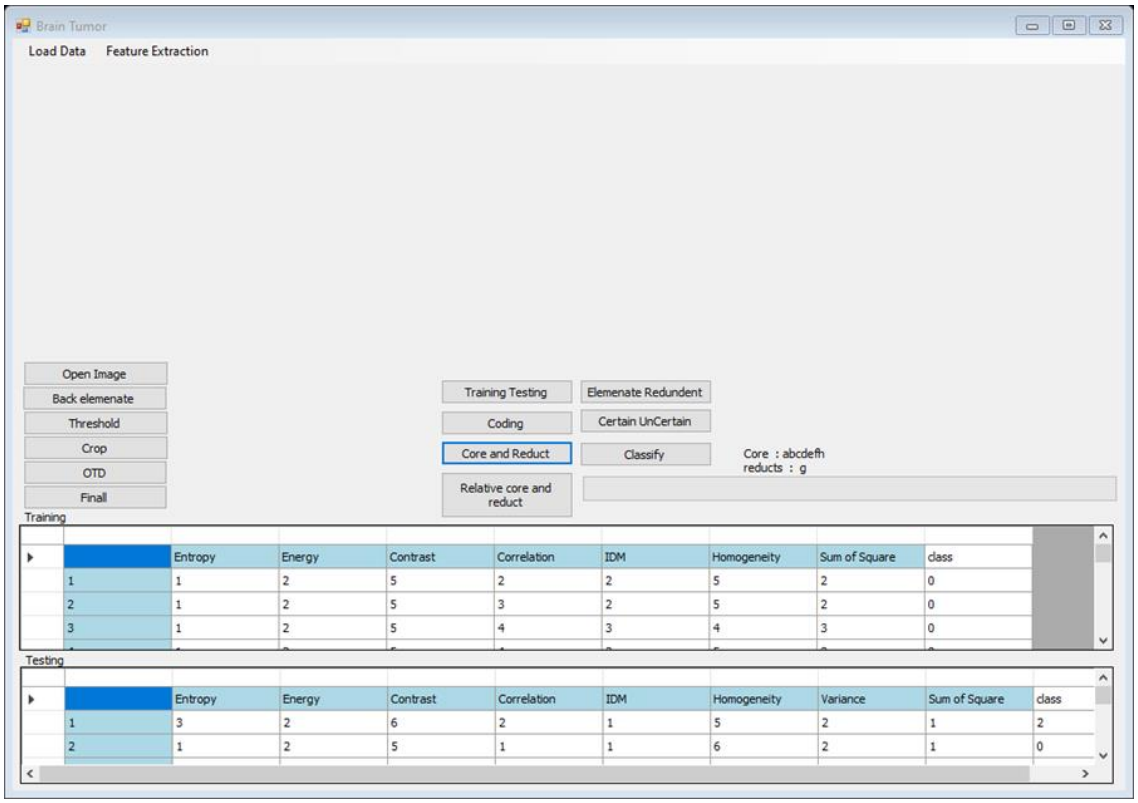

Figure B. 12 Find core and reduct step

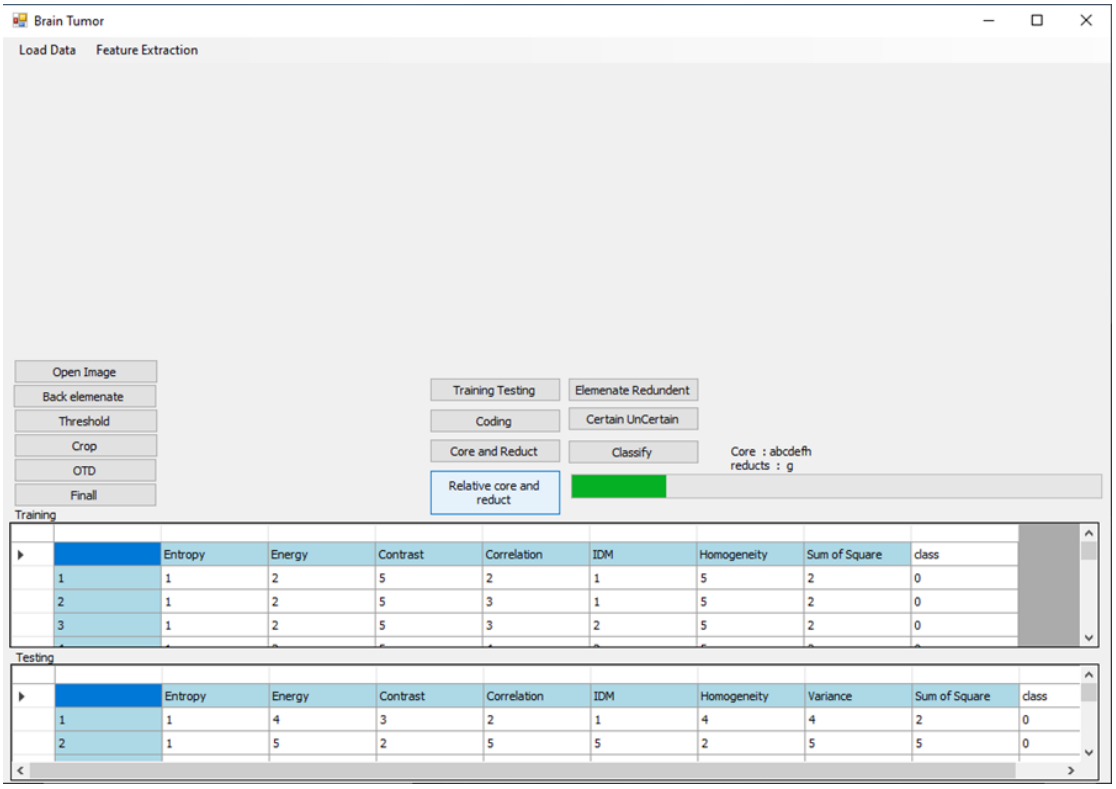

Figure B. 13 Relative core and reduct step

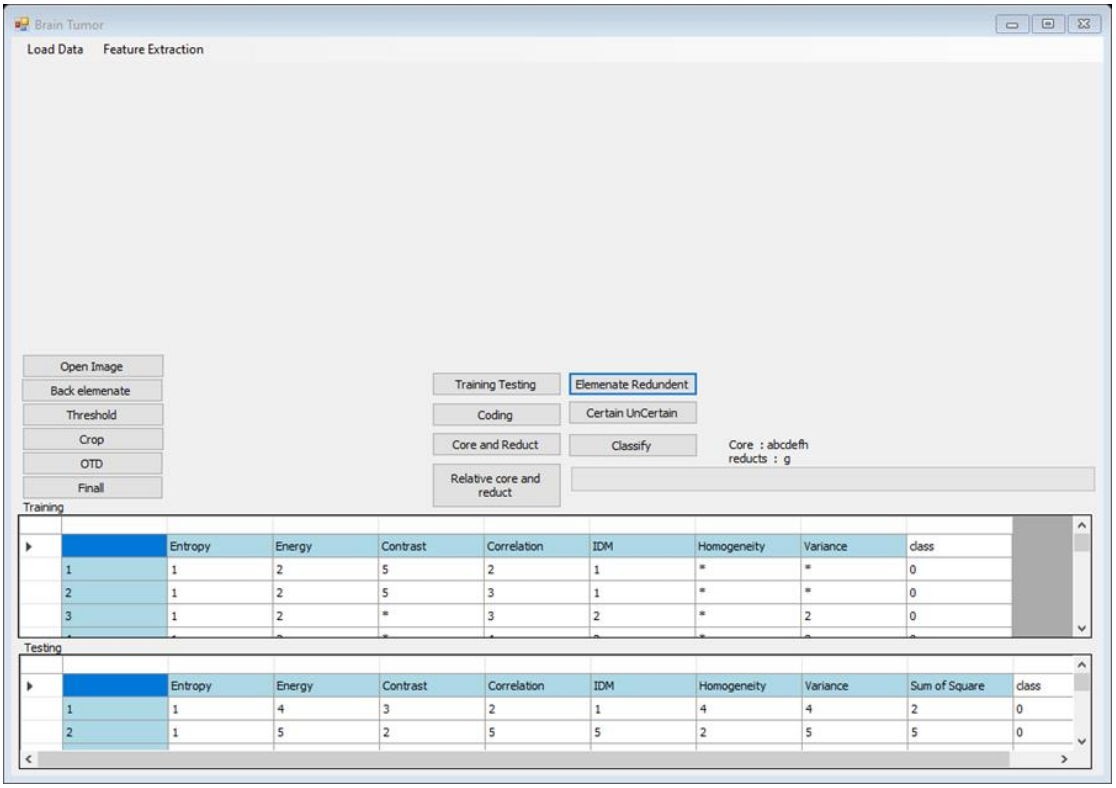

Figure B. 14 Eliminate redundant step

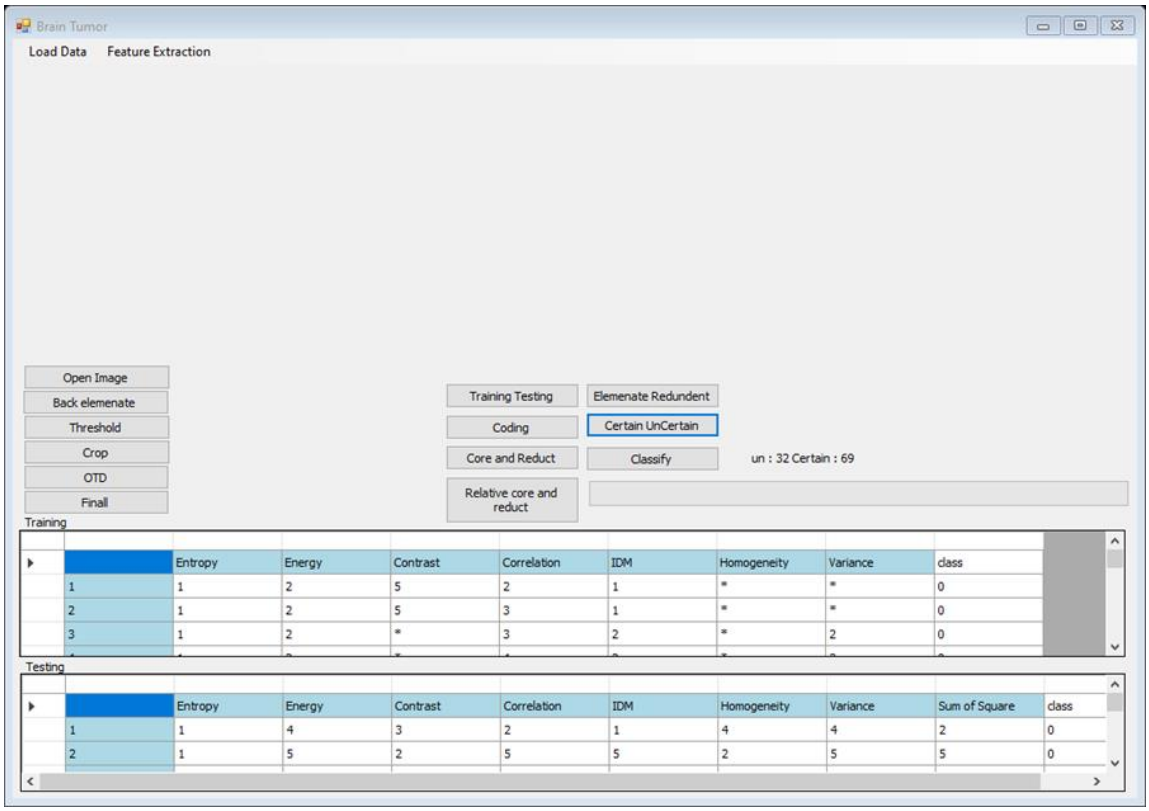

Figure B. 15 Certain uncertain splitting step

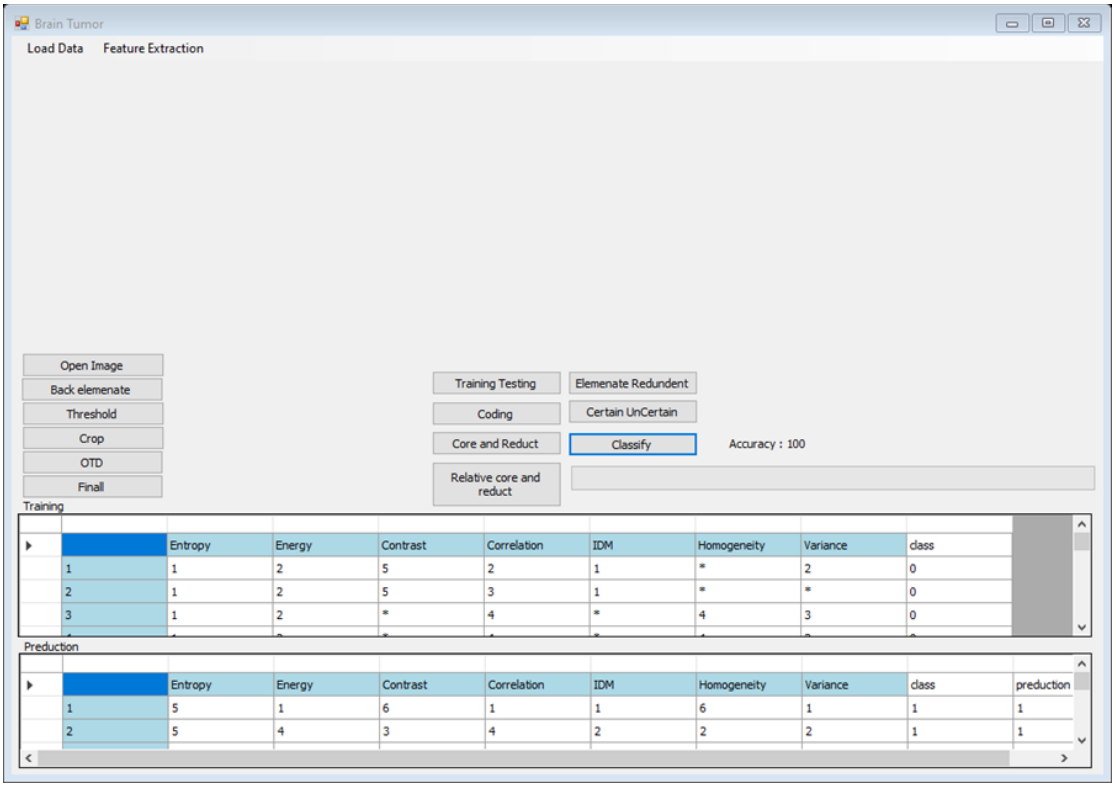

Figure B. 16 Classification step

حکومەتی هەرێمی کوردستان
وەزارەتی خوێندنی باڵا و توێژینەوەی زانستی
زانکۆی سلێمانی
کۆلێجی زانست

دەستنیشانکردنی یارمەتیدەری کۆمپیوتەر بۆ زوو دیاریکردنی وەرەمی مێشک

تێزی دکتۆرایە
پێشکەشکراوە بە ئەنجومەنی کۆلێجی زانست لە
زانکۆی سلێمانی وەك بەشێك لە پێداویستیەکانی بەدەست
هێنانی بڕوانامەی دکتۆرای فەلسەفە لە
(زانستی کۆمپیوتەر)
پڕۆسێسکردنی وێنە

لە لایەن

دالیا محمد توفیق

ماستەر لە تەکنەلۆجیای زانیاری (2011)، زانکۆی جواهرلال نهرو حیدراباد

بە سەرپەرشتی

د. علی مکی صغیر
پرۆفیسۆر

د. هادی وەیسی
پرۆفیسۆری یاریدەدەر

ئۆکتوبر 2022

ڕەزبەر 2722

پوختەی تێز

گرێی مێشك پێناسە ئەكرێت وەكو شانەیەكی نائاسایی كە كاریگەری دەكاتە سەر ناوەندی سیستمی دەماری (CNS)، مێشك و دڕكە پەتك كە دەبێتە هۆیی تێكچوونی كاركردنی هەندێك لە چالاكییەكانی مێشك. ئەتوانین گرێی مێشك دابەش بكەین بۆ دوو جۆری سەرەكی كەبریتین لە جۆری بێ زیان یاخود باش (benign) وە جۆری كوشندە شێرپەنجەیی (malignant) لەسەر بنەمایی سروشتی شەڕەنگێزی وخراپیەكەی. ئەوەی پێشوو یان پێی دەوترێت گرێی مێشكی بێ زیان كەهیچ خانەیەكی شێرپەنجەی تیادا نییە ووردە ووردە گەشە ئەكات ، سنووردێكی جیاوازی هەیە.ئەوەی كۆتاییان پێدەوترێت گرێی شێرپەنجەیی خراپی مێشك كە شەڕانگێزو خراپترە لە جۆری یەكەم وە ئەم جۆرە خانەی شێرپەنجەی تیادایەو سنووردێكی دیاریكراوی نییە . ئەم جۆرە گرێیە ئەتوانێت زۆر بەخێرایی بلاّوببێتەوە و زیان بەخانەكانی نزیكی خۆیی بگەیەنێت . جۆری جیاواز لەپشكنینی وێنەیی (سكان) هەیە كە بەتایبەتی بەكاردێن بۆ دەستنیشانكردنی گرێی مێشك. بەلاّم جۆرە زیاتر باوەكانی پشكنینی وێنەیی كە بەكاردێت بۆ ناسینەوەو دەستنیشانكردنی نەخۆشییەكانی مێشك بریتین لە وێنەی برِگەیی بە دەردانی پۆزیترۆنی (ئەلیكترۆنی بارگە موجەب) (PET)، وێنەگری دەماری، هێلّكاری مۆخ، وێنەی برِگەیی كۆمپیوتەری، (CT) وە جۆری وێنەگرتن بە لەرینەوەی موگناتیسی (MRI) ، ئەم جۆرە وێنانە زۆر كاریگەرن لە پێشكەش كردنی ووردەكاری بنەڕەتی سەبارەت بە بوون و شوێنی گرێیەكە. جۆری (MRI) باوترە بۆ دەستنیشانكردن لە جیاتی جۆری تیشكی ئێكس X-rays، (MRI) شەپۆلی ڕادیۆیی و بواری موگناتیسی بەهێز بەكاردێنێت پشكنینی (MRI)خوازراوترە بە بەراورد بە شێواز و تەكنیكەكانی تری وێنەگرتن لەبەرئەوەی بلاّونابێتەوە وكاریگەری شێرپەنجەیی نییە و لەڕووی ئابووریەوە تێچوویی كەمترە و دەركەوتنێكی ڕوونی هەیە بۆ گرێ شێرپەنجەییەكان، هەروەها (MRI) پێویستی بە كاتێكی كەمترە بۆ پشكنینی وێنەیی تەوای جەستە بەراورد بە PET و تیشكی ئێكس X-rays ، سەرەڕای ئەوە ی وێنەیەكی ووردتری پێكهاتەی ئێسك و ئەو ئەندامانەی كە لە پشتەوەن و شاراوەن وەكو مێشك كە لەژێر كاسەی سەردایە و سییەكان كە لەناو ئێسكی پەراسوودایە. شیكردنەوە و خوێندنەوەی بەشە سەرەكییەكانی وێنەی (MRI) بەشێوەی دەستی و لەلایەن ستافی پزیشكیەوە كاتێكی زۆری ئەوێت و ئەركێكی زۆری ئەوێت لەوەش زیاتر پرۆسەیەكی قورسە كاتێك

پێداچوونەوە و لێکدانەوە بۆ بڕێکی زۆر لە زانیاری دەکرێت لەگەڵ فراوانی و جۆراوجۆری شێوەی دەرکەوتنی شانەکانی گرێی مێشك هەربۆیە سیستمی خودکاری بۆ پۆلێنکردنی گرێ شێرپەنجەییەکان کارێکی بنەڕەتییە بۆ هاوکاریکردنی پسپۆرانی بواری تیشك وپزیشکان بە گشتی بۆناسینەوەی گرێ شێرپەنجەییەکان.

سیستمی دەستنیشانکردن بەیارمەتی کۆمپیوتەر (CAD) ئامرازێکی ناسینەوەی نەخشەییە کە یارمەتی پزیشکان و پسپۆرانی تیشك ئەدات بۆ دەستنیشانکردنێکی وورد. هەر بەهۆی سەختی لە شیکردنەوەی زانیاریە پزیشکییەکان (وینە ، هێما) و پشتبەستن بە شارەزایی پزیشك کارێکی قورسە، بۆیە سیستمی CAD گرنگە و سەرکەووتوە لە شیکردنەوەی وێنە پزیشکییەکان، دەرهێنانی تایبەتمەندییەکان و دەستنیشانکردن لە هەنگاوە بنەڕەتییەکانە.ژمارەیەك لە شێواز و ڕێگای دەرهێنان و جیاکردنەوەی تایبەتمەندی سەرنجڕاکێش هەیە بۆ پۆلێنکردنی گرێی مێشك لە وێنەی (MRI) لە چاپکراوەکاندا. تایبەتمەندییەکانی پێکهاتەو گۆڕینی شەپۆلی جیاکراوە دوو شێواز و ڕێگایە بۆ دەرهێنانی تایبەتمەندییەکان کە زۆرجار بەکاردەهێنرێن. ئەم تێزە دوو شێوازی کارکردنی پێشکەش کردووە کە بەم شێوەیەی لای خوارەوە پۆلێنکراوە:

- لە ڕێگاو شیوازی یەکەمدا ئەم تێزە تەکنیکێکی پێشکەش کردووە بۆ پۆلێنکردنی وێنەی (MRI) مێشك بۆ ئاسایی و نائاسایی ، ئەم شێوازە و تەکنیکە پێشنیارکراوە تایبەتمەندی دەرهێنانی تێکەڵاو بەکارهێناوە بۆ گەشەدان بە ئەنجامی پۆلێنکردنەکە، ئەم شێوازە سێ هەنگاو لە خۆدەگرێت یەکەم: گۆڕینی شەپۆلی جیاکراوەی 3 ئاستی (DWT) بەکار هاتووە، دووەم: شیکاری پێکهاتەی بنەڕەتی (PCA) بە کارهاتووە بۆ کەمکردنەوەی قەبارەی تایبەتمەندییەکان،لەکۆتایبدا تابەتمەندییەکان دەرهێنرا بە بەکارهێنانی ماتریکسی هاوڕوودانی ئاستی خۆڵەمێشی (GLCM) لەبەشەکانی (PCA). پۆلێنکەری دارستانی هەڕەمەکی (RF) بەکارهێنرا لەگەڵ دەستنیشانکردنی تایبەتمەندی بۆ ناسینەوە،پاشان بۆ هەڵسەنگاندنی ئەم پرۆژەیە هەندێك وێنەی (MRI) کۆکرایەوە (81 ئاسایی و 100 نائاسایی). ئەنجامە تاقیکارییەکان ڕێژەی 98.3٪ ووردی و دروستی بەدەست هێناوە هەروەها ڕێژەی هەستیاری بەدەست هاتوو 99٪ وە ڕێژەیی تایبەتمەندی ئەنجامدراو بەدەست هاتوو 97.6٪ شێوازی پێشنیارکراو کاریگەریەکی بەرزی نیشانداوە بە بەراورد لەگەڵ زۆربەی ئەو توێژینەوانەی تر کە لەم بوارەدا نووسراون.

- لەڕێگاو شێوازی دووەم ئەم تێزە ڕێگای جیاوازییەکی ئاستدار (OTD) و بیردۆزی کۆمەڵەی زبری (RST) پێشکەش کردووە بۆ پارچەکردنی وێنەی گرێیی مێشك بەشێوەیەکی ئۆتۆماتیکی. لەم شێوازە دا دوو قۆناغ هەیە: لەقۆناغی یەکەمدا پارچەکردنی ڕووبەری ناوچەکانی مێشك و ناسینەوەی کاسە سەر لەخۆ ئەگرێت بۆ باشترکردنی پارچە کردنەکە، ئەم قۆناغە بریتیە لەپارچە کردنی ڕووبەری ناوچەکانی مێشك و جیاکردنەوەی لە کاسەی سەر. قۆناغی دووەمیش بریتی یە لەدووئاست :لەئاستی یەکەمدا دروستکردنی وێنەیەکی ڕووپۆشکراو (overlay image) کە بریتیە لەتێکڕایی چڕی هەموو ئەوخاڵانەی ڕووبەری مێشك کەلەقۆناغی یەکەمدا بەش بەشکراون. بۆئاستی دووەمیش جێبەجێکردنی لەنێوان ڕووبەری مێشك و وێنەی ڕووپۆشکراو پشت بەست بە چوارچێوەیەکی دیاری کراو. بە بەکارهێنانی ماتریکسی هاوڕوودانی ئاستی خۆڵەمێشی (GLCM) بۆ دەرهێنانی تایبەتمەندیەکان لە وێنە پارچەکراوەکان، پاشان بەکارهێنانی (RST) بۆ تایبەتمەندیە دەرهێنراوەکان و باشترکردنی کارە ئەنجامدراوەکە. هەر بۆ هەڵسەنگاندنیش وێنەی داتابەیسی Figshare بەرزکراوە بە کێشی T1، لەگەڵ وێنەی 233 نەخۆش وەرگیرا کە سێ جۆر گرێیی مێشکیان هەبوو : (93 توێ) گرێی پەردەی مێشك (meningioma) ، (103 توێ) گرێیی دەمارەخانەکان (glioma) ، وە (56 توێ) گرێی ڕژێنی مۆخ (Pituitary). ئەنجامە تاقیکارییەکان ووردی بەرزیان نیشاندا وە بەگشتی ڕێژەی ووردی و دروستی 98.9٪ بەدەست هاتووە بەراورد بە هەموو ئەوتوێژینەوانەی پێشوو کە لەسەر هەمان داتا ئەنجامدرابو.

حكومة اقليم كوردستان
وزارة التعليم العالي و البحث العلمي
جامعة السليمانية
كلية العلوم

التشخيص بمساعدة الكمبيوتر للكشف المبكر عن ورم الدماغ

أطروحة

مقدمة الى مجلس كلية العلوم في جامعة السليمانية كجزء من متطلبات نيل شهادة دكتورا فلسفة في (**علوم حاسبات**)

معالجة الصورة

من قبل

داليا مُحَمَّد توفيق

ماجستير في تكنلوجيا المعلومات (2011)،جامعة جواهرلال نهرو حيدراباد

بأشراف

د. علي مكي صغير
أستاذ

د. هادي ويسي
أستاذ مساعد

شوال 1444

آكتوبر 2022

المستخلص

يُعرف ورم الدماغ بأنه أي نسيج غير طبيعي يؤثر على الجهاز العصبي المركزي (CNS) ، الدماغ والحبل الشوكي ، مما يتسبب في حدوث خلل في بعض أنشطة الدماغ. يمكن تقسيم أورام الدماغ إلى نوعين رئيسيين ، هما أورام حميدة وخبيثة ، بناءً على طبيعة عدوانيتها. يُطلق على النوع الأول ورم دماغي حميد لأنه لا يحتوي على خلايا سرطانية ويتطور تدريجياً داخل الدماغ فقط وله حدود مميزة. يسمى النوع الأخر ورم دماغي خبيث وهو أكثر عدوانية من أورام الدماغ الحميدة لأنها تحتوي على خلايا سرطانية تفتقر إلى الحدود. يمكن لهذا النوع من الورم أن ينتشر بسرعة ويلحق الضرر بمناطق الدماغ القريبة. تُستخدم أنواع مختلفة من الفحوصات عادةً لتشخيص أورام الدماغ. تشمل أنواع الفحص الأكثر استخداماً لتحديد أمراض الدماغ التصوير المقطعي بالإصدار البوزيتروني (PET) ، تصوير الأوعية الدموية ، تصوير النخاع ، التصوير المقطعي المحوسب (CT) ، والتصوير بالرنين المغناطيسي (MRI). هذه الصور فعالة للغاية لدرجة أنها قد تقدم تفاصيل أساسية فيما يتعلق بوجود الورم وموقعه. التصوير بالرنين المغناطيسي هو أكثر أنواع الفحص التشخيصي شيوعًا. بدلاً من الأشعة السينية X-ray، يستخدم التصوير بالرنين المغناطيسي موجات الراديو والمجالات المغناطيسية القوية. تُفضل صور التصوير بالرنين المغناطيسي عند مقارنتها بتقنيات التصوير الأخرى لأنها غير جراحية واقتصادية وتوفر تبايناً جيداً لأي أورام دماغية قد تكون موجودة. وقت اكتساب التصوير بالرنين المغناطيسي (مسح كامل للجسم) أقصر من وقت التصوير المقطعي بالإصدار البوزيتروني والأشعة السينية. بالإضافة إلى ذلك ، فإنه يوفر تفاصيل أفضل عن بنية العظام والأعضاء المخفية خلفها ، مثل الدماغ تحت الجمجمة والرئتين خلف الضلوع. تعد معالجة صور التصوير بالرنين المغناطيسي يدوياً على أساس منتظم من قبل الطاقم الطبي مهمة تستغرق وقتاً طويلاً وتتطلب الكثير. علاوة على ذلك ، إنها عملية صعبة عندما يكون هناك كمية كبيرة من البيانات لمراجعتها مع مجموعة متنوعة من مظاهر أورام المخ. يعد نظام تصنيف الأورام الآلي ضرورياً لمساعدة أخصائيي الأشعة والأطباء في تحديد أورام المخ.

يعد نظام التشخيص بمساعدة الكمبيوتر (CAD) أداة للتعرف على الأنماط تُستخدم لمساعدة أخصائيي الأشعة في إجراء تشخيصات دقيقة. نظراً لصعوبات تحليل البيانات الطبية (الإشارات أو الصور) والاعتماد على خبرة الطبيب ، يعد نظام CAD أمراً بالغ الأهمية لتحليل الصور الطبية ، يعد استخراج الميزات واختيارها من الخطوات الأساسية. هناك عدد من طرق استخراج الميزات المثيرة للاهتمام لتصنيف أورام الدماغ في صور التصوير بالرنين المغناطيسي في مراجعة الدراسات سابقة. ميزات النسيج وتحويل المويجات المنفصل هما طريقتان لاستخراج الميزات الأكثر استخدامًا. قدمت هذه الرسالة طريقتين يمكن تصنيفهما على النحو التالي:

- في الطريقة الأولى ، قدمت الأطروحة تقنية لتصنيف صور الدماغ بالرنين المغناطيسي على أنها طبيعية وغير طبيعية. التقنية المقترحة هي استخلاص خاصية هجينة تم استخدامها لتحسين نتائج التصنيف. تتكون هذه التقنية من ثلاث خطوات. أولاً ، يتم استخدام التحويل المويجي المنفصل من 3 مستويات (DWT). ثانياً، يتم تطبيق تحليل المكون الأساسي (PCA) لتقليل حجم الخصائص. أخيراً ، يتم استخراج الميزات باستخدام مصفوفة التكرار ذات المستوى الرمادي (GLCM) من

مكونات PCA. تم استخدام مصنف الغابة العشوائي (RF) مع اختيار ميزة لتحديد الهوية. لتقييم هذا المخطط ، تم جمع صور الدماغ بالرنين المغناطيسي (81 طبيعي و 100 غير طبيعي). النتائج التجريبية حصلت على دقة 98.3 ٪ والحساسية المحققة 99 ٪ والنوعية المحققة 97.6٪. أظهر المخطط المقترح كفاءة عالية مقارنة بالعديد من مراجعة الدراسات سابقة.

- في الطريقة الثانية ، قدمت الأطروحة فرقاً محسناً في العتبة (OTD) وطريقة نظرية المجموعة التقريبية (RST) لتقسيم أورام الدماغ تلقائياً. تتكون هذه الطريقة من مرحلتين: الأولى تتضمن تقسيم مناطق الدماغ وتحديد الجمجمة لتعزيز التجزئة. تقسم هذه المرحلة منطقة الدماغ وتفصل الجمجمة عنها. تتكون المرحلة الثانية من مستويين: في المستوى الأول ، يتم إنشاء صورة تراكب ، وهو متوسط الكثافة لجميع وحدات البكسل في منطقة الدماغ التي تم تقسيمها في المرحلة الأولى. يتم تطبيق المستوى الثاني بين منطقة الدماغ وصورة التراكب اعتماداً على العتبة المحددة. يتم استخدام مصفوفة التكرار ذات المستوى الرمادي (GLCM) لاستخراج الميزات من الصور المجزأة. يتم استخدام RST مع الميزات المستخرجة لتحسين الأداء. للتقييم ، تم استخدام مجموعة بيانات مفتوحة ، وهي عبارة عن قاعدة بيانات Figshare للصور المحسّنة بالتباين T1 الموزونة مع 233 صورة للمريض مع ثلاثة أنواع من أورام الدماغ: الورم السحائي (93 شريحة) ، الورم الدبقي (105 شريحة) ، والغدة النخامية (56 شريحة) . حصلت النتائج التجريبية على دقة عالية حيث حققت بشكل عام حوالي 98.9٪ مقارنة بالدراسات الأخرى التي استخدمت نفس مجموعة البيانات.